THESIS FOR THE DEGREE OF LICENTIATE OF ENGINEERING

Three-wave mixing in Josephson travelling-wave parametric amplifiers

A theoretical and experimental study of three-wave mixing processes in Josephson junction based lumped-element travelling-wave parametric amplifiers

HAMPUS RENBERG NILSSON

Department of Microtechnology and Nanoscience
Chalmers University of Technology
Gothenburg, Sweden, 2022

Three-wave mixing in Josephson travelling-wave parametric amplifiers
A theoretical and experimental study of three-wave mixing processes in Josephson junction based lumped-element travelling-wave parametric amplifiers

Hampus Renberg Nilsson

Technical Report No. MC2-451
ISSN 1652-0769
This thesis has been prepared using LaTeX.

Department of Microtechnology and Nanoscience
Chalmers University of Technology
SE-412 96 Gothenburg, Sweden
Phone: +46 (0)31 772 1000
`www.chalmers.se`

The project was supported by the Knut and Alice Wallenberg foundation via the Wallenberg Centre for Quantum Technology

Cover
One of the TWPA samples wired to a sample box

Printed by Chalmers Reproservice
Gothenburg, Sweden, May 2022

To Seline, Sammet and Kasper

Three-wave mixing in Josephson travelling-wave parametric amplifiers
A theoretical and experimental study of three-wave mixing processes in Josephson junction based lumped-element travelling-wave parametric amplifiers
HAMPUS RENBERG NILSSON
Department of Microtechnology and Nanoscience
Gothenburg, Sweden, May 2022

Abstract

This work explores possibilities of building a wide-band, quantum-limited low-noise amplifier by means of three-wave mixing (3WM) in different kinds of Josephson travelling-wave parametric amplifiers (TWPAs). We extend the theory of the continuous three-mode model to include any number of up-converted modes in the small frequency limit where the frequency dispersion is close to linear. We also extend the theory to describe a discrete chain at frequencies close to the spectral cutoff where there is no up-conversion. In both cases we find that the gain is significantly reduced compared to the prediction by the continuous three-mode model. At the high frequencies we cannot pump strongly enough to overcome the increasingly strong dispersion, while in the small frequency limit, the dispersion can be overcome but the gain is then reduced by up-conversion processes. The developed theory is in quantitative agreement with experimental observations.

To recover the high gain predicted by the continuous three-mode model, we propose to engineer a TWPA with dispersive features to create a two-band dispersion relation, either by adding resonant phase matching (RPM) features, or by periodically modulating the parameters of the chain. By placing the pump frequency within the upper band, close to the cutoff frequency, while placing the signal in the lower band, we prove that there exists a sweet spot where the signal and the pump are phase matched while the up-conversion is inhibited. We solve the discrete equations for the RPM-based TWPA and show that the gain is expected to grow exponentially with the length of the TWPA.

Keywords: Josephson junction, rf-SQUID, SNAIL, parametric amplifier, parametric amplification, travelling-wave parametric amplifier, three-wave mixing, four-wave mixing, lumped-element, resonant phase matching.

List of Publications

This thesis is based on the following publications:

[A] **Hampus Renberg Nilsson**, Anita Fadavi Roudsari, Daryoush Shiri, Per Delsing, Vitaly Shumeiko, “A high gain travelling-wave parametric amplifier based on three-wave mixing”. `http://arxiv.org/abs/2205.07758`.

Other publications by the author, not included in this thesis, are:

[B] **Hampus Renberg Nilsson**, “Characterisation of a travelling-wave parametric amplifier for improved qubit measurements”. *Master’s thesis*, Chalmers University of Technology, Gothenburg, Sweden, June 2019.

Acknowledgements

This thesis is the result of almost four years of work at the Quantum Technology Laboratory at Chalmers University of Technology, first during the work on my Master's thesis, and then as a doctoral student. During this time I have got help and support from multiple people, to whom I wish to show my gratitude.

First and foremost I would like to thank Prof. Vitaly Shumeiko for all your support with theory, calculations, discussions, feedback, *etc.* If it were not for you, I would probably still be stuck with one calculation or another and not know how to move forward. I am very grateful for all your support.

Then I would like to thank Prof. Per Delsing who has been my main supervisor. Despite having very little time, due to all your different responsibilities, you have still given me a lot of support through many meetings and discussions. All your different perspectives on both theory and experiments have been very insightful and helpful.

I would also like to show my gratitude to Dr. Anita Fadavi Roudsari for all your weekly discussions, training with certain equipment, all the TWPA devices we have done measured on, support and help in general, *etc.* Much of the weekly work was done with your help.

Furthermore, there are several other people that are, or have been, in the group that have been helpful for me and my project: Daryoush Shiri, Avgust Yurgens, Giovanna Tancredi, Ida-Maria Svensson, Jonas Bylander, Amr Osman, Marco Scigliuzzo, Christopher Warren, Marina Kudra, Christian Križan, Yong Lu, Linda Brånell, Liangyu Chen, David Niepce, Andreas Bengtsson, Robert Rehammar and others. I am also thankful for the fast work with our patent application, done by Navid Fallah. If it were not for you, this work would either have to be delayed, or the patent application skipped altogether.

Last but not least, I would like to thank my family for the support through depressing Coronatimes, and reminding me that one's value is not solely based on one's achievements: Gudrun Renberg, Martin Nilsson, Amanda Renberg, Anton Nilsson, Ella Nilsson, Alvin Nilsson, Emilia Renberg, Momo Renberg, Karin Renberg, Gudrun Nilsson, Bo Nilsson, Seline Renberg, Sammet Nilsson, Kasper Grenander Renberg and Gabriella Grenander. A special thanks to Kasper for reminding me that there is no point in sleeping or resting when one could go out for a walk or eat one's favorite food instead.

Hampus Renberg Nilsson, Göteborg, May 2022

Acronyms

cQED:	circuit Quantum Electrodynamics
TWPA:	Travelling-wave parametric amplifier
3WM:	Three-wave mixing
4WM:	Four-wave mixing
JJ:	Josephson junction
SQUID:	Superconducting quantum interference device
rf-SQUID:	Radio-frequency SQUID
SNAIL:	Superconducting nonlinear asymmetric inductive element
c.c.:	Complex conjugate
LHS:	Left-hand side
RHS:	Right-hand side
RPM:	Resonant phase matching

List of Definitions

Name/Symbol	**Value/Formula**	**Description**
Φ_0	$\frac{h}{2e}$	The superconducting magnetic flux quantum.
φ_0	$\frac{\hbar}{2e}$	The reduced superconducting magnetic flux quantum.
I_c	–	The critical current of a Josephson junction.
Δ	$\theta_2 - \theta_1$	The phase difference between two neighbouring nodes.
I_J	$I_\mathrm{c} \sin \Delta$	The current through a Josephson junction.
U_J	$\varphi_0 \dot{\Delta}$	The voltage over a Josephson junction.
i	$\mathrm{i}^2 = -1$	The imaginary unit.
i	$\frac{I}{I_\mathrm{c}}$	A normalised and unitless current variable.
L_J0	$\frac{\varphi_0}{I_\mathrm{c}}$	The inductance of a Josephson junction at zero bias.
L_J	$\frac{L_\mathrm{J0}}{\cos(\Delta_0)}$	The inductance of a Josephson junction.

Continued on next page

Continued from previous page

Name/Symbol	**Value/Formula**	**Description**
L_{rf}	$\dfrac{L_{\mathrm{J0}}}{\frac{L_{\mathrm{J0}}}{L} + \cos(\Delta_0)}$	The inductance of an rf-SQUID.
$L_{\circledcirc}$	See Eq. (3.26).	The inductance of a SNAIL.
L_0	–	The line inductance of a TWPA.
C_{J}	–	The intrinsic capacitance of a Josephson junction.
$C_{\circledcirc}$	$C_{\mathrm{J},1}\left(\dfrac{1}{\mathcal{N}} + \alpha\right)$	The approximate capacitance of a SNAIL.
C	–	The line capacitance of a TWPA.
C_0	–	The ground capacitance of a TWPA.
$\tilde{C}$	$\dfrac{C}{C_0}$	The capacitance ratio between line and ground capacitances.
N	–	The number of unit cells.
$\mathcal{N}$	–	The number of junctions in arm 1 of a SNAIL.
$\tilde{x}$	$\dfrac{x}{a}$	A normalised spatial variable.
$\tilde{t}$	$t\omega_0$	A normalised time variable.
$\bar{A}$	–	The complex conjugate of A.
ω_0	$\dfrac{1}{\sqrt{L_0 C_0}}$	An important reference frequency of a TWPA.

Continued on next page

Continued from previous page

Name/Symbol	**Value/Formula**	**Description**
ω_{pl}	$\frac{1}{\sqrt{L_0 C}}$	The plasma frequency of the TWPA.
ω_{c}	$\frac{2\omega_0}{\sqrt{1+4\tilde{C}}}$	The cutoff frequency of a TWPA.
ω_{p}	–	The angular frequency of the pump.
ω_{s}	–	The angular frequency of the signal.
ω_{i}	$\omega_{\mathrm{p}} - \omega_{\mathrm{s}}$	The angular frequency of the idler.
$\omega_{m\mathrm{p}}$	$m\omega_{\mathrm{p}}$	The m:th harmonic of the pump.
$\omega_{\mathrm{s}+m\mathrm{p}}$	$\omega_{\mathrm{s}} + m\omega_{\mathrm{p}}$	Short notation for the m:th up-converted signal frequency.
$\omega_{\mathrm{i}+m\mathrm{p}}$	$\omega_{\mathrm{i}} + m\omega_{\mathrm{p}}$	Short notation for the m:th up-converted idler frequency.
$\tilde{\omega}_m$	$\frac{\omega_m}{\omega_0}$	The frequency ω_m normalised.
a	–	The unit cell length.
$\tilde{k}_m$	$k_m a$	The wave number k_m normalised.
c_3	See Table 3.1.	The three-wave mixing coefficient.
c_4	See Table 3.1.	The four-wave mixing coefficient.

Continued on next page

Continued from previous page

Name/Symbol	**Value/Formula**	**Description**
A_m	–	The amplitude of wave m.
$A_{\mathrm{p}0}$	$A_{\mathrm{p}}(0)$	The initial amplitude of the pump.
$A_{\mathrm{s}0}$	$A_{\mathrm{s}}(0)$	The initial amplitude of the signal.
A'_m	$\dfrac{\partial A_m}{\partial \tilde{x}}$	The derivative of A_m with respect to $\tilde{x}$.
a_m	$\dfrac{\omega_m}{\omega_{\mathrm{p}}}\dfrac{A_m}{A_{\mathrm{p}0}}$	The rescaled amplitude of wave m.
g	–	The gain coefficient.
G	$\left\lvert\dfrac{A_{\mathrm{s}}(N)}{A_{\mathrm{s}0}}\right\rvert^2$	The power gain.
M	–	The number of each mode.
δ	$\dfrac{\omega_{\mathrm{s}} - \omega_{\mathrm{p}}/2}{\omega_{\mathrm{p}}/2}$	The signal detuning from half of the pump frequency.

Contents

Part I

Thesis

CHAPTER 1

Introduction

During recent years, the interest for quantum computing and quantum processing has grown significantly. To build a large-scale, multiqubit quantum processor based on superconducting transmon qubits, high fidelity qubit readout is necessary, which requires amplifiers with high gain, large bandwidth, and low added noise.

1.1 Parametric amplifiers

Parametric amplifiers [1], which are built with nonlinear, superconducting lumped element oscillators or as transmission lines, demonstrate high gain and near quantum-limited noise performance [2]–[6] and have become an essential part of the circuit Quantum Electrodynamics (cQED) [7] toolbox. Especially interesting are the transmission line based parametric amplifiers, also known as travelling-wave parametric amplifiers (TWPAs), which provide a larger bandwidth than the cavity based parametric amplifiers (JPAs).

The general principle of parametric amplification is based on having a system that can be modulated by a parameter. By varying the parameter back and forth, energy can, under certain conditions, be transferred into a signal, while not necessarily require any energy dissipation. The absence of dissipation removes additional noise, which implies that parametric amplifiers have the potential to realise quantum-limited noise performance [8], [9].

The specific principle of amplification in a TWPA is based on a nonlinearity of the transmission line. Early works on TWPAs utilise the nonlinearity of capacitors, such as varactor diodes, as well inductors based on ferromagnetic materials [10], [11]. For cryogenic applications, the environment required for superconducting qubits, we are not aware of many nonlinear elements. While some work has been done on nonlinear capacitances [12], this work will be limited to the use of nonlinear inductances based on Josephson junctions.

The nonlinear inductance allows a nonlinear interaction between the small-amplitude propagating signal with a large-amplitude copropagating wave known as the pump. Under a phase-matching condition this results in an exponential spatial growth of the signal amplitude [10], [11], [13]. In the quantum regime, the TWPA is capable to generate signal squeezing and photon entanglement [14], [15], but this is not investigated in this thesis.

There are two types of TWPAs within the cQED platform that are investigated both theoretically and experimentally: one uses the nonlinear inductance of a chain of Josephson junctions [15]–[26] while the other uses the nonlinear kinetic inductance of a superconducting transmission line [27]–[34]. The TWPAs are further distinguished depending on the type of nonlinear interaction they employ: three-wave mixing (3WM) or four-wave mixing (4WM). In this thesis we concentrate on TWPAs based on the Josephson nonlinearitity and we focus on three-wave mixing.

1.2 Nonlinear interactions

In the 3WM interaction, two photons mix into a third, hence involving three waves. The process uses the lowest order, cubic, nonlinearity of the inductive energy, which is similar to the $\chi^{(2)}$ nonlinearity in optical crystals [35]. Such nonlinearity is associated with the broken time-reversal symmetry, which can be introduced by applying a current-bias, or a magnetic flux-bias. The amplification occurs due to a down-conversion process, which is capable to provide an efficient amplification within a large bandwidth in a weakly dispersive medium already at relatively small pump intensity [10]. An important property of this regime is the separation of the amplification band from the pump, and also the possibility of phase-preserving as well as phase-sensitive amplification [36]–[38]. In practice, however, the amplification performance of 3WM devices with weak frequency dispersion is compromised by the generation of pump harmonics [35] as well as signal and idler up-conversion [29], [39].

In the 4WM interaction, three photons mix into a fourth, hence involving four waves. The process uses the next order, quartic, nonlinearity of the inductive energy, which is similar to the $\chi^{(3)}$ nonlinearity in optical fibers [35]. Amplification in this regime is less efficient since it is a higher order effect with respect to the pumping strength, and it also suffers from dephasing due to Kerr effect that makes exponential amplification impossible without dispersion engineering [17]–[19], [40]. Furthermore, the pump position in the middle of the gain band is undesirable for certain applications. However, an advantage with 4WM is that it does not require any bias.

1.3 Focus of this thesis

In this thesis we theoretically investigate the efficiency of 3WM for several different TWPA designs. We develop several models, especially a generalised model capturing all relevant up-conversion processes in the small frequency limit, and an extended model of the continuous three-mode model by Tien [10] to describe a discrete chain close to the spectral cutoff. The generalised model we also compare to, and verify with, experimental data. Our quest throughout the thesis is to investigate whether it is practically possible to realise the full exponential amplification with 3WM predicted by the three-mode model [10] and, if it is not possible, how to solve the problems we identify.

1.4 Thesis outline

The structure of this thesis is very similar to the structure of our paper [A], but the thesis includes more details and calculations, and the order of the different calculations is changed somewhat. The only work that is not present in the thesis, but is present in the paper, is the study of 4WM up-conversion processes for a single input.

In Chapter 2 we derive the characteristics of a discrete and fully linear transmission line, including the dispersion relation, the characteristic impedance and the transmission. The structure of this transmission line is identical to the TWPAs studied, except that there are no mixing processes since there are no nonlinearities.

In Chapter 3 we derive both the discrete and the continuous wave equations for a general TWPA with general mixing coefficients c_3 and c_4. Then we derive the expressions for these mixing coefficients for three different TWPA designs that use either i) current-biased Josephson junctions, ii) magnetically flux-biased radio-frequency superconducting quantum interference devices (rf-SQUIDs) [22], or iii) magnetically flux-biased superconducting nonlinear asymmetric inductive elements (SNAILs) [25].

In Chapter 4 we investigate the small frequency limit. We begin by deriving differential equations, known as the propagation equations [9] or the coupled mode equations [39], for an arbitrary set of waves. Then we investigate the transmission of a small signal for many different sets of waves and develop a general multimode model. With this model we show that generation of up-converted modes makes it practically hard to achieve high exponential gain (*cf.* Ref. [39]). We also compare this model with experimental data obtained from a SNAIL-based TWPA, and find a very good quantitative agreement.

In Chapter 5 we derive the discrete equivalent of the propagation equations which can be used to study waves of arbitrary frequencies, but especially frequencies close to the cutoff frequency. We use these equations to derive the exact solution to the model containing only the three modes in the down-conversion process, which is a generalisation of the solution for a continuous medium in Ref. [10]. We investigate whether it is possible to place the frequencies of the waves close enough to the cutoff frequency to eliminate up-conversion, and how much pumping strength is required to do so.

In Section 5.4 we show how perfect phase matching at zero detuning can be achieved, while up-conversion is prohibited, with two different designs: the resonant phase matching technique, similar to the work in Ref. [18], and by periodically modulating the chain [29]. We also solve the discrete propagation equations for the former and show the existence of pure exponential gain for a fairly wide band for reasonably small pumping strengths.

Finally, in Chapter 6, we summarise the conclusions from the thesis. This includes both the conclusions from the small frequency limit as well as the conclusions from the study of the discrete equations.

The different models we use in this work, and the different assumptions they rely on, are illustrated in Figure 1.1.

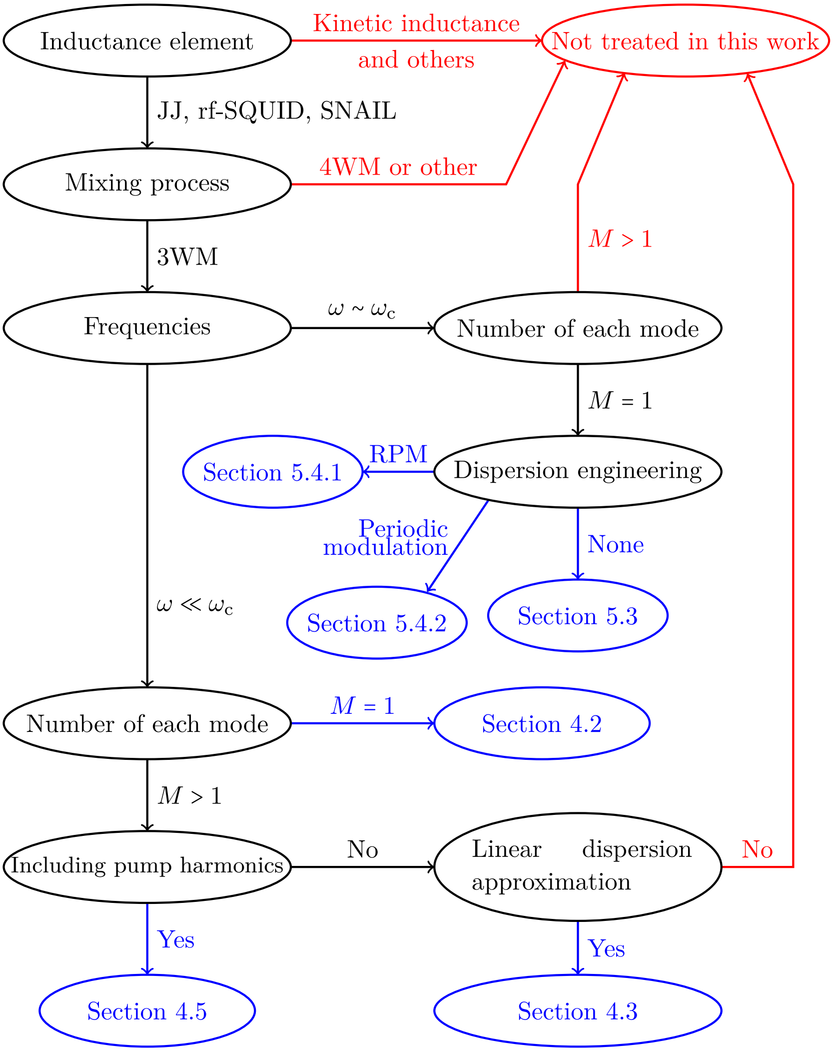

Figure 1.1: An overview of the different regimes investigated in this thesis, and where to read about them.

1.5 Amplifier figures of merit

The different figures of merit for an amplifier are typically its gain, bandwidth, noise temperature and saturation power. The definitions may vary slightly between different works, so here we clarify what definitions are used in this work.

The gain typically refers to transmission larger than 1. Furthermore, it may refer to either the voltage gain $|S_{21}|$, or the power gain $|S_{21}|^2$, where we will use the latter. However, the definition of dB for the voltage gain is $20\log_{10}(|S_{21}|)$ and for the power gain it is defined as $10\log_{10}\left(|S_{21}|^2\right)$, which ensures that both the voltage and the power gain will have the same values when expressed in dB. In certain cases, the transmission may be smaller than 1, *i.e.* there is loss, but for simplicity we will refer to this as negative gain.

The bandwidth typically refers to the frequency range where the gain is either nonzero or above a threshold value. While it is common to use the latter, with the threshold value equal to the maximum gain minus 3 dB, we will use the former in this work.

The noise temperature of an amplifier is one way of expressing the noise performance of an amplifier. Another way is the number of noise photons. Both these measures relate to the output noise power divided by the gain G at a given frequency. In other words, an amplifier can be thought of as an ideal amplifier, which adds no noise, with a noise source in front of it, and the noise temperature relates to how much noise this noise source adds. While this is an interesting measure, and something that needs to be measured when characterising an amplifier, we will not go deeper into it in this work.

Finally we have the saturation power, also known as the 1 dB compression point, which relates to the input power where the amplifier can no longer provide full amplification. More specifically, it is the input power where the gain is 1 dB lower than the gain for much smaller powers. While this is an interesting measure, and important for multiple applications, in this work we will only discuss it briefly in Section 4.5.6.

1.6 Josephson junctions

Before we can study any kind of TWPA, we must determine how to construct our nonlinear inductance element. The basic building block of nonlinear inductance elements in the TWPAs we study is the Josephson junction. The Josephson junction consists of two superconductors separated by a thin insulating barrier, see Figure 1.2.

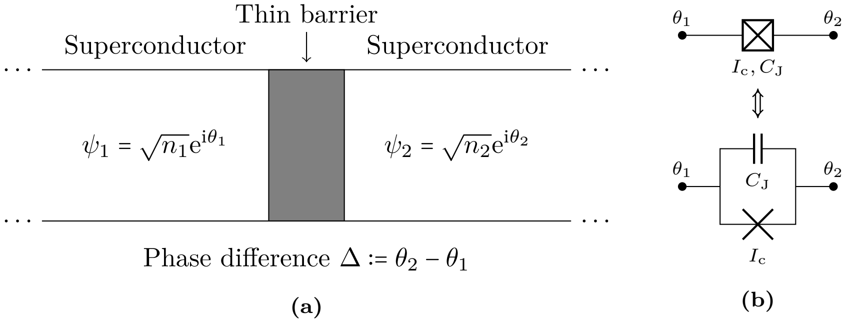

Figure 1.2: Illustrations of a Josephson junction. In (a) a sketch of the superconductors and the thin barrier that make the junction. In (b) the pictogram for a real Josephson junction (the upper) and the pictogram for an ideal junction in parallel with a capacitance equal to the junction intrinsic capacitance.

For an ideal Josephson junction the Josephson relations [41] are

$$I_\mathrm{J} = I_\mathrm{c} \sin\Delta \qquad \text{“Josephson I”,} \tag{1.1a}$$

$$U_\mathrm{J} = \varphi_0 \dot{\Delta} \qquad \text{“Josephson II”,} \tag{1.1b}$$

where U_J is the voltage over the junction, I_J is the current passing through the junction, I_c is the Josephson junction critical current, $\varphi_0 = \hbar/(2e)$ is the reduced superconducting magnetic flux quantum and Δ is the phase difference across the junction. Using these equations we can find the inductance of a Josephson junction as

$$L_\mathrm{J} = \frac{U_\mathrm{J}}{\frac{\mathrm{d}}{\mathrm{d}t} I_\mathrm{J}} = \frac{\varphi_0 \dot{\Delta}}{I_\mathrm{c} \cos\Delta \cdot \dot{\Delta}} = \frac{L_\mathrm{J0}}{\cos\Delta} \tag{1.2}$$

where $L_\mathrm{J0} = \varphi_0 / I_\mathrm{c}$ is the inductance at zero-bias. Note that the Josephson inductance is dependent on the phase difference Δ. The Josephson junction is hence a nonlinear inductor. Furthermore, using $\cos\Delta = \sqrt{1 - \sin^2\Delta}$ and the first Josephson relation, we can write it as

$$L_{\mathrm{J}} = \frac{L_{\mathrm{J0}}}{\sqrt{1 - i^2}} \tag{1.3}$$

where $i = I_{\mathrm{J}}/I_{\mathrm{c}}$ is the normalised current. Here we clearly see that the inductance increases as the current gets larger, and diverges as the current approaches the critical current. The current hence acts as a parameter that determines the inductance.

Josephson junctions can be combined in different ways to build different nonlinear inductance elements. In Chapter 3 we will derive the linear part of the inductance as well as the mixing coefficients c_3, c_4 for different kinds of inductance elements.

It is worth noting that the Josephson relations apply only to an ideal junction. In reality, since the junction is constructed as two conductors close to each other, there will also be a capacitance between them. This gives rise to the junction's intrinsic capacitance C_{J}, shown in Figure 1.2b, which in our TWPA structure will take the role of capacitance in parallel with the inductance of the transmission line.

CHAPTER 2

Transmission lines

The focus of this thesis is nonlinear transmission lines. However, to understand how *nonlinear* transmission lines work, it is crucial to first understand how *linear* transmission lines work, which will be the focus of this chapter.

2.1 The linear, discrete wave equation

In this section we will derive the wave equation for plane waves propagating through a linear and discrete LC-C-chain. With *linear*, we refer to all inductances and capacitances having fixed values. With *discrete*, we refer to the elements being much smaller than the wavelengths of the waves propagating through the chain. Each unit cell has a capacitance C_0 to ground and an LC parallel resonator on the line to the next node, thus making an LC-C*-chain*. Each unit cell has a physical length a and a voltage U_n at node n. Let us zoom in to the n:th node and investigate relations between currents, see definitions in Figure 2.1.

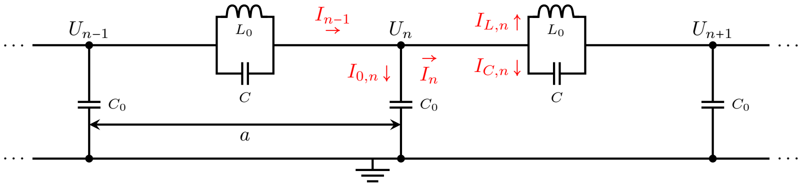

Figure 2.1: An LC-C-chain with definitions of currents, voltage U_n at the node n, and physical length a.

From Kirchhoff's current law it follows that

$$I_{0,n} = I_{n-1} - I_n, \tag{2.1a}$$

$$I_n = I_{C,n} + I_{L,n}. \tag{2.1b}$$

Let us define the node fluxes as

$$\Phi_n(t) := \int U_n(t)\,\mathrm{d}t \tag{2.2}$$

and the node phases as $\phi_n := \Phi_n/\varphi_0$, where $\varphi_0 = \hbar/(2e)$ is the reduced superconducting magnetic flux quantum. We normalise the node fluxes with φ_0 for reasons that will become apparent later. For now, let us simply consider it to be a normalisation factor. Now the currents, which are time-dependent but we will skip explicitly writing the time-dependence, can be expressed as

$$I_{0,n} = C_0 \frac{\mathrm{d}}{\mathrm{d}t}(U_n - 0) = C_0 \varphi_0 \frac{\mathrm{d}^2}{\mathrm{d}t^2}\phi_n, \tag{2.3a}$$

$$I_{C,n} = C \frac{\mathrm{d}}{\mathrm{d}t}(U_n - U_{n+1}) = -C\varphi_0 \frac{\mathrm{d}^2}{\mathrm{d}t^2}(\phi_{n+1} - \phi_n), \tag{2.3b}$$

$$L_0 \frac{\mathrm{d}I_{L,n}}{\mathrm{d}t} = U_n - U_{n+1} \implies I_{L,n} = -\frac{\varphi_0}{L_0}(\phi_{n+1} - \phi_n). \tag{2.3c}$$

Substituting the currents from Equations (2.3a) to (2.3c) into Equations (2.1a) and (2.1b) we get

$$\begin{aligned}\overbrace{C_0\varphi_0\frac{\mathrm{d}^2}{\mathrm{d}t^2}\phi_n}^{I_{0,n}} &= \overbrace{-C\varphi_0\frac{\mathrm{d}^2}{\mathrm{d}t^2}(2\phi_n-\phi_{n+1}-\phi_{n-1})}^{I_{C,n-1}-I_{C,n}} \overbrace{-\frac{\varphi_0}{L_0}(2\phi_n-\phi_{n+1}-\phi_{n-1})}^{I_{L,n-1}-I_{L,n}} \\ \implies C_0\varphi_0\frac{\mathrm{d}^2}{\mathrm{d}t^2}\phi_n &- \left[C\varphi_0\frac{\mathrm{d}^2}{\mathrm{d}t^2}+\frac{\varphi_0}{L_0}\right](\phi_{n+1}-2\phi_n+\phi_{n-1}) = 0.\end{aligned} \tag{2.4}$$

This equation has the unit of current. We can divide it by φ_0/L_0 to make it unitless. We get

$$L_0C_0\frac{\mathrm{d}^2}{\mathrm{d}t^2}\phi_n - \left[L_0C\frac{\mathrm{d}^2}{\mathrm{d}t^2}+1\right](\phi_{n+1}-2\phi_n+\phi_{n-1}) = 0. \tag{2.5}$$

Finally, let us define the resonance frequency ω_0 and the plasma frequency ω_{pl}. Equation (2.5) becomes

$$\frac{1}{\omega_0^2}\frac{\mathrm{d}^2}{\mathrm{d}t^2}\phi_n - \left[\frac{1}{\omega_{\mathrm{pl}}^2}\frac{\mathrm{d}^2}{\mathrm{d}t^2}+1\right](\phi_{n+1}-2\phi_n+\phi_{n-1}) = 0. \tag{2.6}$$

We call this equation the linear, discrete wave equation.

2.2 The dispersion relation

Now let us assume that we have plane waves. We use the ansatz that the phase at each node n is $\phi_n = A\mathrm{e}^{\mathrm{i}(\tilde{k}n-\omega t)}$, where $\tilde{k} = ka$ is the relation between the wave vector k and the length of a unit cell a. Inserting this ansatz into Equation (2.6) we get

$$\begin{aligned} 0 &= \frac{1}{\omega_0^2}(-\mathrm{i}\omega)^2\phi_n - \left(\frac{1}{\omega_{\mathrm{pl}}^2}(-\mathrm{i}\omega)^2+1\right)\left(\phi_{n+1}-2\phi_n+\phi_{n-1}\right) \\ &= -\frac{\omega^2}{\omega_0^2}\phi_n + \left(\frac{\omega^2}{\omega_{\mathrm{pl}}^2}-1\right)\left(\mathrm{e}^{\mathrm{i}\tilde{k}}\phi_n - 2\phi_n + \mathrm{e}^{-\mathrm{i}\tilde{k}}\phi_n\right)\end{aligned} \tag{2.7}$$

Dividing by ϕ_n simplifies this to

$$\begin{aligned} 0 &= -\frac{\omega^2}{\omega_0^2} + \left(\frac{\omega^2}{\omega_{\mathrm{pl}}^2} - 1\right)\left(\mathrm{e}^{\mathrm{i}\tilde{k}} - 2 + \mathrm{e}^{-\mathrm{i}\tilde{k}}\right) \\ &= -\frac{\omega^2}{\omega_0^2} + 2\left(\frac{\omega^2}{\omega_{\mathrm{pl}}^2} - 1\right)\left(\cos\left(\tilde{k}\right) - 1\right) \\ &= -\frac{\omega^2}{\omega_0^2} - 4\left(\frac{\omega^2}{\omega_{\mathrm{pl}}^2} - 1\right)\sin^2\left(\frac{\tilde{k}}{2}\right) \end{aligned} \tag{2.8}$$

which can be written as

$$\omega^2 = 4\omega_0^2\left(1 - \frac{\omega^2}{\omega_{\mathrm{pl}}^2}\right)\sin^2\left(\frac{\tilde{k}}{2}\right). \tag{2.9}$$

For $C \to 0 \implies \omega_{\mathrm{pl}} \to \infty$ we get the well-known dispersion for a discrete LC-chain, namely

$$\omega^2 = 4\omega_0^2\sin^2\left(\frac{\tilde{k}}{2}\right) \tag{2.10}$$

where the maximum frequency $\omega = 2\omega_0$ is trivially found for $\tilde{k} = \pi$. However, $C \neq 0$ gives rise to an additional term. Defining $\tilde{C} = \frac{C}{C_0} = \frac{\omega_0^2}{\omega_{\mathrm{pl}}^2}$, we solve for this term and get

$$\begin{aligned} \omega^2 + 4\tilde{C}\omega^2\sin^2\left(\frac{\tilde{k}}{2}\right) &= 4\omega_0^2\sin^2\left(\frac{\tilde{k}}{2}\right), \\ \omega^2\left(1 + 4\tilde{C}\sin^2\left(\frac{\tilde{k}}{2}\right)\right) &= 4\omega_0^2\sin^2\left(\frac{\tilde{k}}{2}\right), \\ \implies \omega^2 &= \frac{4\omega_0^2\sin^2\left(\frac{\tilde{k}}{2}\right)}{1 + 4\tilde{C}\sin^2\left(\frac{\tilde{k}}{2}\right)}. \end{aligned} \tag{2.11}$$

2.2.1 Unitless solution and cutoff frequency

Let us now normalise the frequency ω with ω_0. Then we can write Equation (2.11) in a unitless manner as

$$\tilde{\omega}^2 := \frac{\omega^2}{\omega_0^2} = \frac{4\sin^2\left(\frac{\tilde{k}}{2}\right)}{1 + 4\tilde{C}\sin^2\left(\frac{\tilde{k}}{2}\right)} \tag{2.12}$$

The largest value of $\tilde{\omega}$ that can propagate through the transmission line, known as the cutoff frequency $\tilde{\omega}_{\mathrm{c}}$, which is obtained when the sine-factors in Equation (2.12) equal one, *i.e.* when $\tilde{k} = \pi$. The value of $\tilde{\omega}_{\mathrm{c}}$ is hence

$$\tilde{\omega}_{\mathrm{c}}^2 := \frac{\omega_{\mathrm{c}}^2}{\omega_0^2} = \frac{4}{1 + 4\tilde{C}} \qquad \Longrightarrow \qquad \tilde{\omega}_{\mathrm{c}} = \frac{2}{\sqrt{1 + 4\tilde{C}}}. \tag{2.13}$$

We see here that the cutoff has the largest value when $\tilde{C} = 0$, then $\tilde{\omega}_{\mathrm{c}} = 2$, but is reduced the larger $\tilde{C}$ is. For example, if $\tilde{C} = \frac{3}{4}$ then $\tilde{\omega}_{\mathrm{c}} = 1$, or if $\tilde{C} = 2$ then $\tilde{\omega}_{\mathrm{c}} = \frac{2}{3}$. If we let $\tilde{C} \to \infty$ then $\tilde{\omega}_{\mathrm{c}} \to 0$.

2.2.2 Dispersion as a function of frequency

Let us now solve Equation (2.12) for $\tilde{k}$. We have

$$\begin{aligned}
\tilde{\omega}^2\left(1 + 4\tilde{C}\sin^2\left(\frac{\tilde{k}}{2}\right)\right) &= 4\sin^2\left(\frac{\tilde{k}}{2}\right), \\
\tilde{\omega}^2 + 4\sin^2\left(\frac{\tilde{k}}{2}\right)\left(\tilde{C}\tilde{\omega}^2 - 1\right) &= 0, \\
\sin^2\left(\frac{\tilde{k}}{2}\right) &= \frac{1}{4}\cdot\frac{\tilde{\omega}^2}{1 - \tilde{C}\tilde{\omega}^2}, \\
\sin\left(\frac{\tilde{k}}{2}\right) &= \frac{1}{2}\cdot\frac{\tilde{\omega}}{\sqrt{1 - \tilde{C}\tilde{\omega}^2}}.
\end{aligned} \tag{2.14}$$

The dispersion relation is hence

$$\tilde{k} = 2\cdot\arcsin\left(\frac{1}{2}\cdot\frac{\tilde{\omega}}{\sqrt{1 - \tilde{C}\tilde{\omega}^2}}\right). \tag{2.15}$$

The dispersion relation is plotted for multiple values of $\tilde{C}$ in Figure 2.2. In the continuous limit, $a \ll \lambda \Leftrightarrow \tilde{k} \ll \pi$, we can simplify this with a first order Taylor expansion of the arcsin-function, see Table 2.1. If $\tilde{C}$ is small, *i.e.* if the frequency is much smaller than the plasma frequency, we can do another simplification, which is also presented in Table 2.1.

For very small frequencies $\tilde{\omega} \ll \tilde{\omega}_c$ we can approximation the dispersion relation with $\tilde{k} \approx \tilde{\omega}$, as shown in Table 2.1. For frequencies that are not small enough to have the linear approximation we add the next order term from the Taylor expansion. The dispersion relation then takes the form

$$\tilde{k}\left(\tilde{\omega}\right) \approx \tilde{\omega} + \frac{1 + 12\tilde{C}}{24}\tilde{\omega}^3 := \tilde{\omega} + b\tilde{\omega}^3. \tag{2.16}$$

Here b is the cubic order coefficient which equals $1/24$ when $\tilde{C} = 0$ and increases as $\tilde{C}$ increases.

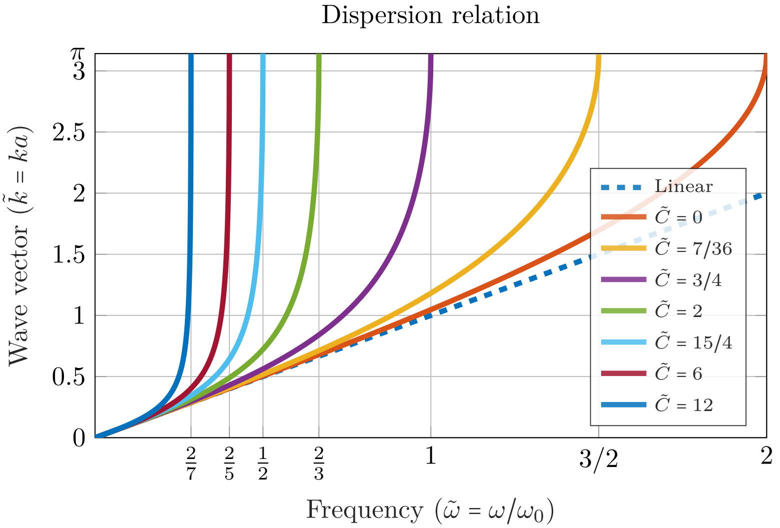

Figure 2.2: The dispersion relation of an LC-C-chain for different values of $\tilde{C}$. For small frequencies, $\omega \ll \omega_c$, the dispersion relation is linear regardless of $\tilde{C}$. For frequencies approaching the cutoff, $\omega \to \omega_c$, the wave vector quickly increases to π. The larger $\tilde{C}$ is, the sharper the dispersion relation becomes.

Table 2.1: The full dispersion relation and the dispersion relation with different simplifications.

$\tilde{k}(\tilde{\omega})$	$\forall\omega_{\mathrm{pl}}$	$\omega \ll \omega_{\mathrm{pl}}$
Discrete	$2\cdot\arcsin\left(\frac{1}{2}\cdot\frac{\tilde{\omega}}{\sqrt{1-\tilde{C}\tilde{\omega}^2}}\right)$	$2\cdot\arcsin\left(\frac{\tilde{\omega}}{2}\right)$
Continuous $(a \ll \lambda \Leftrightarrow \tilde{k} \ll \pi)$	$\frac{\tilde{\omega}}{\sqrt{1-\tilde{C}\tilde{\omega}^2}}$	$\tilde{\omega}$

2.3 Impedance and transmission

The characteristic impedance Z_{char} of an LC-C-chain is given by

$$\begin{aligned} Z_{\mathrm{line}} &= \frac{\mathrm{i}\omega L_0}{1-\omega^2 L_0 C}, \quad Y_{\mathrm{ground}} = \mathrm{i}\omega C_0, \\ Z_{\mathrm{char}} &= \sqrt{\frac{Z_{\mathrm{line}}}{Y_{\mathrm{ground}}}} = \frac{1}{\sqrt{1-\omega^2 L_0 C}}\sqrt{\frac{L_0}{C_0}} = \frac{Z_0}{\sqrt{1-\tilde{C}\tilde{\omega}^2}}. \end{aligned} \tag{2.17}$$

where $Z_0 = \sqrt{L_0/C_0}$ is the characteristic impedance of the transmission line for small frequencies ($\tilde{C}\tilde{\omega}^2 \ll 1$), while for large frequencies the impedance is larger if $\tilde{C} > 0$, see Figure 2.3. The maximum impedance is found at the cutoff frequency, $\tilde{\omega}_{\mathrm{c}} = 2/\sqrt{1+4\tilde{C}}$. Inserting the cutoff frequency into the characteristic impedance, Equation (2.17), we get that the maximum impedance is

$$Z_{\mathrm{char}}(\tilde{\omega}_{\mathrm{c}}) = \frac{Z_0}{\sqrt{1-\tilde{C}\cdot 4/(1+4\tilde{C})}} = Z_0\sqrt{1+4\tilde{C}}. \tag{2.18}$$

To find the transmission, the scattering parameter S_{21}, of the LC-C-chain with N unit cells, it is easier to start with the transmission matrix, and then convert the results into S_{21} [42]. The transmission matrix of one unit cell is given by

$$\boldsymbol{M} = \begin{bmatrix} 1 + Z_{\mathrm{line}}Y_{\mathrm{ground}} & Z_{\mathrm{line}} \\ Y_{\mathrm{ground}} & 1 \end{bmatrix}. \tag{2.19}$$

The transmission matrix of the full chain is then simply $\boldsymbol{M}^N$. If its elements are

$$\boldsymbol{M}^N = \begin{bmatrix} A & B \\ C & D \end{bmatrix} \tag{2.20}$$

and the chain is connected to an environment with characteristic impedance Z_0, we can extract the transmission S_{21} of the chain using the formula

$$S_{21} = 2\left(A + \frac{B}{Z_0} + CZ_0 + D\right)^{-1} . \tag{2.21}$$

The transmission for 25 unit cells and two values of $\tilde{C}$ are shown in Figure 2.4, normalised by the cutoff frequency. The discrete nature of the chain leads to the creation of standing waves in the line that are manifested by ripples (oscillations) in the transmission, which are clearly seen in Figure 2.4. For more unit cells there would be more oscillations.

Note that in Figure 2.3, frequencies are normalised with ω_0, while in Figure 2.4, frequencies are normalised by the cutoff frequency ω_c. Normalising with ω_0 is what will be done for most cases throughout the thesis. We normalise with ω_c in the latter figure to be able to compare the ripples. As can be seen in the figure, the ripples are in fact smaller when $\tilde{C} > 0$, in relation to the cutoff frequency, despite the larger characteristic impedance of the line.

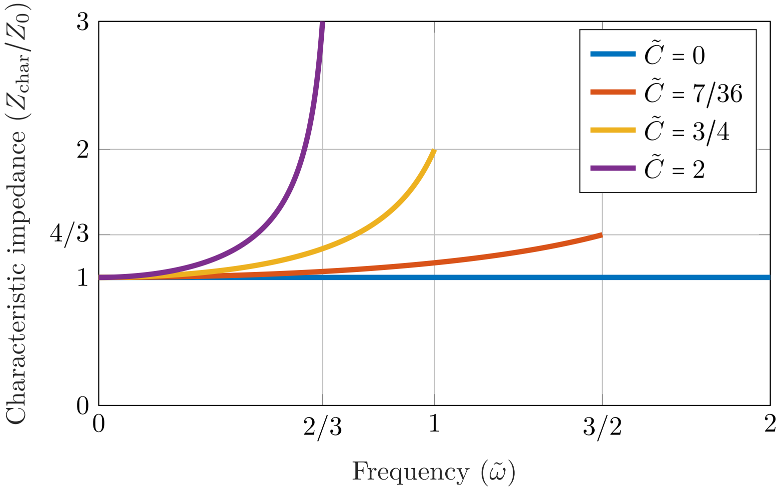

Figure 2.3: The characteristic impedance Z_{char}, expressed in terms of Z_0, as a function of normalised frequency $\tilde{\omega} = \omega/\omega_0$, for different values of $\tilde{C}$.

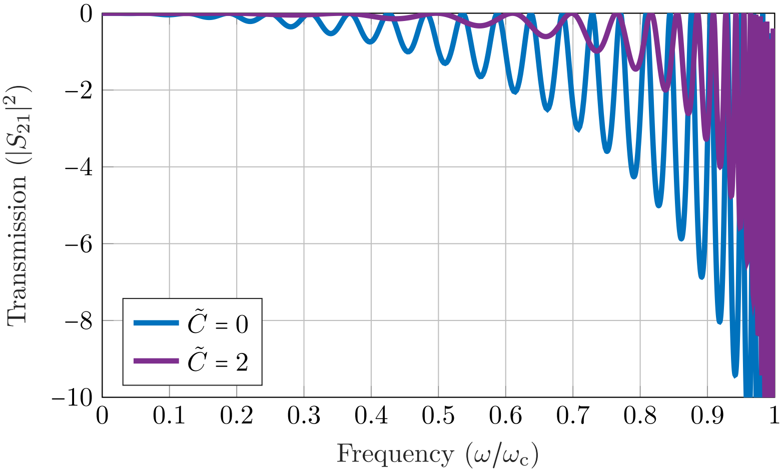

Figure 2.4: The transmission for an LC-C-chain with 25 unit cells and $\tilde{C} = 0$ (blue) and $\tilde{C} = 2$ (purple), as a function of frequency normalised by the cutoff frequency.

CHAPTER 3

Travelling-wave parametric amplifiers

In this chapter we will continue the work from Chapter 2, but now with one key difference: the inductance is now dependent on the phase difference between the nodes, see Figure 3.1, which makes the transmission line a TWPA.

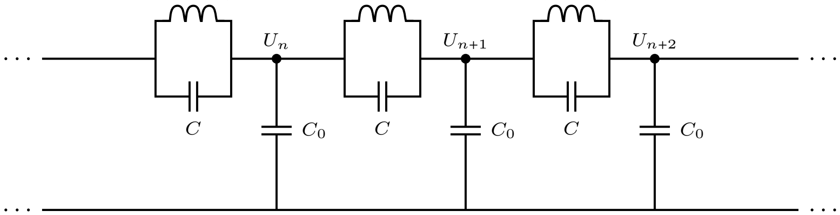

Figure 3.1: General schematic of a TWPA: an *LC*-*C*-chain with nonlinear inductances depending on the phase differences between the nodes.

3.1 TWPA discrete wave equation

Since the only difference between Figures 2.1 and 3.1 is the inductance element, Equation (2.4) is almost unchanged, with the exception of the expression for $I_{L,n}$, where there are additional terms that reflect the nonlinearity of the inductance. Defining the phase difference $\Delta_n = \phi_{n+1} - \phi_n$, where ϕ_n are the node phases as defined in Section 2.1, and the static phase-bias Δ_0, we can in general describe the current as

$$I_{L,n} = \frac{\varphi_0}{L_0} f(\Delta_n) = I_0 \sum_{j=0}^{\infty} \frac{f^{(j)}(\Delta_0)}{j!} (\Delta_n - \Delta_0)^j \,. \tag{3.1}$$

Here $I_0 = \varphi_0 / L_0$ is the current set by the static inductance L_0 of the inductive element, the function f is a general function describing the current phase relation of the inductive element, and the sum in the right hand side of the equation is the Taylor expansion of f around Δ_0. Let us now define the phase variation

$$\delta_n = \Delta_n - \Delta_0 \tag{3.2}$$

and the coefficients

$$b_j := \frac{f^{(j)}(\Delta_0)}{j!}. \tag{3.3}$$

Note that the static inductance per definition is such that $b_1 = 1$. In the absence of a bias current we also know that $b_0 = 0$. However, a more general relation is taking a bias current I_b into consideration, which gives the constraint $I_\mathrm{b} = I_0 b_0$. The inductance current difference becomes

$$I_{L,n-1} - I_{L,n} = I_0 \sum_{j=0}^{\infty} b_j \left(\delta_{n-1}^j - \delta_n^j \right). \tag{3.4}$$

The first term in the sum is trivially zero and, since $b_1 = 1$, the second term equals the same difference as in Equation (2.3c). The discrete wave equation with a nonlinear inductance can then be rewritten as

$$\begin{aligned} &L_0 C_0 \frac{\mathrm{d}^2}{\mathrm{d}t^2} \phi_n - \left[L_0 C \frac{\mathrm{d}^2}{\mathrm{d}t^2} + 1 \right] (\phi_{n+1} - 2\phi_n + \phi_{n-1}) \\ &= \sum_{j=2}^{\infty} b_j \left((\phi_{n+1} - \phi_n)^j - (\phi_n - \phi_{n-1})^j \right). \end{aligned} \tag{3.5}$$

Compared with the linear discrete wave equation, Equation (2.6), the only difference is the right-hand side of the equation, due to the nonlinear inductance. It is the right-hand side that allows different frequency mixing processes, as we will see in Chapter 4.

Finally we will assume small phase variations $\delta_n \ll 1$, which allows us to drop higher order terms. Due to conventions we define

$$c_3 = -2b_2, \quad c_4 = -3b_3. \tag{3.6}$$

In this work, c_3 and c_4 are called the 3-wave mixing (3WM) and 4-wave mixing (4WM) coefficients respectively[1][2]. With these coefficients, we modify Equation (3.5) to reach the final form of the discrete wave equation,

$$\begin{aligned} L_0 C_0 \frac{\mathrm{d}^2}{\mathrm{d}t^2}\phi_n - \left[L_0 C \frac{\mathrm{d}^2}{\mathrm{d}t^2} + 1\right](\phi_{n+1} - 2\phi_n + \phi_{n-1}) \\ = -\frac{c_3}{2}\left((\phi_{n+1} - \phi_n)^2 - (\phi_n - \phi_{n-1})^2\right) \\ - \frac{c_4}{3}\left((\phi_{n+1} - \phi_n)^3 - (\phi_n - \phi_{n-1})^3\right). \end{aligned} \tag{3.7}$$

3.2 TWPA continuous wave equation

A common simplification of Equation (3.7) is assuming that wavelengths are much longer than the unit cell length, $\tilde{k} \ll \pi$. Then the node phase $\phi_n(t)$ can be replaced by a continuous flux variable $\phi(x,t)$ and the differences can be expressed with derivatives,

$$\phi_{n+1} - \phi_n = \sum_{j=1}^{\infty} \frac{(a\partial_x)^j}{j!}\phi(x,t) = \left[\mathrm{e}^{a\partial_x} - 1\right]\phi(x,t), \tag{3.8a}$$

$$\phi_n - \phi_{n-1} = \sum_{j=1}^{\infty} -\frac{(-a\partial_x)^j}{j!}\phi(x,t) = \left[1 - \mathrm{e}^{-a\partial_x}\right]\phi(x,t) \tag{3.8b}$$

---

[1] Note: The c_3, c_4 here are not the same coefficients as c_3 and c_4 in Ref. [43].

[2] Note: In some literature [22], [24], [44], the mixing coefficients are expressed with $\beta = -b_2$ and $\gamma = -b_3$.

where a is the physical length of the unit cell. For the linear part of the wave equation we can simplify the differential operator as

$$\left(\mathrm{e}^{a\partial_x}-1\right)-\left(1-\mathrm{e}^{-a\partial_x}\right)=2\left(\frac{\mathrm{e}^{a\partial_x}+\mathrm{e}^{-a\partial_x}}{2}-1\right)=-4\sin^2\!\left(\frac{1}{2}\mathrm{i}a\partial_x\right). \tag{3.9}$$

The continuous wave equation hence becomes

$$\begin{aligned} L_0C_0\frac{\partial^2\phi}{\partial t^2}&+4\left[L_0C\frac{\partial^2}{\partial t^2}+1\right]\sin^2\!\left(\frac{1}{2}\mathrm{i}a\partial_x\right)\phi \\ &=-\frac{c_3}{2}\left(\left(\left[\mathrm{e}^{a\partial_x}-1\right]\phi\right)^2-\left(\left[1-\mathrm{e}^{-a\partial_x}\right]\phi\right)^2\right) \\ &\quad-\frac{c_4}{3}\left(\left(\left[\mathrm{e}^{a\partial_x}-1\right]\phi\right)^3-\left(\left[1-\mathrm{e}^{-a\partial_x}\right]\phi\right)^3\right). \end{aligned} \tag{3.10}$$

We simplify Equation (3.10) by keeping only the lowest order terms with respect to the unit cell length a. For the linear part of equation we get

$$4\sin^2\!\left(\frac{1}{2}\mathrm{i}a\partial_x\right)\phi\approx4\left(\frac{1}{2}\mathrm{i}a\partial_x\right)^2\phi=-a^2\frac{\partial^2\phi}{\partial x^2}, \tag{3.11a}$$

for the quadratic part we get

$$\begin{aligned} \left(\left[\mathrm{e}^{a\partial_x}-1\right]\phi\right)^2&\approx\left(a\frac{\partial\phi}{\partial x}\right)^2+a^3\frac{\partial\phi}{\partial x}\frac{\partial^2\phi}{\partial x^2}+\left(\frac{a^2}{2}\frac{\partial^2\phi}{\partial x^2}\right)^2, \\ \left(\left[1-\mathrm{e}^{-a\partial_x}\right]\phi\right)^2&\approx\left(a\frac{\partial\phi}{\partial x}\right)^2-a^3\frac{\partial\phi}{\partial x}\frac{\partial^2\phi}{\partial x^2}+\left(\frac{a^2}{2}\frac{\partial^2\phi}{\partial x^2}\right)^2, \\ \left(\left[\mathrm{e}^{a\partial_x}-1\right]\phi\right)^2-\left(\left[1-\mathrm{e}^{-a\partial_x}\right]\phi\right)^2&\approx2a^3\frac{\partial\phi}{\partial x}\frac{\partial^2\phi}{\partial x^2}, \end{aligned} \tag{3.11b}$$

and for the cubic part we get

$$\begin{aligned} \left(\left[\mathrm{e}^{a\partial_x}-1\right]\phi\right)^3&\approx\left(a\frac{\partial\phi}{\partial x}\right)^3+\frac{3}{2}a^4\left(\frac{\partial\phi}{\partial x}\right)^2\frac{\partial^2\phi}{\partial x^2}+\frac{3}{2}a^4\frac{\partial\phi}{\partial x}\left(\frac{\partial^2\phi}{\partial x^2}\right)^2+\left(a^2\frac{\partial^2\phi}{\partial x^2}\right)^3, \\ \left(\left[1-\mathrm{e}^{-a\partial_x}\right]\phi\right)^3&\approx\left(a\frac{\partial\phi}{\partial x}\right)^3-\frac{3}{2}a^4\left(\frac{\partial\phi}{\partial x}\right)^2\frac{\partial^2\phi}{\partial x^2}+\frac{3}{2}a^4\frac{\partial\phi}{\partial x}\left(\frac{\partial^2\phi}{\partial x^2}\right)^2-\left(a^2\frac{\partial^2\phi}{\partial x^2}\right)^3, \\ \left(\left[\mathrm{e}^{a\partial_x}-1\right]\phi\right)^3-\left(\left[1-\mathrm{e}^{-a\partial_x}\right]\phi\right)^3&\approx3a^4\left(\frac{\partial\phi}{\partial x}\right)^2\frac{\partial^2\phi}{\partial x^2}. \end{aligned} \tag{3.11c}$$

Now Equation (3.10) can be simplified to

$$\begin{aligned}&\left[L_0C_0\frac{\partial^2}{\partial t^2} - L_0Ca^2\frac{\partial^2}{\partial t^2}\frac{\partial^2}{\partial x^2} - a^2\frac{\partial^2}{\partial x^2}\right]\phi \\ &= -c_3a^3\frac{\partial\phi}{\partial x}\frac{\partial^2\phi}{\partial x^2} - c_4a^4\left(\frac{\partial\phi}{\partial x}\right)^2\frac{\partial^2\phi}{\partial x^2}.\end{aligned} \tag{3.12}$$

As a final step of simplification, let us introduce the normalised TWPA units $\tilde{t} = t\omega_0$ and $\tilde{x} = x/a$. These can either be thought of as unitless variables for time and space, normalised with ω_0 and a, or simply as time and space measured in units of ω_0 and a. With these, and the previously defined relation $\tilde{C} = C/C_0$, we reach the most simplified form of the continuous wave equation,

$$\left[\frac{\partial^2}{\partial\tilde{t}^2} - \tilde{C}\frac{\partial^2}{\partial\tilde{t}^2}\frac{\partial^2}{\partial\tilde{x}^2} - \frac{\partial^2}{\partial\tilde{x}^2}\right]\phi = -c_3\frac{\partial\phi}{\partial\tilde{x}}\frac{\partial^2\phi}{\partial\tilde{x}^2} - c_4\left(\frac{\partial\phi}{\partial\tilde{x}}\right)^2\frac{\partial^2\phi}{\partial\tilde{x}^2}. \tag{3.13}$$

This is the wave equation we will use for most of the analysis of mixing processes within the TWPA. It is worth remembering that this equation is an approximation of the exact discrete wave equation, and holds as long as wavelengths are much longer than the unit cell, which is equivalent with $\tilde{k} \ll \pi$, *i.e.* in the quasilinear regime, recall Section 2.2. If wavelengths are *not* much longer than a unit cell, one should use the discrete wave equation instead, which we will do in Chapter 5.

In the regime where the continuous wave equation can be used, the linear approximation of the dispersion relation holds most of the time. However, as we will show later, for the phase mismatches we will need to use the cubic approximation, recall Equation (2.16). Therefore we call this regime the *quasilinear* regime.

3.3 Josephson junction TWPA

The simplest kind of cryogenic, inductive element is a single Josephson junction, possibly biased with a DC-current. Utilising Equation (3.1), we can approximate the current through the junction at each node n as

$$\begin{aligned}
I_\mathrm{J} &= I_\mathrm{c}\sin(\Delta_n) = I_\mathrm{c}\sin(\Delta_0+\delta_n) \\
&= I_\mathrm{c}\sin\Delta_0\cos\delta_n + I_\mathrm{c}\sin\delta_n\cos\Delta_0 \\
&\approx I_\mathrm{c}\sin\Delta_0\left(1-\frac{1}{2}\delta_n^2\right) + I_\mathrm{c}\cos\Delta_0\left(\delta_n-\frac{1}{6}\delta_n^3\right) \\
&= I_\mathrm{c}\cos\Delta_0\left(\tan\Delta_0\left(1-\frac{1}{2}\delta_n^2\right)+\left(\delta_n-\frac{1}{6}\delta_n^3\right)\right).
\end{aligned} \tag{3.14}$$

Let us define normalised currents as $i = I/I_\mathrm{c}$. Then the phase-bias Δ_0 is determined by the bias current as

$$i_\mathrm{b} = \sin\Delta_0 \qquad \Longrightarrow \qquad \Delta_0 = \arcsin(i_\mathrm{b})\,. \tag{3.15}$$

The reference current is $I_0 = I_\mathrm{c}\cos\Delta_0$, therefore the static inductance in Figure 3.1 is the junction inductance given by

$$L_\mathrm{J} = \frac{\varphi_0}{I_0} = \frac{\varphi_0}{I_\mathrm{c}\cos\Delta_0} \tag{3.16}$$

while the line capacitance is simply the junction intrinsic capacitance, $C = C_\mathrm{J}$. The quadratic and cubic coefficients, as defined in Equation (3.3), are $b_2 = -\frac{1}{2}\tan\Delta_0$ and $b_3 = -\frac{1}{6}$. The mixing coefficients, as defined in Equation (3.6), are hence

$$c_3 = \tan\Delta_0, \quad c_4 = \frac{1}{2}. \tag{3.17}$$

The 4WM coefficient c_4 is fixed, *i.e.* 4WM is unaffected by the bias current. The 3WM coefficient on the other hand is

$$c_3 = \tan\Delta_0 = \frac{\sin\Delta_0}{\cos\Delta_0} = \frac{i_\mathrm{b}}{\sqrt{1-i_\mathrm{b}^2}}. \tag{3.18}$$

In words, without a bias current the 3WM coefficient is zero, while for a bias current close to the critical current, the coefficient diverges towards infinity. However, this does not mean that we can get an arbitrarily strong 3WM process, which will investigate closer in Chapter 5.

3.4 RF-SQUID TWPA

Another inductive element for the TWPA is the rf-SQUID [22]. It consists of a superconducting loop where one arm has an inductor with linear inductance L and another arm has a Josephson junction with critical current I_c. There is also a static external magnetic field applying a magnetic flux bias. The rf-SQUID is depicted in Figure 3.2.

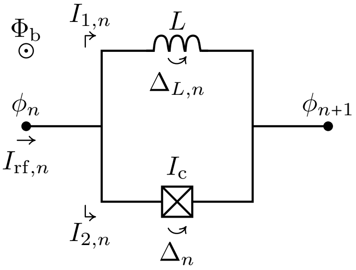

Figure 3.2: The rf-SQUID.

The phase drop over the upper arm is $\Delta_{L,n}$ and the phase drop over the lower arm is Δ_n. To relate the magnetic flux bias Φ_b to the phase, let us define $F := 2\pi\Phi_\mathrm{b}/\Phi_0$. This gives the constraint that $\Delta_{L,n} - \Delta_n = F$, or in other words, that the phase drop over the linear inductance is $\Delta_{L,n} = F + \Delta_n$.

The rf-SQUID current is given by

$$\begin{aligned} I_{\mathrm{rf},n}(F,\Delta_n) &= I_{1,n} + I_{2,n} = \frac{\varphi_0}{L}(F+\Delta_n) + I_\mathrm{c}\sin(\Delta_n) \\ \implies i_{\mathrm{rf},n} &= \frac{L_\mathrm{J0}}{L}(F+\Delta_n) + \sin(\Delta_n)\,. \end{aligned} \tag{3.19a}$$

where $i_{\mathrm{rf},n} = I_{\mathrm{rf},n}/I_\mathrm{c}$ is the normalised rf-SQUID current and $L_\mathrm{J0} = \varphi_0/I_\mathrm{c}$ is the unbiased junction inductance. Let us now insert the small phase variation,

$\Delta_n = \Delta_0 + \delta_n$. The current becomes

$$\begin{aligned} i_{\mathrm{rf},n} &= \frac{L_{\mathrm{J0}}}{L}\left(F + \Delta_0 + \delta_n\right) + \sin\left(\Delta_0 + \delta_n\right) \\ &= \frac{L_{\mathrm{J0}}}{L}\left(F + \Delta_0 + \delta_n\right) + \sin\left(\Delta_0\right)\cos\left(\delta_n\right) + \sin\left(\delta_n\right)\cos\left(\Delta_0\right) \\ &\approx \frac{L_{\mathrm{J0}}}{L}\left(F + \Delta_0 + \delta_n\right) + \sin\left(\Delta_0\right)\left(1 - \frac{1}{2}\delta_n^2\right) + \left(\delta_n - \frac{1}{6}\delta_n^3\right)\cos\left(\Delta_0\right). \end{aligned} \tag{3.19b}$$

Rearranging the equation so that the different orders of small phase variation are gathered we get

$$\begin{aligned} i_{\mathrm{rf},n} &= 1 \cdot \left[\frac{L_{\mathrm{J0}}}{L}\left(F + \Delta_0\right) + \sin\left(\Delta_0\right)\right] \\ &+ \delta_n \cdot \left[\frac{L_{\mathrm{J0}}}{L} + \cos\left(\Delta_0\right)\right] \\ &- \frac{1}{2}\delta_n^2 \cdot \sin\left(\Delta_0\right) - \frac{1}{6}\delta_n^3 \cdot \cos\left(\Delta_0\right). \end{aligned} \tag{3.19c}$$

We factor out $L_{\mathrm{J0}}/L + \cos(\Delta_0)$, to ensure that $b_1 = 1$ as we have previously mentioned follows from the definition of the b_j-coefficients. The first term in Equation (3.19c) is the normalised bias current i_{b} and gives the constraint

$$i_{\mathrm{b}} = \frac{L_{\mathrm{J0}}}{L}\left(F + \Delta_0\right) + \sin\left(\Delta_0\right), \tag{3.20}$$

which lets us find the value of Δ_0 numerically, given the value of the flux bias F and the bias current i_{b}. Typically we use $i_{\mathrm{b}} = 0$. From Equation (3.19c) we extract the inductance of the rf-SQUID to be

$$L_0 = L_{\mathrm{rf}} = \frac{L_{\mathrm{J0}}}{\frac{L_{\mathrm{J0}}}{L} + \cos\left(\Delta_0\right)}, \tag{3.21}$$

see Figure 3.3.

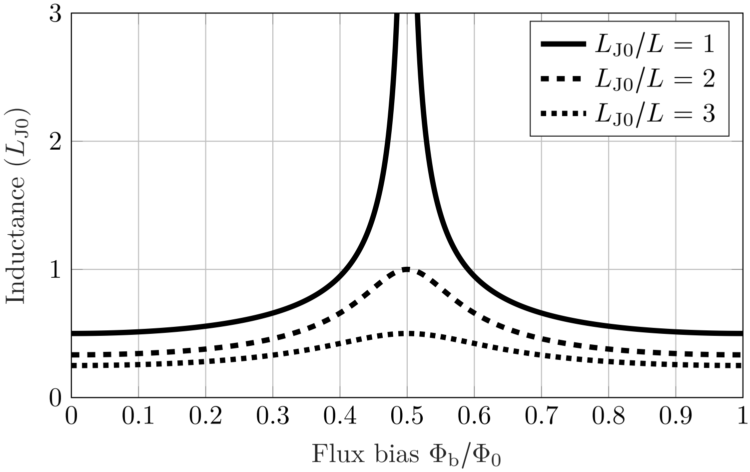

Figure 3.3: The inductance of an rf-SQUID, expressed in terms of L_{J0} for 3 different values of the fraction L_{J0}/L, as a function of magnetic flux bias. The maximum inductance is found for a bias equal to half of a flux quantum, $\Phi_b = \Phi_0/2$. The inductance is periodic, *i.e.* for larger or smaller fluxes than the ones displayed, the pattern repeats.

We can also extract the mixing coefficients now, as defined in Equation (3.6), as

$$c_3 = \frac{\sin(\Delta_0)}{\frac{L_{J0}}{L} + \cos(\Delta_0)}, \tag{3.22a}$$

$$c_4 = \frac{1}{2}\frac{\cos(\Delta_0)}{\frac{L_{J0}}{L} + \cos(\Delta_0)}. \tag{3.22b}$$

These mixing coefficients are shown in Figures 3.4 and 3.5 as a function of magnetic flux bias. Note that there are bias points where $c_3 \neq 0, c_4 = 0$ as well as bias points where $c_3 = 0, c_4 \neq 0$. In other words, the rf-SQUID-TWPA can be magnetically biased such that we get pure 3WM or pure 4WM, unlike the single junction TWPA. To get pure 3WM, the flux bias F needs to be such that

$$\cos(\Delta_0) = 0 \quad \implies \quad c_3 = \frac{1}{\frac{L_{J0}}{L} + 0} = \frac{L}{L_{J0}}. \tag{3.23}$$

At this bias point, the inductance becomes $L_0 = L$.

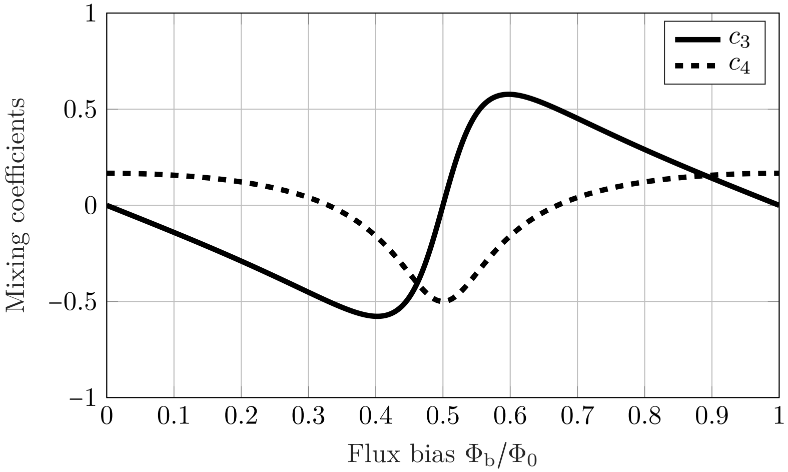

Figure 3.4: The mixing coefficients c_3, c_4 of an rf-SQUID-TWPA with $L_{J0}/L = 2$ as a function of magnetic flux bias. For flux biases $\sim 0.33\Phi_0$ and $\sim 0.67\Phi_0$, we get pure three-wave mixing as $c_4 = 0$ and $c_3 = 1/2$.

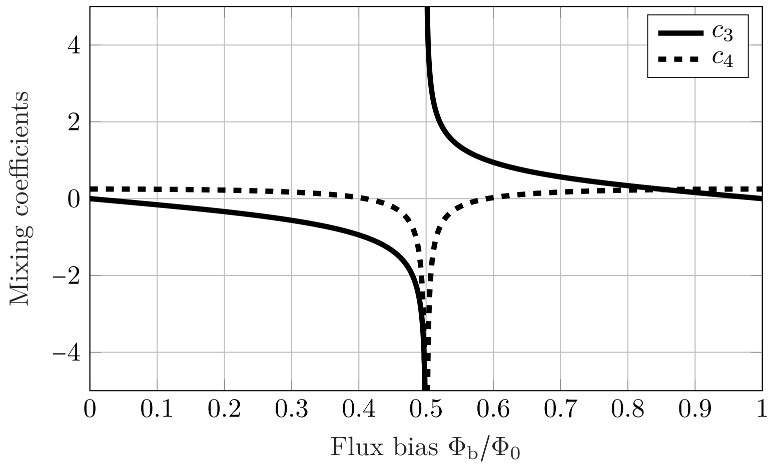

Figure 3.5: The mixing coefficients c_3, c_4 of an rf-SQUID-TWPA with $L_{J0}/L = 1$ as a function of magnetic flux bias. For flux biases $\sim 0.41\Phi_0$ and $\sim 0.59\Phi_0$, we get pure three-wave mixing as $c_4 = 0$ and $c_3 = 1$.

3.5 SNAIL TWPA

Another TWPA inductance element is the SNAIL, which is an acronym for the Superconducting Nonlinear Asymmetric Inductance eLement [25]. It consists of a loop, where one arm has $\mathcal{N}$ identical Josephson junctions with critical current I_c, while the other has a single Josephson junction with critical current αI_c where $\alpha < 1$. There is also a static external magnetic field applying a magnetic flux bias. The SNAIL is depicted in Figure 3.6.

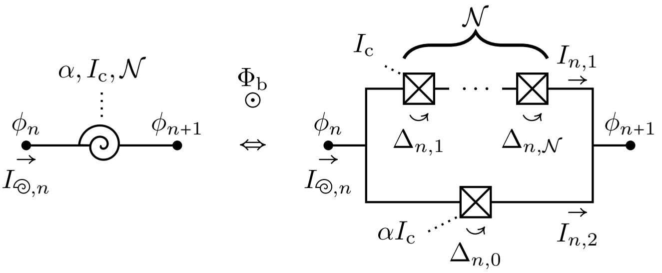

Figure 3.6: The Superconducting Nonlinear Asymmetric Inductance eLement.

In Figure 3.6, let us call the lone junction “junction 0”, and those on the top arm “junction 1”, ..., “junction $\mathcal{N}$”. Since the same current that flows through junction 1 will also flow through junction 2 to junction $\mathcal{N}$, and they have the same critical currents, the phase differences over these junctions are identical. If we call the total phase drop over these junctions Δ_n, the phase drop over one of them is hence $\Delta_n/\mathcal{N}$.

The phase drop over the upper arm is Δ_n and the phase drop over the lower arm is $\Delta_{n,0}$. To relate the external magnetic flux Φ_b to phase, let us define $F := 2\pi\Phi_\mathrm{b}/\Phi_0$. This gives us the constraint that $\Delta_{n,0} - \Delta_n = F$, or in other words, that the phase drop over junction 0 is $\Delta_{n,0} = F + \Delta_n$.

The SNAIL current is given by

$$\begin{aligned} I_{@,n} &= I_{n,1} + I_{n,2} = \alpha I_\mathrm{c} \sin(\Delta_{n,0}) + I_\mathrm{c} \sin(\Delta_{n,1}) \\ &= I_\mathrm{c}\left(\alpha \sin(F + \Delta_n) + \sin\left(\frac{\Delta_n}{\mathcal{N}}\right)\right). \end{aligned} \tag{3.24a}$$

To make the equations slightly cleaner, let us define the normalised SNAIL current $i_{@,n} = I_{@,n}/I_\mathrm{c}$. Let us also insert the small phase variation $\Delta_n =$

$\Delta_0 + \delta_n$. The current becomes

$$\begin{aligned}
i_{@,n} &= \alpha \sin(F + \Delta_0 + \delta_n) + \sin\left(\frac{\Delta_0 + \delta_n}{\mathcal{N}}\right) \\
&= \alpha\big[\sin(F + \Delta_0)\cos(\delta_n) + \sin(\delta_n)\cos(F + \Delta_0)\big] \\
&+ \sin\left(\frac{\Delta_0}{\mathcal{N}}\right)\cos\left(\frac{\delta_n}{\mathcal{N}}\right) + \sin\left(\frac{\delta_n}{\mathcal{N}}\right)\cos\left(\frac{\Delta_0}{\mathcal{N}}\right) \\
&\approx \alpha\left[\sin(F + \Delta_0)\left(1 - \frac{1}{2}\delta_n^2\right) + \left(\delta_n - \frac{1}{6}\delta_n^3\right)\cos(F + \Delta_0)\right] \\
&+ \sin\left(\frac{\Delta_0}{\mathcal{N}}\right)\left(1 - \frac{1}{2}\left(\frac{\delta_n}{\mathcal{N}}\right)^2\right) + \left(\frac{\delta_n}{\mathcal{N}} - \frac{1}{6}\left(\frac{\delta_n}{\mathcal{N}}\right)^3\right)\cos\left(\frac{\Delta_0}{\mathcal{N}}\right).
\end{aligned} \tag{3.24b}$$

Rearranging the equation so that the different orders of small phase variation are gathered we get

$$\begin{aligned}
i_{@,n} \approx 1 &\cdot \left[\alpha \sin(F + \Delta_0) + \sin\left(\frac{\Delta_0}{\mathcal{N}}\right)\right] \\
+ \delta_n &\cdot \left[\alpha \cos(F + \Delta_0) + \frac{1}{\mathcal{N}}\cos\left(\frac{\Delta_0}{\mathcal{N}}\right)\right] \\
- \frac{1}{2}\delta_n^2 &\cdot \left[\alpha \sin(F + \Delta_0) + \frac{1}{\mathcal{N}^2}\sin\left(\frac{\Delta_0}{\mathcal{N}}\right)\right] \\
- \frac{1}{6}\delta_n^3 &\cdot \left[\alpha \cos(F + \Delta_0) + \frac{1}{\mathcal{N}^3}\cos\left(\frac{\Delta_0}{\mathcal{N}}\right)\right].
\end{aligned} \tag{3.24c}$$

We factor out the factor multiplied with δ_n, to ensure that $b_1 = 1$ as we have previously mentioned follows from the definition of the b_j-coefficients. The first term in Equation (3.24c) is the normalised bias current i_b and then we get the constraint

$$i_\mathrm{b} = \alpha \sin(F + \Delta_0) + \sin\left(\frac{\Delta_0}{\mathcal{N}}\right), \tag{3.25}$$

which lets us find the value of Δ_0 numerically, given the value of the flux bias F and the bias current i_b. Typically we use $i_\mathrm{b} = 0$. We extract the inductance of the SNAIL from Equation (3.24c) as

$$L_0 = L_{@} = \frac{L_{\mathrm{J}0}}{\alpha \cos(F + \Delta_0) + \frac{1}{\mathcal{N}}\cos\left(\frac{\Delta_0}{\mathcal{N}}\right)}, \tag{3.26}$$

see Figure 3.7.

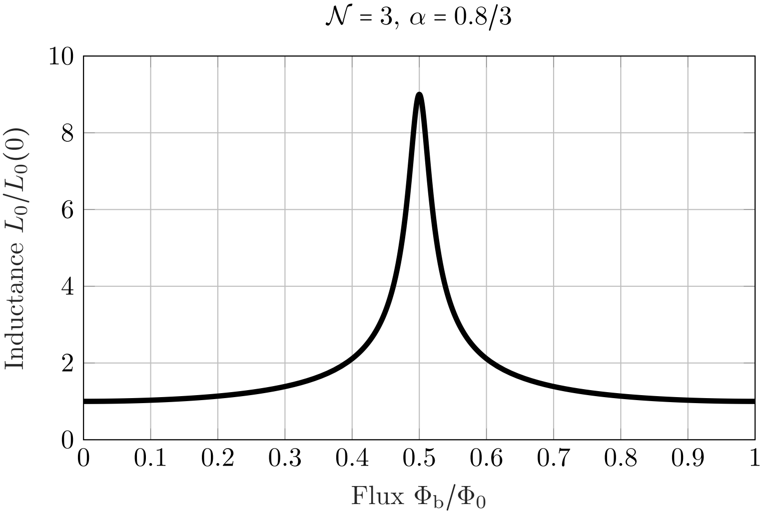

Figure 3.7: The inductance of a SNAIL with $\mathcal{N} = 3$ and $\alpha = 0.8/3$ as a function of flux, normalised to the inductance at zero flux, $L_0(0)$.

The capacitance of the SNAIL is given by

$$C = C_{\circledcirc} = \frac{C_{\mathrm{J},1}}{\mathcal{N}} + C_{\mathrm{J},2} \approx \frac{C_{\mathrm{J},1}}{\mathcal{N}} + \alpha C_{\mathrm{J},1} = C_{\mathrm{J},1}\left(\frac{1}{\mathcal{N}} + \alpha\right). \tag{3.27}$$

where $C_{\mathrm{J},1}$ is the capacitance of each junction in the upper arm in Figure 3.6 and $C_{\mathrm{J},2}$ is the capacitance of the single junction.

We can also extract the mixing coefficients now, as defined in Equation (3.6), as

$$c_3 = \frac{\alpha \sin(F + \Delta_0) + \frac{1}{\mathcal{N}^2} \sin\left(\frac{\Delta_0}{\mathcal{N}}\right)}{\alpha \cos(F + \Delta_0) + \frac{1}{\mathcal{N}} \cos\left(\frac{\Delta_0}{\mathcal{N}}\right)}, \tag{3.28a}$$

$$c_4 = \frac{1}{2} \frac{\alpha \cos(F + \Delta_0) + \frac{1}{\mathcal{N}^3} \cos\left(\frac{\Delta_0}{\mathcal{N}}\right)}{\alpha \cos(F + \Delta_0) + \frac{1}{\mathcal{N}} \cos\left(\frac{\Delta_0}{\mathcal{N}}\right)}. \tag{3.28b}$$

These mixing coefficients are shown in Figure 3.8 as a function of flux bias. Note that there are bias points where $c_3 \neq 0, c_4 = 0$ as well as bias points where $c_3 = 0, c_4 \neq 0$. In other words, the SNAIL-TWPA can be biased such that we get pure 3WM or pure 4WM, just like the rf-SQUID-TWPA.

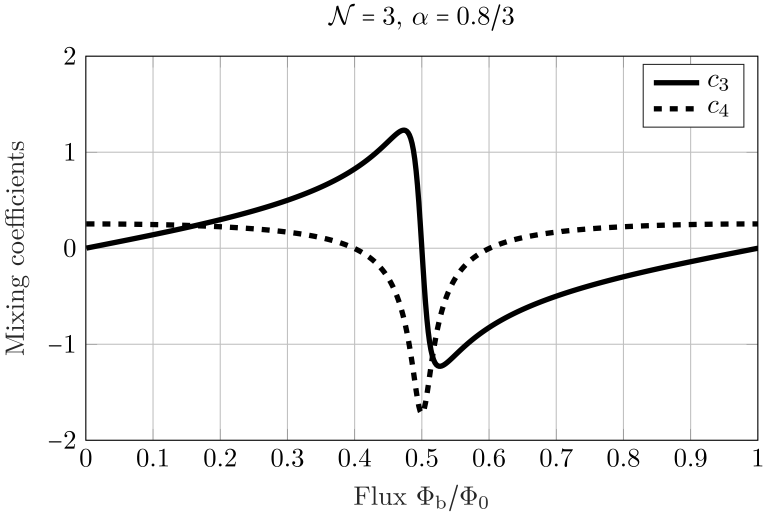

Figure 3.8: The mixing coefficients c_3, c_4 of a SNAIL-TWPA with $\mathcal{N} = 3, \alpha = 0.8/3$ as a function of magnetic flux bias.

3.6 Summary

A summary of the different TWPA elements is presented in Table 3.1.

Table 3.1: The capacitance, phase-bias equation, inductance and the mixing coefficients for the three different TWPA elements.

	JJ	rf-SQUID	SNAIL
C	C_J	C_J	$C_{\mathrm{J},1}\left(\frac{1}{\mathcal{N}}+\alpha\right)$
i_b	$\sin(\Delta_0)$	$\frac{L_{\mathrm{J}0}}{L}(F+\Delta_0)+\sin(\Delta_0)$	$\alpha\sin(F+\Delta_0)+\sin\left(\frac{\Delta_0}{\mathcal{N}}\right)$
L_0	$\frac{L_{\mathrm{J}0}}{\cos(\Delta_0)}$	$\frac{L_{\mathrm{J}0}}{\frac{L_{\mathrm{J}0}}{L}+\cos(\Delta_0)}$	$\frac{L_{\mathrm{J}0}}{\alpha\cos(F+\Delta_0)+\frac{1}{\mathcal{N}}\cos\left(\frac{\Delta_0}{\mathcal{N}}\right)}$
c_3	$\tan(\Delta_0)$	$\frac{\sin(\Delta_0)}{\frac{L_{\mathrm{J}0}}{L}+\cos(\Delta_0)}$	$\frac{\alpha\sin(F+\Delta_0)+\frac{1}{\mathcal{N}^2}\sin\left(\frac{\Delta_0}{\mathcal{N}}\right)}{\alpha\cos(F+\Delta_0)+\frac{1}{\mathcal{N}}\cos\left(\frac{\Delta_0}{\mathcal{N}}\right)}$
c_4	$\frac{1}{2}$	$\frac{1}{2}\frac{\cos(\Delta_0)}{\frac{L_{\mathrm{J}0}}{L}+\cos(\Delta_0)}$	$\frac{1}{2}\frac{\alpha\cos(F+\Delta_0)+\frac{1}{\mathcal{N}^3}\cos\left(\frac{\Delta_0}{\mathcal{N}}\right)}{\alpha\cos(F+\Delta_0)+\frac{1}{\mathcal{N}}\cos\left(\frac{\Delta_0}{\mathcal{N}}\right)}$

CHAPTER 4

Three-wave mixing in the small frequency limit

In this chapter we will explore effects of three-wave mixing (3WM), its gain as well as other characteristics, in the limit where frequencies are well below the cutoff frequency where dispersion is small. We refer to this regime as the quasilinear regime. The process is induced by a nonzero 3WM coefficient c_3 and gets its name from two photons mixing into a third, hence involving three waves.

An advantage with 3WM is that the energy source for amplification, the pump, is placed outside the gain band, unlike four-wave mixing (4WM) [17], [40]. Another common characteristic for 3WM is the absence of Kerr effect, which makes phase match between pump, signal and idler inherently small. The absence of Kerr effect creates other problems though, as we will explore in this chapter. Throughout this chapter we will ignore effects of 4WM.

4.1 General mixing equations

In this section we will derive general expressions for the differential equations describing the 3WM processes in the quasilinear regime, which we will later use to predict gain and other 3WM characteristics. These equations are known as the propagation equations [9], or the coupled mode equations [39]. We will completely ignore effects of four-wave mixing for now. By doing so, the continuous wave equation (Equation (3.13)) now reads

$$\left[\frac{\partial^2}{\partial\tilde{t}^2} - \tilde{C}\frac{\partial^2}{\partial\tilde{t}^2}\frac{\partial^2}{\partial\tilde{x}^2} - \frac{\partial^2}{\partial\tilde{x}^2}\right]\phi = -c_3\frac{\partial\phi}{\partial\tilde{x}}\frac{\partial^2\phi}{\partial\tilde{x}^2}. \tag{4.1}$$

Furthermore, to solve the wave equation, we begin with the ansatz that the solutions are travelling-waves given by the form

$$\phi = \sum_m \phi_m = \frac{1}{2}\sum_m A_m(\tilde{x})\mathrm{e}^{\mathrm{i}\left(\tilde{k}_m\tilde{x}-\tilde{\omega}_m\tilde{t}\right)} + \bar{A}_m(\tilde{x})\mathrm{e}^{-\mathrm{i}\left(\tilde{k}_m\tilde{x}-\tilde{\omega}_m\tilde{t}\right)} \tag{4.2}$$

where m is the index of each wave, the tilde-notation means units normalised as defined in the end of Section 3.2 and $\bar{A}_m$ is the complex conjugate of the amplitude A_m.

4.1.1 Simplifying the free wave part

The left-hand side of Equation (4.1) comes from propagation of free waves in a linear medium, as we know from Section 2.1. However, now that the right-hand side of the equation is not equal to zero, the derivatives of the amplitudes are not necessarily equal to zero either. We begin by calculating the derivatives for each ϕ_m,

$$\frac{\partial^2\phi_m}{\partial\tilde{t}^2} = -\tilde{\omega}_m^2\phi_m, \tag{4.3a}$$

$$\frac{\partial\phi_m}{\partial\tilde{x}} = \frac{1}{2}\left[\left(A_m' + \mathrm{i}\tilde{k}_m A_m\right)\mathrm{e}^{\mathrm{i}\left(\tilde{k}_m\tilde{x}-\tilde{\omega}_m\tilde{t}\right)} + \text{c.c.}\right], \tag{4.3b}$$

$$\frac{\partial^2\phi_m}{\partial\tilde{x}^2} = \frac{1}{2}\left[\left(A_m'' + 2\mathrm{i}\tilde{k}_m A_m' - \tilde{k}_m^2 A_m\right)\mathrm{e}^{\mathrm{i}\left(\tilde{k}_m\tilde{x}-\tilde{\omega}_m\tilde{t}\right)} + \text{c.c.}\right], \tag{4.3c}$$

$$\tilde{C}\frac{\partial^2}{\partial\tilde{t}^2}\frac{\partial^2\phi_m}{\partial\tilde{x}^2} = -\tilde{C}\tilde{\omega}_m^2\frac{\partial^2\phi_m}{\partial\tilde{x}^2}, \tag{4.3d}$$

where +c.c. refers to adding the complex conjugate of what was just written, and A_m' and A_m'' are the first and second derivatives with respect to $\tilde{x}$. Now we apply the slowly varying envelope approximation

$$\left|\frac{\partial^2 A_m}{\partial \tilde{x}^2}\right| \ll \left|\tilde{k}_m \frac{\partial A_m}{\partial \tilde{x}}\right| \tag{4.4}$$

to neglect the second derivative, and we can hence write the left-hand side of the equation for each wave m as

$$\begin{aligned} \mathrm{LHS}_m &\approx -\tilde{\omega}_m^2 \phi_m - \frac{1-\tilde{C}\tilde{\omega}_m^2}{2}\left[\left(2\mathrm{i}\tilde{k}_m A_m' - \tilde{k}_m^2 A_m\right)\mathrm{e}^{\mathrm{i}\left(\tilde{k}_m\tilde{x}-\tilde{\omega}_m\tilde{t}\right)} + \mathrm{c.c.}\right] \\ &= \left(-\tilde{\omega}_m^2 - \tilde{C}\tilde{\omega}_m^2\tilde{k}_m^2 + \tilde{k}_m^2\right)\phi_m \\ &+ \left[\mathrm{i}\tilde{k}_m\left(\tilde{C}\tilde{\omega}_m^2 - 1\right)A_m'\mathrm{e}^{\mathrm{i}\left(\tilde{k}_m\tilde{x}-\tilde{\omega}_m\tilde{t}\right)} + \mathrm{c.c.}\right]. \end{aligned} \tag{4.5}$$

Applying the continuous dispersion relation, recall Table 2.1, the first term equals zero. The second term can also be simplified using the continuous dispersion relation,

$$\mathrm{i}\tilde{k}_m\left(\tilde{C}\tilde{\omega}_m^2 - 1\right) = -\mathrm{i}\frac{\tilde{\omega}_m^2}{\tilde{k}_m}\frac{\tilde{k}_m^2}{\tilde{\omega}_m^2}\left(1-\tilde{C}\tilde{\omega}_m^2\right) = -\mathrm{i}\frac{\tilde{\omega}_m^2}{\tilde{k}_m} \tag{4.6}$$

To summarise, the left-hand side of the wave equation can be simplified to

$$\mathrm{LHS} = \sum_m -\mathrm{i}\frac{\tilde{\omega}_m^2}{\tilde{k}_m}\left(A_m'\mathrm{e}^{\mathrm{i}\left(\tilde{k}_m\tilde{x}-\tilde{\omega}_m\tilde{t}\right)} - \bar{A}_m'\mathrm{e}^{-\mathrm{i}\left(\tilde{k}_m\tilde{x}-\tilde{\omega}_m\tilde{t}\right)}\right). \tag{4.7}$$

4.1.2 Simplifying the mixing part

The right-hand side of Equation (4.1) is the part giving rise to the mixing between different waves and, potentially, gain. We have already calculated the derivatives that are on this side of the equation, recall Equations (4.3b) and (4.3c). However, on this side, the amplitudes without derivatives do not cancel and we can apply yet another approximation,

$$\left|\frac{\partial A_m}{\partial \tilde{x}}\right| \ll \left|\tilde{k}_m A_m\right|. \tag{4.8}$$

This allows us to approximate the derivatives as

$$\frac{\partial \phi_m}{\partial \tilde{x}} \approx \frac{\mathrm{i}}{2}\tilde{k}_m \left(A_m \mathrm{e}^{\mathrm{i}\left(\tilde{k}_m\tilde{x}-\tilde{\omega}_m\tilde{t}\right)} - \bar{A}_m \mathrm{e}^{-\mathrm{i}\left(\tilde{k}_m\tilde{x}-\tilde{\omega}_m\tilde{t}\right)} \right), \tag{4.9a}$$

$$\frac{\partial^2 \phi_m}{\partial \tilde{x}^2} \approx -\frac{1}{2}\tilde{k}_m^2 \left(A_m \mathrm{e}^{\mathrm{i}\left(\tilde{k}_m\tilde{x}-\tilde{\omega}_m\tilde{t}\right)} + \bar{A}_m \mathrm{e}^{-\mathrm{i}\left(\tilde{k}_m\tilde{x}-\tilde{\omega}_m\tilde{t}\right)} \right). \tag{4.9b}$$

The full expression of the right-hand side of the wave equation is

$$\mathrm{RHS} = -c_3 \left(\sum_m \frac{\partial \phi_m}{\partial \tilde{x}} \right) \left(\sum_m \frac{\partial^2 \phi_m}{\partial \tilde{x}^2} \right), \tag{4.10}$$

which, given that the total number of waves is M, is an expression with $4M^2$ terms and will be hard to fit on this page, and even harder to analyse completely. However, not all terms are equally important. Given that we study wave m, only some of the terms will be resonant with this wave. In other words, we only care about the terms that have the frequency $\tilde{\omega}_m$ in the exponent, and neglect the rest.

Assume we have the three waves m, n, q, and that the frequencies have the relationship $\tilde{\omega}_m = \tilde{\omega}_n - \tilde{\omega}_q$, *i.e.* a down-conversion process. Then there are two terms in the right-hand side that will be resonant with m: one from $\phi_n' \cdot \phi_q''$, and the one from $\phi_q' \cdot \phi_n''$. The resulting terms are hence

$$\frac{\mathrm{i}}{2}\tilde{k}_n A_n \mathrm{e}^{\mathrm{i}\left(\tilde{k}_n\tilde{x}-\tilde{\omega}_n\tilde{t}\right)} \cdot \left(-\frac{1}{2}\tilde{k}_q^2\right) \bar{A}_q \mathrm{e}^{-\mathrm{i}\left(\tilde{k}_q\tilde{x}-\tilde{\omega}_q\tilde{t}\right)} = -\frac{\mathrm{i}}{4}\tilde{k}_n\tilde{k}_q^2 A_n \bar{A}_q \mathrm{e}^{\mathrm{i}\left(\left(\tilde{k}_n-\tilde{k}_q\right)\tilde{x}-\tilde{\omega}_m\tilde{t}\right)}$$

and

$$-\frac{\mathrm{i}}{2}\tilde{k}_q \bar{A}_q \mathrm{e}^{-\mathrm{i}\left(\tilde{k}_q\tilde{x}-\tilde{\omega}_q\tilde{t}\right)} \cdot \left(-\frac{1}{2}\tilde{k}_n^2\right) A_n \mathrm{e}^{\mathrm{i}\left(\tilde{k}_n\tilde{x}-\tilde{\omega}_n\tilde{t}\right)} = \frac{\mathrm{i}}{4}\tilde{k}_n^2\tilde{k}_q A_n \bar{A}_q \mathrm{e}^{\mathrm{i}\left(\left(\tilde{k}_n-\tilde{k}_q\right)\tilde{x}-\tilde{\omega}_m\tilde{t}\right)}.$$

Note the difference of the sign for the latter. If the relationship is instead $\tilde{\omega}_m = \tilde{\omega}_n + \tilde{\omega}_q$, *i.e.* an up-conversion process, the terms become

$$\frac{\mathrm{i}}{2}\tilde{k}_n A_n \mathrm{e}^{\mathrm{i}\left(\tilde{k}_n\tilde{x}-\tilde{\omega}_n\tilde{t}\right)} \cdot \left(-\frac{1}{2}\tilde{k}_q^2\right) A_q \mathrm{e}^{\mathrm{i}\left(\tilde{k}_q\tilde{x}-\tilde{\omega}_q\tilde{t}\right)} = -\frac{\mathrm{i}}{4}\tilde{k}_n\tilde{k}_q^2 A_n A_q \mathrm{e}^{\mathrm{i}\left(\left(\tilde{k}_n+\tilde{k}_q\right)\tilde{x}-\tilde{\omega}_m\tilde{t}\right)}$$

and

$$\frac{\mathrm{i}}{2}\tilde{k}_q A_q \mathrm{e}^{\mathrm{i}\left(\tilde{k}_q\tilde{x}-\tilde{\omega}_q\tilde{t}\right)} \cdot \left(-\frac{1}{2}\tilde{k}_n^2\right) A_n \mathrm{e}^{\mathrm{i}\left(\tilde{k}_n\tilde{x}-\tilde{\omega}_n\tilde{t}\right)} = -\frac{\mathrm{i}}{4}\tilde{k}_n^2\tilde{k}_q A_n A_q \mathrm{e}^{\mathrm{i}\left(\left(\tilde{k}_n+\tilde{k}_q\right)\tilde{x}-\tilde{\omega}_m\tilde{t}\right)}.$$

The last case is for addition with degeneracy, *i.e.* when $\tilde{\omega}_m = 2\tilde{\omega}_n$. Then there will only be one term, given by

$$\frac{\mathrm{i}}{2}\tilde{k}_n A_n \mathrm{e}^{\mathrm{i}\left(\tilde{k}_n\tilde{x}-\tilde{\omega}_n\tilde{t}\right)} \cdot \left(-\frac{1}{2}\tilde{k}_n^2\right) A_n \mathrm{e}^{\mathrm{i}\left(\tilde{k}_n\tilde{x}-\tilde{\omega}_n\tilde{t}\right)} = -\frac{\mathrm{i}}{4}\tilde{k}_n^3 A_n^2 \mathrm{e}^{\mathrm{i}\left(2\tilde{k}_n\tilde{x}-\tilde{\omega}_m\tilde{t}\right)}. \tag{4.11}$$

4.1.3 Constructing the propagation equations

Now that we have simplified both sides of Equation (4.1), we can construct the differential equations describing wave propagation, *i.e.* the propagation equations. On the left-hand side of the wave equation, each amplitude derivative A_m' has the prefactor $-\mathrm{i}\frac{\tilde{\omega}_m^2}{\tilde{k}_m}$ and on the right hand-side each term has the prefactor $\mp c_3\frac{\mathrm{i}}{4}$. Solving for A_m', the prefactors on the right-hand side hence become $\pm\frac{c_3}{4}\frac{\tilde{k}_m}{\tilde{\omega}_m^2}$. When solving for A_m' the time dependence will disappear, since we have only kept the resonant terms. The propagation equation for each wave m hence becomes

$$\begin{aligned} A_m' = &\sum_{n,q:\ \tilde{\omega}_m=\tilde{\omega}_n-\tilde{\omega}_q} \frac{c_3}{4}\frac{\tilde{k}_n\tilde{k}_q\tilde{k}_m\left(\tilde{k}_n-\tilde{k}_q\right)}{\tilde{\omega}_m^2} A_n\bar{A}_q \mathrm{e}^{\mathrm{i}\left(\tilde{k}_n-\tilde{k}_q-\tilde{k}_m\right)\tilde{x}} \\ -\frac{1}{2}&\sum_{n,q:\ \tilde{\omega}_m=\tilde{\omega}_n+\tilde{\omega}_q} \frac{c_3}{4}\frac{\tilde{k}_n\tilde{k}_q\tilde{k}_m\left(\tilde{k}_n+\tilde{k}_q\right)}{\tilde{\omega}_m^2} A_n A_q \mathrm{e}^{-\mathrm{i}\left(\tilde{k}_m-\tilde{k}_n-\tilde{k}_q\right)\tilde{x}}. \end{aligned} \tag{4.12}$$

The factor $\frac{1}{2}$ adjusts for the degeneracy problem raised in Equation (4.11), since for every $a \neq b$ there will be two terms in the sum for $(n,q) = (a,b)$ and $(n,q) = (b,a)$, while for every $a = b$, there will only be term $(n,q) = (a,a)$. Since we are working in the long wave limit, we can simplify this expression by approximating wave vectors in coefficients with linear dispersion, *i.e.* $\tilde{k} \approx \tilde{\omega}$. However, we do not use this approximation, yet, for the phase mismatches, as they would then be equal to zero. The propagation equation for wave m now becomes

$$\begin{aligned} A_m' \approx &\sum_{n,q:\ \tilde{\omega}_m=\tilde{\omega}_n-\tilde{\omega}_q} \frac{c_3}{4}\tilde{\omega}_n\tilde{\omega}_q A_n\bar{A}_q \mathrm{e}^{\mathrm{i}\left(\tilde{k}_n-\tilde{k}_q-\tilde{k}_m\right)\tilde{x}} \\ -\frac{1}{2}&\sum_{n,q:\ \tilde{\omega}_m=\tilde{\omega}_n+\tilde{\omega}_q} \frac{c_3}{4}\tilde{\omega}_n\tilde{\omega}_q A_n A_q \mathrm{e}^{-\mathrm{i}\left(\tilde{k}_m-\tilde{k}_n-\tilde{k}_q\right)\tilde{x}}. \end{aligned} \tag{4.13}$$

4.2 The single idler model

In this section we will go through how to solve the propagation equations for three waves: the pump, which serves as the energy source, the signal, which is what we want to amplify, and the idler, a necessary third wave that is generated by the mixing process. This case is a highly idealised scenario, which we will later show is not particularly accurate, but it still serves as a benchmark showing what 3WM is capable of, if the necessary requirements are fulfilled.

4.2.1 The propagation equations

To begin let us assume we have three waves, the pump 'p', the signal 's' fulfilling $\tilde{\omega}_\mathrm{s} < \tilde{\omega}_\mathrm{p}$ and the idler 'i' given by $\tilde{\omega}_\mathrm{i} = \tilde{\omega}_\mathrm{p} - \tilde{\omega}_\mathrm{s}$. The full propagation equations, using the form in Equation (4.12), for these three waves are

$$A'_\mathrm{p} = -\frac{c_3}{4}\frac{\tilde{k}_\mathrm{p}\tilde{k}_\mathrm{s}\tilde{k}_\mathrm{i}\left(\tilde{k}_\mathrm{s}+\tilde{k}_\mathrm{i}\right)}{\tilde{\omega}_\mathrm{p}^2}A_\mathrm{s}A_\mathrm{i}\mathrm{e}^{-\mathrm{i}\left(\tilde{k}_\mathrm{p}-\tilde{k}_\mathrm{s}-\tilde{k}_\mathrm{i}\right)\tilde{x}}, \tag{4.14a}$$

$$A'_\mathrm{s} = \frac{c_3}{4}\frac{\tilde{k}_\mathrm{p}\tilde{k}_\mathrm{s}\tilde{k}_\mathrm{i}\left(\tilde{k}_\mathrm{p}-\tilde{k}_\mathrm{i}\right)}{\tilde{\omega}_\mathrm{s}^2}A_\mathrm{p}\bar{A}_\mathrm{i}\mathrm{e}^{\mathrm{i}\left(\tilde{k}_\mathrm{p}-\tilde{k}_\mathrm{s}-\tilde{k}_\mathrm{i}\right)\tilde{x}}, \tag{4.14b}$$

$$A'_\mathrm{i} = \frac{c_3}{4}\frac{\tilde{k}_\mathrm{p}\tilde{k}_\mathrm{s}\tilde{k}_\mathrm{i}\left(\tilde{k}_\mathrm{p}-\tilde{k}_\mathrm{s}\right)}{\tilde{\omega}_\mathrm{i}^2}A_\mathrm{p}\bar{A}_\mathrm{s}\mathrm{e}^{\mathrm{i}\left(\tilde{k}_\mathrm{p}-\tilde{k}_\mathrm{s}-\tilde{k}_\mathrm{i}\right)\tilde{x}}. \tag{4.14c}$$

Now using the simplification step as in Equation (4.13), the equations become

$$A'_\mathrm{p} = -\frac{c_3}{4}\tilde{\omega}_\mathrm{s}\tilde{\omega}_\mathrm{i}A_\mathrm{s}A_\mathrm{i}\mathrm{e}^{-\mathrm{i}\left(\tilde{k}_\mathrm{p}-\tilde{k}_\mathrm{s}-\tilde{k}_\mathrm{i}\right)\tilde{x}}, \tag{4.15a}$$

$$A'_\mathrm{s} = \frac{c_3}{4}\tilde{\omega}_\mathrm{p}\tilde{\omega}_\mathrm{i}A_\mathrm{p}\bar{A}_\mathrm{i}\mathrm{e}^{\mathrm{i}\left(\tilde{k}_\mathrm{p}-\tilde{k}_\mathrm{s}-\tilde{k}_\mathrm{i}\right)\tilde{x}}, \tag{4.15b}$$

$$A'_\mathrm{i} = \frac{c_3}{4}\tilde{\omega}_\mathrm{p}\tilde{\omega}_\mathrm{s}A_\mathrm{p}\bar{A}_\mathrm{s}\mathrm{e}^{\mathrm{i}\left(\tilde{k}_\mathrm{p}-\tilde{k}_\mathrm{s}-\tilde{k}_\mathrm{i}\right)\tilde{x}}. \tag{4.15c}$$

Now let us define the phase mismatch $\Delta\tilde{k} = \tilde{k}_\mathrm{p} - \tilde{k}_\mathrm{s} - \tilde{k}_\mathrm{i}$ and the pumping strength $\chi = \frac{1}{4}c_3\tilde{\omega}_\mathrm{p}A_\mathrm{p}$. Let us also assume that the signal and idler amplitudes are much smaller than the pump amplitude, $A_\mathrm{s}, A_\mathrm{i} \ll A_\mathrm{p}$, which makes the pump equation $A'_\mathrm{p} = 0$, *i.e.* a constant pump, also known as the *stiff pump* *approximation.* Then we get the equations

$$A_{\mathrm{s}}' = \chi\tilde{\omega}_{\mathrm{i}}\bar{A}_{\mathrm{i}}\mathrm{e}^{\mathrm{i}\Delta\tilde{k}\tilde{x}}, \tag{4.16a}$$

$$A_{\mathrm{i}}' = \chi\tilde{\omega}_{\mathrm{s}}\bar{A}_{\mathrm{s}}\mathrm{e}^{\mathrm{i}\Delta\tilde{k}\tilde{x}}. \tag{4.16b}$$

4.2.2 Solving the propagation equations

To solve these differential equations, we begin with the transformation

$$A_{\mathrm{s}} = B_{\mathrm{s}}\mathrm{e}^{\mathrm{i}\frac{\Delta\tilde{k}}{2}\tilde{x}}, \tag{4.17a}$$

$$A_{\mathrm{i}} = \bar{B}_{\mathrm{i}}\mathrm{e}^{\mathrm{i}\frac{\Delta\tilde{k}}{2}\tilde{x}}. \tag{4.17b}$$

Then we get the equations

$$B_{\mathrm{s}}' = -\mathrm{i}\frac{\Delta\tilde{k}}{2}B_{\mathrm{s}} + \chi\tilde{\omega}_{\mathrm{i}}B_{\mathrm{i}}, \tag{4.18a}$$

$$B_{\mathrm{i}}' = \mathrm{i}\frac{\Delta\tilde{k}}{2}B_{\mathrm{i}} + \bar{\chi}\tilde{\omega}_{\mathrm{s}}B_{\mathrm{s}}, \tag{4.18b}$$

which we can write on the form

$$\begin{bmatrix} B_{\mathrm{s}}' \\ B_{\mathrm{i}}' \end{bmatrix} = \underbrace{\begin{bmatrix} -\mathrm{i}\frac{\Delta\tilde{k}}{2} & \chi\tilde{\omega}_{\mathrm{i}} \\ \bar{\chi}\tilde{\omega}_{\mathrm{s}} & \mathrm{i}\frac{\Delta\tilde{k}}{2} \end{bmatrix}}_{\mathcal{M}} \begin{bmatrix} B_{\mathrm{s}} \\ B_{\mathrm{i}} \end{bmatrix}. \tag{4.19}$$

A system of differential equations of this form can be solved by finding the eigenvalues to the coefficient matrix $\mathcal{M}$. The eigenvalues are $\pm g$ where

$$g = \sqrt{\tilde{\omega}_{\mathrm{s}}\tilde{\omega}_{\mathrm{i}}\left|\chi\right|^2 - \left(\frac{\Delta\tilde{k}}{2}\right)^2}, \tag{4.20}$$

and the corresponding eigenvectors

$$\vec{v}_{\pm} = \begin{bmatrix} \tilde{\omega}_{\mathrm{i}}\chi \\ \mathrm{i}\frac{\Delta\tilde{k}}{2} \pm g \end{bmatrix}. \tag{4.21}$$

The general solution can hence be written as

$$\begin{bmatrix} B_\mathrm{s} \\ B_\mathrm{i} \end{bmatrix} = b_1 \mathrm{e}^{g\tilde{x}} \begin{bmatrix} \tilde{\omega}_\mathrm{i}\chi \\ \mathrm{i}\frac{\Delta\tilde{k}}{2} + g \end{bmatrix} + b_2 \mathrm{e}^{-g\tilde{x}} \begin{bmatrix} \tilde{\omega}_\mathrm{i}\chi \\ \mathrm{i}\frac{\Delta\tilde{k}}{2} - g \end{bmatrix}. \tag{4.22}$$

Using the boundary conditions $B_\mathrm{s}(0) = B_\mathrm{s0}, B_\mathrm{i}(0) = B_\mathrm{i0}$, we can solve for the constants b_1, b_2 and, after working out a lot of algebra, we reach the explicit solution,

$$B_\mathrm{s}(\tilde{x}) = B_\mathrm{s0}\left(\cosh(g\tilde{x}) - \frac{\mathrm{i}\Delta\tilde{k}}{2g}\sinh(g\tilde{x})\right) + \frac{\tilde{\omega}_\mathrm{i}\chi}{g} B_\mathrm{i0}\sinh(g\tilde{x}), \tag{4.23a}$$

$$B_\mathrm{i}(\tilde{x}) = B_\mathrm{i0}\left(\cosh(g\tilde{x}) + \frac{\mathrm{i}\Delta\tilde{k}}{2g}\sinh(g\tilde{x})\right) + \frac{\tilde{\omega}_\mathrm{s}\bar{\chi}}{g} B_\mathrm{s0}\sinh(g\tilde{x}), \tag{4.23b}$$

which, with the fact that $A_\mathrm{s0} = B_\mathrm{s0}, A_\mathrm{i0} = \bar{B}_\mathrm{i0}$, gives us the final solutions for $A_\mathrm{s}, A_\mathrm{i}$,

$$A_\mathrm{s}(\tilde{x}) = \left[A_\mathrm{s0}\left(\cosh(g\tilde{x}) - \frac{\mathrm{i}\Delta\tilde{k}}{2g}\sinh(g\tilde{x})\right) + \frac{\tilde{\omega}_\mathrm{i}\chi}{g} A_\mathrm{i0}\sinh(g\tilde{x})\right]\mathrm{e}^{\mathrm{i}\Delta\tilde{k}\tilde{x}/2}, \tag{4.24a}$$

$$A_\mathrm{i}(\tilde{x}) = \left[A_\mathrm{i0}\left(\cosh(g\tilde{x}) - \frac{\mathrm{i}\Delta\tilde{k}}{2g}\sinh(g\tilde{x})\right) + \frac{\tilde{\omega}_\mathrm{s}\chi}{g} A_\mathrm{s0}\sinh(g\tilde{x})\right]\mathrm{e}^{\mathrm{i}\Delta\tilde{k}\tilde{x}/2}. \tag{4.24b}$$

To get the gain we assume zero initial idler, $A_\mathrm{i0} = 0$, in Equation (4.24a) and we get that the power gain G is given by

$$G := \left|\frac{A_\mathrm{s}(\tilde{x})}{A_\mathrm{s0}}\right|^2 = \cosh^2(g\tilde{x}) + \frac{\Delta\tilde{k}^2}{4g^2}\sinh^2(g\tilde{x}). \tag{4.25}$$

4.2.3 Analysis in the purely linear dispersion regime

The purely linear regime is the regime where the dispersion relation is linear. In this regime the phase mismatch is zero ($\Delta\tilde{k} \approx 0$), or more accurately, negligibly small. Then we get that

$$G = \cosh^2(g\tilde{x}), \quad \text{and} \quad g = \chi\sqrt{\tilde{\omega}_\mathrm{s}\tilde{\omega}_\mathrm{i}}. \tag{4.26}$$

In other words, we obtain exponential growth of the signal set by the gain coefficient g. By expressing the frequencies as

$$\tilde{\omega}_{\mathrm{s}} = \frac{1+\delta}{2}\tilde{\omega}_{\mathrm{p}}, \quad \tilde{\omega}_{\mathrm{i}} = \frac{1-\delta}{2}\tilde{\omega}_{\mathrm{p}}, \quad \delta = \frac{\tilde{\omega}_{\mathrm{s}} - \tilde{\omega}_{\mathrm{p}}/2}{\tilde{\omega}_{\mathrm{p}}/2} \in (-1,1), \tag{4.27}$$

where δ is the signal detuning from half of the pump frequency, we can express the gain coefficient as

$$g = \chi\sqrt{\frac{1+\delta}{2}\frac{1-\delta}{2}\tilde{\omega}_{\mathrm{p}}^{2}} = \frac{\chi\tilde{\omega}_{\mathrm{p}}}{2}\sqrt{1-\delta^{2}}. \tag{4.28}$$

The gain coefficient has the shape of a semicircle with radius $\frac{1}{2}\chi\tilde{\omega}_{\mathrm{p}}$ and its maximum at $\delta = 0$, *i.e.* when the signal frequency is equal to half of the pump frequency.

4.2.4 Analysis of critical pumping strength and pump frequency

It is clear from Equation (4.28) that the larger the pump frequency is, the larger the gain coefficient becomes. However, if we increase the pump frequency enough, we will no longer be in the purely linear regime and the phase mismatch can no longer be neglected. Let us recall the definition of the gain coefficient with phase mismatch, Equation (4.20), and we see that when the phase mismatch $\Delta\tilde{k}$ is too large $\left(\Delta\tilde{k} > \chi\tilde{\omega}_{\mathrm{p}}\left(1-\delta^{2}\right)\right)$, the gain coefficient will become imaginary. Then exponential gain will be replaced by a transmission that oscillates along the TWPA, *i.e.* oscillatory gain. This leads to the question: How large can the pump frequency become, without the phase mismatch becoming too large?

To be able to analyse larger frequencies, but still small with respect to the cutoff frequency, we go to the quasilinear regime, where we can assume linear dispersion for wave vectors except for the phase mismatch, where we instead need to use the lowest order nonzero approximation. This will be a cubic approximation, recall Equation (2.16). The phase mismatch is then approximated as

$$\begin{aligned}\Delta\tilde{k} &\approx b\tilde{\omega}_\mathrm{p}^3 - b\tilde{\omega}_\mathrm{s}^3 - b\tilde{\omega}_\mathrm{i}^3 \\ &= b\tilde{\omega}_\mathrm{p}^3\left(1 - \left(\frac{1+\delta}{2}\right)^3 - \left(\frac{1-\delta}{2}\right)^3\right) \\ &= \frac{3}{4}b\tilde{\omega}_\mathrm{p}^3\left(1-\delta^2\right)\end{aligned} \tag{4.29}$$

where b is the cubic coefficient in Equation (2.16). The crossover between exponential gain and oscillatory gain happens when the gain coefficient is zero. Solving Equation (4.20) for $g = 0$, and using Equation (4.29) to approximate the phase mismatch, we get that the critical pumping strength χ_c is given by

$$\begin{aligned}\frac{\chi_\mathrm{c}^2\tilde{\omega}_\mathrm{p}^2}{4} &= \frac{1}{4}\frac{9}{16}b^2\tilde{\omega}_\mathrm{p}^6\left(1-\delta^2\right)^2, \\ \chi_\mathrm{c}^2 &= \frac{9}{16}b^2\tilde{\omega}_\mathrm{p}^4\left(1-\delta^2\right)^2, \\ \chi_\mathrm{c} &= \frac{3}{4}b\tilde{\omega}_\mathrm{p}^2\left(1-\delta^2\right).\end{aligned} \tag{4.30}$$

As expected, the critical strength goes to zero for very small pump frequencies. Also note that it varies with detuning δ and is maximum at zero detuning. In other words, for large enough pumping strengths there will be exponential gain in the full band. For small enough pumping strengths there will not be exponential gain anywhere in the band and for pumping strengths in between there is exponential gain at the edges of the band, but not in the centre.

We can also solve for the critical pump frequency, *i.e.* the pump frequency, given a pumping strength χ, where the crossover between exponential gain and oscillatory takes place. We simply solve Equation (4.30) for $\tilde{\omega}_\mathrm{p}$ and we get

$$\tilde{\omega}_\mathrm{p,c} = \frac{4\chi}{3b}\frac{1}{1-\delta^2}. \tag{4.31}$$

4.2.5 Analysis of optimal pump frequency

Above we solved for when the gain coefficient goes to zero, *i.e.* when exponential gain is eliminated. Another interesting question is when the gain coefficient has its maximum value. To find this, we differentiate the gain coefficient with respect to the pump frequency and set the derivative to zero,

$$\begin{aligned}\frac{\mathrm{d}}{\mathrm{d}\tilde{\omega}_\mathrm{p}}4g^2 &\approx \frac{\mathrm{d}}{\mathrm{d}\tilde{\omega}_\mathrm{p}}\left(\chi^2\left(1-\delta^2\right)\cdot\tilde{\omega}_\mathrm{p}^2-\frac{9}{16}b^2\left(1-\delta^2\right)^2\cdot\tilde{\omega}_\mathrm{p}^6\right)\\ &=2\chi^2\left(1-\delta^2\right)\cdot\tilde{\omega}_\mathrm{p}-\frac{54}{16}b^2\left(1-\delta^2\right)^2\cdot\tilde{\omega}_\mathrm{p}^5=0 \qquad (4.32)\\ \implies \tilde{\omega}_\mathrm{p,opt}^4&=\frac{16\chi^2}{27b^2}\frac{1}{1-\delta^2}.\end{aligned}$$

This frequency, the optimal pump frequency, is shown in Figure 4.1 for zero detuning together with the critical pump frequency, the gain coefficient using the full expressions (Equations (4.15b) and (4.15c)) and the gain coefficient using the simplified expressions (Equations (4.16a) and (4.16b)). We could also plot the gain coefficient as a function of detuning now, but we will wait with that until we have developed the general model in Section 4.5, see Figure 4.15.

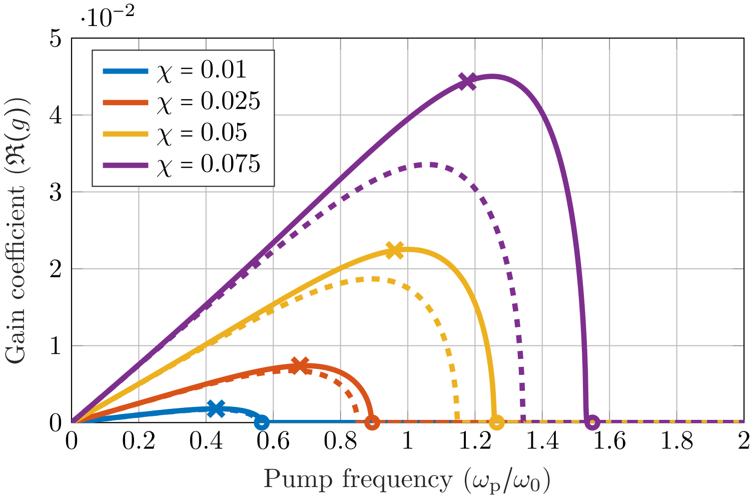

Figure 4.1: The real part of the gain coefficient $\Re(g)$ at $\delta = 0$ and $\tilde{C} = 0$ for the 3WM single idler model, using the full expression (solid) as defined in Equation (4.12), linear coupling coefficients approximation (dashed) as defined in Equation (4.13), critical pump frequency (circle) and approximated optimal pump frequency (cross), for different values of χ.

Note that the derived optimal pump frequency in Figure 4.1 is slightly below the actual optimal pump frequency, especially for large pumping strengths. This is not surprising, since we used the cubic approximation of the dispersion in order to find it, an approximation that only holds for small frequencies. It is worth pointing out that we should not pay too much attention to the gain coefficient at large frequencies, since the propagation equations used to derive it also used the small frequency assumption. In other words, the equations are not valid for too large frequencies.

4.3 Signal and idler up-conversion for purely linear dispersion

In Section 4.2 we studied 3WM when the only waves present were pump, signal and idler. In this section we will study what happens if we also include up-converted modes of signal and idler, but ignore up-conversion of the pump. We will study this case for purely linear dispersion, as this will result in linear differential equations.

The argument for ignoring up-conversion of the pump is that it will reduce the pump amplitude, which can be taken into consideration by using a smaller value for the pump amplitude. The argument for studying effects in the purely linear regime is that we can design the TWPA to have a much larger ω_0 than signal and idler frequencies, up to some number of up-converted modes, which would put all waves in the purely linear regime.

We remark that neither of these two assumptions are particularly accurate. Up-conversion of the pump does not only reduce the pump amplitude, but also allows up-converted modes of the signal and the idler to be amplified as the pump harmonics can act as a pump for these modes. As for the purely linear regime, it turns out that all waves will continue to up-convert until there are modes outside the purely linear regime, so it will never be a valid approximation.

In this section we will study this scenario anyways, since the realisation that the assumptions were not accurate partly come from the analysis done in this chapter. However, the less interested reader can jump to either Section 4.4, where we thoroughly investigate the relations between phase mismatch and up-conversion, or to Section 4.5, where we develop the final, generalised, model for 3WM.

4.3.1 The propagation equations

To begin with, let us assume we have M modes of the signal and the idler whose frequencies we denote $\tilde{\omega}_{\mathrm{s}+m\mathrm{p}} = \tilde{\omega}_{\mathrm{s}} + m\tilde{\omega}_{\mathrm{p}}$ and $\tilde{\omega}_{\mathrm{i}+m\mathrm{p}} = \tilde{\omega}_{\mathrm{i}} + m\tilde{\omega}_{\mathrm{p}}$, $m \in [0, M-1] \cap \mathbb{N}$, and their wave vectors similarly. All of these waves, signal, idler and their up-converted modes, are small in amplitude, the pump is hence the only wave that can induce mixing processes. The propagation equations, using the simplified version in Equation (4.13), are thus for the signal

$$A'_{\mathrm{s}} = \frac{c_3}{4}\left(\tilde{\omega}_{\mathrm{p}}\tilde{\omega}_{\mathrm{i}}A_{\mathrm{p}}\bar{A}_{\mathrm{i}}\mathrm{e}^{\mathrm{i}(\tilde{k}_{\mathrm{p}}-\tilde{k}_{\mathrm{s}}-\tilde{k}_{\mathrm{i}})\tilde{x}} + \tilde{\omega}_{\mathrm{s+p}}\tilde{\omega}_{\mathrm{p}}A_{\mathrm{s+p}}\bar{A}_{\mathrm{p}}\mathrm{e}^{\mathrm{i}(\tilde{k}_{\mathrm{s+p}}-\tilde{k}_{\mathrm{p}}-\tilde{k}_{\mathrm{s}})\tilde{x}}\right), \tag{4.33a}$$

for each $m \in [2, M-2] \cap \mathbb{N}$

$$\begin{aligned} A'_{\mathrm{s}+m\mathrm{p}} = \frac{c_3}{4}\Bigg(&\tilde{\omega}_{\mathrm{s}+(m+1)\mathrm{p}}\tilde{\omega}_{\mathrm{p}}A_{\mathrm{s}+(m+1)\mathrm{p}}\bar{A}_{\mathrm{p}}\mathrm{e}^{\mathrm{i}\left(\tilde{k}_{\mathrm{s}+(m+1)\mathrm{p}}-\tilde{k}_{\mathrm{s}+m\mathrm{p}}-\tilde{k}_{\mathrm{p}}\right)\tilde{x}} \\ &- \tilde{\omega}_{\mathrm{s}+(m-1)\mathrm{p}}\tilde{\omega}_{\mathrm{p}}A_{\mathrm{s}+(m-1)\mathrm{p}}A_{\mathrm{p}}\mathrm{e}^{-\mathrm{i}\left(\tilde{k}_{\mathrm{s}+m\mathrm{p}}-\tilde{k}_{\mathrm{s}+(m-1)\mathrm{p}}-\tilde{k}_{\mathrm{p}}\right)\tilde{x}}\Bigg), \end{aligned} \tag{4.33b}$$

and for the highest up-converted signal mode

$$A'_{\mathrm{s}+(M-1)\mathrm{p}} = -\frac{c_3}{4}\tilde{\omega}_{\mathrm{s}+(M-2)\mathrm{p}}\tilde{\omega}_{\mathrm{p}}A_{\mathrm{s}+(M-2)\mathrm{p}}A_{\mathrm{p}}\mathrm{e}^{-\mathrm{i}\left(\tilde{k}_{\mathrm{s}+(M-1)\mathrm{p}}-\tilde{k}_{\mathrm{s}+(M-2)\mathrm{p}}-\tilde{k}_{\mathrm{p}}\right)\tilde{x}}. \tag{4.33c}$$

The equations for the idler and its up-converted modes are given by replacing s↔i in the equations above. Now, if we reintroduce the pumping strength χ, assume a real valued pump amplitude, and assume that we are in the purely linear regime, these equations can be simplified to

$$A'_{\mathrm{s}} = \chi\left(\tilde{\omega}_{\mathrm{i}}\bar{A}_{\mathrm{i}} + \tilde{\omega}_{\mathrm{s+p}}A_{\mathrm{s+p}}\right), \tag{4.34a}$$

$$A'_{\mathrm{s}+m\mathrm{p}} = \chi\left(\tilde{\omega}_{\mathrm{s}+(m+1)\mathrm{p}}A_{\mathrm{s}+(m+1)\mathrm{p}} - \tilde{\omega}_{\mathrm{s}+(m-1)\mathrm{p}}A_{\mathrm{s}+(m-1)\mathrm{p}}\right), \tag{4.34b}$$

$$A'_{\mathrm{s}+(M-1)\mathrm{p}} = -\chi\tilde{\omega}_{\mathrm{s}+(M-2)\mathrm{p}}A_{\mathrm{s}+(M-2)\mathrm{p}}. \tag{4.34c}$$

Let us comment what these equations describe: For the signal, the first term is the same as in the single idler model, *i.e.* the gain-providing down-conversion term, while the second term describes up-conversion of the signal to the mode s+p. For the highest mode in this ansatz, s+$(M-1)$p, there is only one term which describes its down-conversion to the mode s+$(M-2)$p. For the modes $m \in [2, M-2] \cap \mathbb{N}$ between the signal and the highest mode there are two terms, one describing up-conversion to a higher mode and one describing down-conversion to a lower mode.

4.3.2 Two modes

Let us now look closer at Equation (4.34) for $M = 2$, *i.e.* when there are exactly 2 modes each of the signal and of the idler. Then the equations are

$$\begin{aligned} A'_{\mathrm{s}} &= \chi\left(\tilde{\omega}_{\mathrm{i}}\bar{A}_{\mathrm{i}} + \tilde{\omega}_{\mathrm{s+p}}A_{\mathrm{s+p}}\right), && (4.35\mathrm{a}) \\ A'_{\mathrm{i}} &= \chi\left(\tilde{\omega}_{\mathrm{s}}\bar{A}_{\mathrm{s}} + \tilde{\omega}_{\mathrm{i+p}}A_{\mathrm{i+p}}\right), && (4.35\mathrm{b}) \\ A'_{\mathrm{s+p}} &= -\chi\tilde{\omega}_{\mathrm{s}}A_{\mathrm{s}}, && (4.35\mathrm{c}) \\ A'_{\mathrm{i+p}} &= -\chi\tilde{\omega}_{\mathrm{i}}A_{\mathrm{i}}. && (4.35\mathrm{d}) \end{aligned}$$

By complex conjugating the idler mode equations, we can write these equations in a matrix form

$$\begin{bmatrix} A'_{\mathrm{s}} \\ \bar{A}'_{\mathrm{i}} \\ A'_{\mathrm{s+p}} \\ \bar{A}'_{\mathrm{i+p}} \end{bmatrix} = \begin{bmatrix} 0 & \chi\tilde{\omega}_{\mathrm{i}} & \chi\tilde{\omega}_{\mathrm{s+p}} & 0 \\ \bar{\chi}\tilde{\omega}_{\mathrm{s}} & 0 & 0 & \bar{\chi}\tilde{\omega}_{\mathrm{i+p}} \\ -\chi\tilde{\omega}_{\mathrm{s}} & 0 & 0 & 0 \\ 0 & -\bar{\chi}\tilde{\omega}_{\mathrm{i}} & 0 & 0 \end{bmatrix} \begin{bmatrix} A_{\mathrm{s}} \\ \bar{A}_{\mathrm{i}} \\ A_{\mathrm{s+p}} \\ \bar{A}_{\mathrm{i+p}} \end{bmatrix} \tag{4.36}$$

By assuming real-valued pumping strength and using the δ defined in Equation (4.27) to write the frequencies as

$$\begin{aligned} \tilde{\omega}_{\mathrm{s+p}} &= \left(1 + \frac{1+\delta}{2}\right)\tilde{\omega}_{\mathrm{p}} = \frac{3+\delta}{2}\tilde{\omega}_{\mathrm{p}}, && (4.37\mathrm{a}) \\ \tilde{\omega}_{\mathrm{i+p}} &= \left(1 + \frac{1-\delta}{2}\right)\tilde{\omega}_{\mathrm{p}} = \frac{3-\delta}{2}\tilde{\omega}_{\mathrm{p}}, && (4.37\mathrm{b}) \end{aligned}$$

we can write the propagation equations as

$$\begin{bmatrix} A'_{\mathrm{s}} \\ \bar{A}'_{\mathrm{i}} \\ A'_{\mathrm{s+p}} \\ \bar{A}'_{\mathrm{i+p}} \end{bmatrix} = \frac{\chi\tilde{\omega}_{\mathrm{p}}}{2} \begin{bmatrix} 0 & 1-\delta & 3+\delta & 0 \\ 1+\delta & 0 & 0 & 3-\delta \\ -1-\delta & 0 & 0 & 0 \\ 0 & -1+\delta & 0 & 0 \end{bmatrix} \begin{bmatrix} A_{\mathrm{s}} \\ \bar{A}_{\mathrm{i}} \\ A_{\mathrm{s+p}} \\ \bar{A}_{\mathrm{i+p}} \end{bmatrix} \tag{4.38}$$

Let us call this matrix *the propagation matrix.* Note that the value of the pump frequency on its own is not important, assuming it is small enough to be in the purely linear regime, but rather the product of χ and the pump frequency. The relevant measure of TWPA length is thus not simply the number of unit cells $\tilde{x}$, but the effective length $\frac{1}{2}\chi\tilde{\omega}_{\mathrm{p}}\tilde{x}$.

We can solve these equations numerically *e.g.* using the Runge-Kutta based numerical solver `ode45` in MATLAB. The numerically determined solution for the eigenvalue with the largest real part, effectively the gain coefficient, is shown in Figure 4.2.

As we can see, there are two major differences for $M = 1$ versus $M = 2$: i) The bandwidth for the gain coefficient is much smaller for $M = 2$, and ii) the gain coefficient for $M = 2$ is less than half of the gain coefficient of $M = 1$. If we look at gain versus length at zero detuning, see Figure 4.3, we see that not only is the gain less than half in dB, but it also contains oscillations which completely deplete the signal at certain lengths.

We can also solve the propagation equations analytically with the same method as used in Section 4.2, but it is quite tedious so we will skip it here. The analytical solution for transmission, or "gain", at zero detuning is given by

$$\begin{aligned} G = \Bigg(&\cosh\left(\frac{\chi\tilde{\omega}_\mathrm{p}}{4}\tilde{x}\right)\cos\left(\frac{\chi\tilde{\omega}_\mathrm{p}\sqrt{11}}{4}\tilde{x}\right) \\ &+ \frac{1}{\sqrt{11}}\sinh\left(\frac{\chi\tilde{\omega}_\mathrm{p}}{4}\tilde{x}\right)\sin\left(\frac{\chi\tilde{\omega}_\mathrm{p}\sqrt{11}}{4}\tilde{x}\right)\Bigg)^2, \end{aligned} \tag{4.39}$$

which grows indeed, as we observed from the numerical simulation, with half the exponential rate and with oscillations. We have also found the analytical expression for the reduced bandwidth, which is given by

$$|\delta| < \sqrt{\frac{\sqrt{5120} - 70}{10}} \approx 0.3942. \tag{4.40}$$

In other words, the bandwidth is about 39 % of the full bandwidth.

To understand this behaviour we turn to the eigenvalues of the propagation matrix, given in Equation (4.38), and compare with the corresponding propagation matrix for $M = 1$. The eigenvalues at zero detuning are

$$\lambda_\pm = \pm 1 \;\; (M = 1), \quad \lambda_{\pm,\pm} = \frac{\pm 1 \pm \mathrm{i}\sqrt{11}}{2} \;\; (M = 2). \tag{4.41}$$

Firstly, let us note that the real part of the eigenvalues for $M = 2$ is indeed half of the eigenvalues for $M = 1$, which is why it grows with half the exponential rate. Secondly, let us note that for $M = 2$ there is a nonzero imaginary part of the eigenvalues, which is what gives rise to the oscillations.

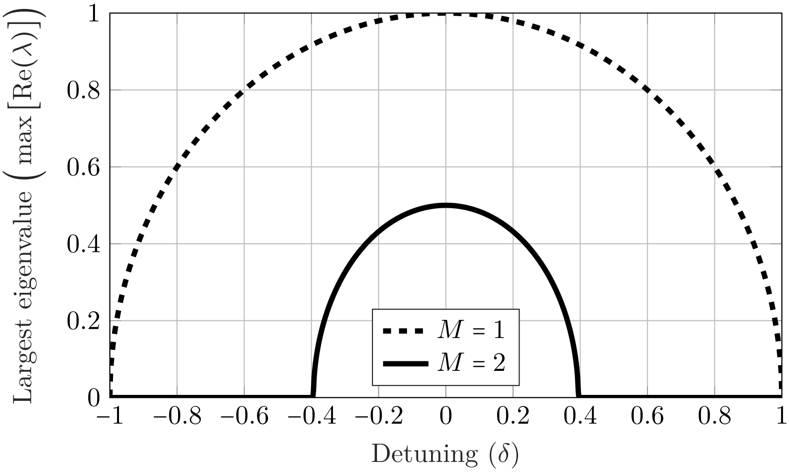

Figure 4.2: The largest real part of the gain coefficient for 3WM with $M = 2$, ignoring pump harmonics, compared with the largest gain coefficient using $M = 1$.

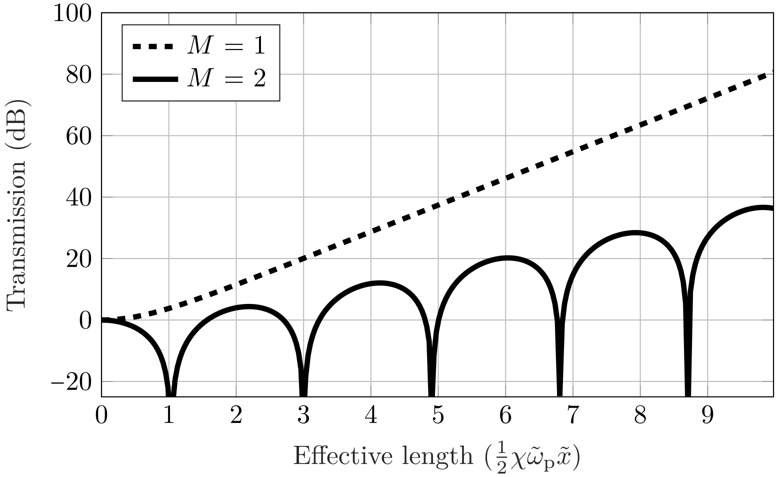

Figure 4.3: Transmission for 3WM with $M = 2$, ignoring pump harmonics, at zero detuning ($\delta = 0$), compared with equivalent simulation results using $M = 1$.

For increasing detuning, the real part of the eigenvalues decreases faster for $M = 2$ than for $M = 1$. When detuning is larger than the critical detuning in Equation (4.40), all the eigenvalues have become imaginary, which is why there are only oscillations without any gain.

In summary, for $M = 2$ in the purely linear regime, the exponential growth rate is less than or equal to half the exponential rate for $M = 1$, and the bandwidth is reduced to about 39 %.

4.3.3 Three modes

When going from $M = 1$ to $M = 2$, both gain and bandwidth were reduced. This brings up the question: will the gain and bandwidth reduce even further when we include even more up-converted modes? In this section we study what happens in the case of $M = 3$.

Using the same assumptions and simplifications as for $M = 2$ in the section above, we can write the propagation equations for $M = 3$ as

$$\begin{bmatrix} A'_{\mathrm{s}} \\ \bar{A}'_{\mathrm{i}} \\ A'_{\mathrm{s+p}} \\ \bar{A}'_{\mathrm{i+p}} \\ A'_{\mathrm{s+2p}} \\ \bar{A}'_{\mathrm{i+2p}} \end{bmatrix} = \frac{\chi\tilde{\omega}_{\mathrm{p}}}{2} \begin{bmatrix} 0 & 1-\delta & 3+\delta & 0 & 0 & 0 \\ 1+\delta & 0 & 0 & 3-\delta & 0 & 0 \\ -1-\delta & 0 & 0 & 0 & 5+\delta & 0 \\ 0 & -1+\delta & 0 & 0 & 0 & 5-\delta \\ 0 & 0 & -3-\delta & 0 & 0 & 0 \\ 0 & 0 & 0 & -3+\delta & 0 & 0 \end{bmatrix} \begin{bmatrix} A_{\mathrm{s}} \\ \bar{A}_{\mathrm{i}} \\ A_{\mathrm{s+p}} \\ \bar{A}_{\mathrm{i+p}} \\ A_{\mathrm{s+2p}} \\ \bar{A}_{\mathrm{i+2p}} \end{bmatrix}. \tag{4.42}$$

This matrix is hence the propagation matrix for $M = 3$. We solve these differential equations numerically, see Figures 4.4 and 4.5, and notice that not only do gain and bandwidth not get worse, but they are in fact improved.

To understand this behaviour, once again we turn to the eigenvalues of the propagation matrix at zero detuning. The analytical expressions for the eigenvalues are quite long so we will skip them here, but they can be approximated as

$$\lambda_{\pm} \approx \pm 0.84, \quad \lambda_{\pm,\pm} \approx \pm 0.08 \pm \mathrm{i} \cdot 4.23. \tag{4.43}$$

Four of them, the values of $\lambda_{\pm,\pm}$, are mostly imaginary and will hence contribute with oscillations. The interesting detail here is that two of them, the values of $\lambda_{\pm}$, are in fact *purely* real. This leads to pure exponential gain. When including detuning, there are always two purely real eigenvalues, which means that we now recover the full bandwidth.

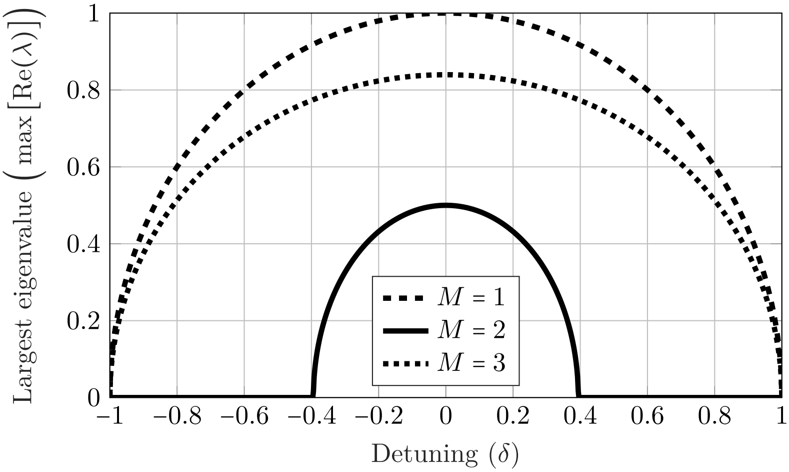

Figure 4.4: The largest real part of the gain coefficient for 3WM with $M = \{1, 2, 3\}$, ignoring pump harmonics.

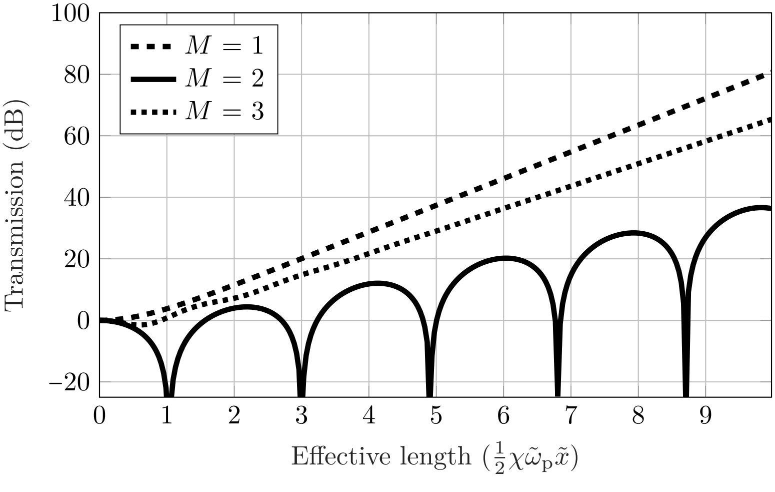

Figure 4.5: Transmission for 3WM for $M = \{1, 2, 3\}$, ignoring pump harmonics, at zero detuning ($\delta = 0$), compared with equivalent simulation results using $M = 1$.

In summary, for $M = 3$ in the purely linear regime, we get an exponential growth in the full band and the exponential growth rate is almost as large as for $M = 1$.

4.3.4 Multiple modes

So far we have not been able to conclude anything definite about the signal and idler up-conversion for purely linear dispersion, since the results have varied a lot for each added up-converted mode. Instead of adding one mode at the time and analyse the resulting behaviour, we now generalise the method for an arbitrary number of modes. If we are to be able to draw any conclusions of what happens in reality, the transmission must converge at some critical number of modes M_c. If it does not converge, which is indeed the case here, we can conclude that it is impossible to keep all signal and idler modes within the purely linear regime of the dispersion relation as they will keep up-converting until they reach a nonlinear dispersive regime.

Let us now develop this general model. Given a number of modes M, the propagation equations can be written as

$$\begin{bmatrix} A'_\mathrm{s} \\ \bar{A}'_\mathrm{i} \\ \vdots \\ A'_{\mathrm{s}+(M-1)\mathrm{p}} \\ \bar{A}'_{\mathrm{i}+(M-1)\mathrm{p}} \end{bmatrix} = \frac{\chi\tilde{\omega}_\mathrm{p}}{2}\mathcal{M} \begin{bmatrix} A_\mathrm{s} \\ \bar{A}_\mathrm{i} \\ \vdots \\ A_{\mathrm{s}+(M-1)\mathrm{p}} \\ \bar{A}_{\mathrm{i}+(M-1)\mathrm{p}} \end{bmatrix} \tag{4.44}$$

where $\mathcal{M}$ is the propagation matrix with size $[2M \times 2M]$ which has the values

$$\begin{aligned} \mathcal{M}_{1,2} &= 1 - \delta, & \mathcal{M}_{2,1} &= 1 + \delta, \\ \mathcal{M}_{2m-1,2m+1} &= 2m + 1 + \delta, & \mathcal{M}_{2m+1,2m-1} &= -2m + 1 - \delta, \\ \mathcal{M}_{2m,2m+2} &= 2m + 1 - \delta, & \mathcal{M}_{2m+2,2m} &= -2m + 1 + \delta \end{aligned} \tag{4.45}$$

for all $m \in [1, M-1] \cap \mathbb{N}$, and zeros in all other positions. The eigenvalues of this matrix determine the behaviour of the propagating waves. For purely real eigenvalues we get pure exponential gain, for purely imaginary eigenvalues we get oscillations, and for complex eigenvalues we get both oscillations and exponential gain.

We find the eigenvalues of $\mathcal{M}$ numerically for values up to $M = 10000$

and note that for large values of M, multiple eigenvalues are either purely imaginary, or have a small real part. These eigenvalues are less interesting as they mostly contribute with oscillations. However, for each value of M we solved, there are either 2 or 4 eigenvalues with a fairly large real part ($|\Re(\lambda)| > \frac{1}{4}$). Let us call these the "dominating eigenvalues". We notice that for each odd M there are 2 purely real dominating eigenvalues, while for each even M there are 4 complex dominating eigenvalues, see Figure 4.6.

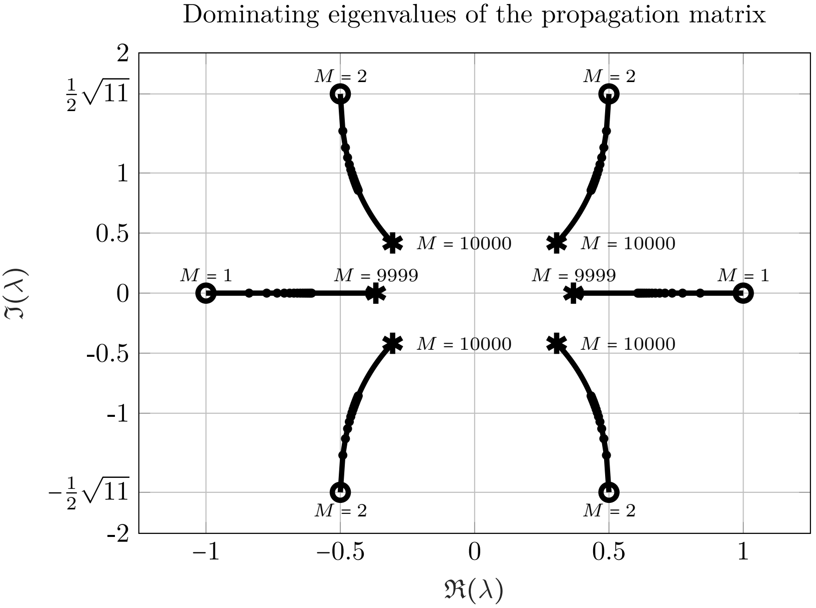

Figure 4.6: The dominating eigenvalues ($|\Re(\lambda)| > 0.25$) of the propagation matrix at zero detuning for multiple values of M, odd values from 1 to 9999 (horizontal lines) and even values from 2 to 10000 (bent lines). The lowest order solutions ($M = \{1, 2\}$) are shown with circles, the highest order solutions ($M = \{9999, 10000\}$) are shown with stars and the 30 second lowest order solutions ($M \in [3, 30] \cap \mathbb{N}$) are shown with dots.

As we can see in Figure 4.6, whether the dominating eigenvalues are purely real or complex depends fully on whether M is even or odd. Furthermore, we note that for at least up to 10000 modes (which is already highly unrealistic on its own), the solution has not converged. In other words, adding more up-converted modes will keep changing the behaviour of transmission of the signal.

From the analysis of the signal and idler up-conversion without pump harmonics in the purely linear regime done in this section, we conclude that it is impossible to keep all the modes in the purely linear regime. The reason is that the waves will keep generating modes of higher and higher frequencies until there are modes outside the purely linear regime of the dispersion relation. It is hence important to investigate the relation between up-conversion and dispersion, which we will do in the next section.

4.4 Single input study

In this section we will study what happens when there is only one input wave into the TWPA, especially in the quasilinear regime, *i.e.* where we use the linear dispersion approximation for the coupling coefficients but the cubic approximation for the phase mismatches, recall Section 3.2. This analysis will mostly be used to understand the propagation and up-conversion of the pump, but is equally applicable for the case of the signal.

In the first subsection we will write down the propagation equations for the single input case with an arbitrary number of harmonics M, and then in the second subsection we apply different simplifications to rescale these equations. Then in the next subsections we will first look closer at different fixed values of M, and then generalise to an arbitrary number of harmonics.

4.4.1 The propagation equations

When there is only one input it can only mix into harmonics of itself. If we assume its frequency is $\tilde{\omega}_1$, the mixing products are thus at the frequencies $\tilde{\omega}_m = m\tilde{\omega}_1$ for $m \in \mathbb{Z}_+$. Let us assume, as previously, that the number of harmonics is M. For each wave $m \in [1, M] \cap \mathbb{N}$, it can then either up-convert to any of the higher frequencies $n \in [m+1, M] \cap \mathbb{N}$, or down-convert into any of the lower frequencies $n \in [1, m-1] \cap \mathbb{N}$. The simplified propagation equations, recall Equation (4.13), are hence

$$\begin{aligned} A'_m = &\sum_{n=m+1}^{M} \frac{c_3}{4}\tilde{\omega}_n\tilde{\omega}_{n-m}A_n\bar{A}_{n-m}\mathrm{e}^{\mathrm{i}\left(\tilde{k}_n-\tilde{k}_m-\tilde{k}_{n-m}\right)\tilde{x}} \\ &-\frac{1}{2}\sum_{n=1}^{m-1}\frac{c_3}{4}\tilde{\omega}_n\tilde{\omega}_{m-n}A_nA_{m-n}\mathrm{e}^{-\mathrm{i}\left(\tilde{k}_m-\tilde{k}_n-\tilde{k}_{m-n}\right)\tilde{x}}. \end{aligned} \tag{4.46}$$

Using the simple relation between the frequencies we can write the frequency product as a number times $\tilde{\omega}_1^2$. Furthermore, instead of assuming zero phase mismatches which we now know is a bad approximation, we use the cubic approximation of the dispersion relation to approximate them,

$$\begin{aligned} \tilde{k}_n - \tilde{k}_m - \tilde{k}_{n-m} &\approx b\tilde{\omega}_n^3 - b\tilde{\omega}_m^3 - b\tilde{\omega}_{n-m}^3 \\ &= b\left(n\tilde{\omega}_1\right)^3 - b\left(m\tilde{\omega}_1\right)^3 - b\left((n-m)\tilde{\omega}_1\right)^3 \\ &= b\tilde{\omega}_1^3\left(n^3 - m^3 - (n-m)^3\right) \\ &= 3b\tilde{\omega}_1^3 mn(n-m) \end{aligned} \tag{4.47}$$

where b is the cubic coefficient in Equation (2.16). For the first phase mismatch this is hence

$$\tilde{k}_2 - 2\tilde{k}_1 \approx 3b\tilde{\omega}_1^3 \cdot 2 \cdot 1 \cdot (2-1) = 6b\tilde{\omega}_1^3. \tag{4.48}$$

The fraction of the general phase mismatch and this first one is

$$\frac{\tilde{k}_n - \tilde{k}_m - \tilde{k}_{n-m}}{\tilde{k}_2 - 2\tilde{k}_1} = \frac{3b\tilde{\omega}_1^3 mn(n-m)}{6b\tilde{\omega}_1^3} = \frac{1}{2}mn(n-m) := d_{n,m}. \tag{4.49}$$

We can hence write the propagation equations as

$$\begin{aligned} A'_m = &\sum_{n=m+1}^{M} \frac{c_3\tilde{\omega}_1^2}{4}n(n-m)A_n\bar{A}_{n-m}\mathrm{e}^{\mathrm{i}\left(\tilde{k}_2-2\tilde{k}_1\right)\tilde{x}d_{n,m}} \\ &-\frac{1}{2}\sum_{n=1}^{m-1}\frac{c_3\tilde{\omega}_1^2}{4}n(m-n)A_nA_{m-n}\mathrm{e}^{-\mathrm{i}\left(\tilde{k}_2-2\tilde{k}_1\right)\tilde{x}d_{m,n}}. \end{aligned} \tag{4.50}$$

4.4.2 Rescaling the propagation equations

Now we will rescale the propagation equations for reasons that will soon become apparent. First let us note that, since energy is conserved and all initial energy is in the first harmonic, if we rescale each amplitude according to

$$b_m(\tilde{x}) = m\frac{A_m(\tilde{x})}{A_1(0)} \tag{4.51}$$

the sum of the absolute value of all amplitudes squared must always be 1, which is convenient. Then the propagation equations become

$$\begin{aligned}\frac{A_1(0)}{m}b_m' = &\sum_{n=m+1}^{M}\frac{c_3\tilde{\omega}_1^2}{4}A_1^2(0)b_n\bar{b}_{n-m}\mathrm{e}^{\mathrm{i}(\tilde{k}_2-2\tilde{k}_1)\tilde{x}d_{n,m}}\\ &-\frac{1}{2}\sum_{n=1}^{m-1}\frac{c_3\tilde{\omega}_1^2}{4}A_1^2(0)b_nb_{m-n}\mathrm{e}^{-\mathrm{i}(\tilde{k}_2-2\tilde{k}_1)\tilde{x}d_{m,n}}.\end{aligned} \tag{4.52}$$

If we now introduce the rescaled length and transformed amplitude

$$\xi(\tilde{x}) = \frac{c_3\tilde{\omega}_1^2}{4}A_1(0)\cdot\tilde{x}, \quad a_m(\xi(\tilde{x})) = b_m(\tilde{x}) \tag{4.53}$$

we get that

$$b_m'(\tilde{x}) = a_m'(\xi(\tilde{x}))\cdot\xi'(x) \quad\Longrightarrow\quad (a_m)_\xi' = (b_m)_{\tilde{x}}'\cdot\frac{1}{A_1(0)c_3\tilde{\omega}_1^2/4}. \tag{4.54}$$

Finally, by defining the parameter

$$\mu = \frac{\tilde{k}_2-2\tilde{k}_1}{c_3\tilde{\omega}_1^2A_1(0)/4} \tag{4.55}$$

we can write the propagation equations as a function of only this one parameter μ and the rescaled length ξ,

$$a_m'(\xi) = m\left(\sum_{n=m+1}^{M}a_n\bar{a}_{n-m}\mathrm{e}^{\mathrm{i}\mu\xi d_{n,m}} - \frac{1}{2}\sum_{n=1}^{m-1}a_na_{m-n}\mathrm{e}^{-\mathrm{i}\mu\xi d_{m,n}}\right). \tag{4.56}$$

Recall that this is a set of equations for all $m \in [1, M] \cap \mathbb{N}$. Let us look closer at these equations. Here we have reduced all values of $c_3, A_1(0), \tilde{\omega}_1, \tilde{C}$ in the quasilinear regime, into a set of equations dependent on the single scaling parameter μ. Regardless of actual initial amplitudes, the rescaled initial amplitudes are 1 for the first harmonic and 0 for the others. Furthermore, we can simplify the expression of the scaling parameter as

$$\mu \approx \frac{b\tilde{\omega}_2^3 - b\tilde{\omega}_1^3}{c_3\tilde{\omega}_1^2 A_1(0)/4} = \frac{6b\tilde{\omega}_1^3}{c_3\tilde{\omega}_1^2 A_1(0)/4} = \frac{24b\tilde{\omega}_1}{c_3 A_1(0)} = \frac{24b\tilde{\omega}_1^2}{c_3\Delta_1(0)} \overset{!}{=} \frac{\tilde{\omega}_1^2}{c_3\Delta_1(0)} \tag{4.57}$$

where $\Delta_1(0) = A_1(0)/\tilde{\omega}_1$ is the phase difference induced by the first harmonic. The last equality, marked with the exclamation mark, is only valid for $\tilde{C} = 0$ since b is the cubic coefficient in Equation (2.16). Now that we have a generalised description dependent only on the parameter μ, let us solve the propagation equations for different number of harmonics M and study the results.

An important question is: what do the rescaled amplitudes a_m, the parameter μ and the rescaled length ξ represent?

- **Normalised amplitudes:** The rescaled amplitudes are simply the amplitudes normalised with respect to energy and initial amplitude such that 1 represents the total injected energy. Expressing the amplitudes this way ensures that the absolute value of each amplitude will always be a number between 0 and 1, and that the sum of the absolute values squared will always be 1.

- **Effective phase mismatch:** The parameter μ describes the relation between phase mismatch and pumping strength, *i.e.* the “effective phase mismatch”. As we know from Section 4.2, and especially Equation (4.20), it is not the value of the phase mismatch on its own that determines the behaviour of the propagating waves, but the relation between the phase mismatch and the pumping strength. The parameter μ captures this relation and puts a number to it. A large number ($\mu \gtrsim 10$) represents a lot of phase mismatch compared with the pumping strength, while a small number ($\mu \lesssim 1$) represents little phase mismatch compared with the pumping strength.

- **Effective length:** The rescaled length ξ describes the “effective length” of the TWPA. It is not the specific number of unit cells $\tilde{x} = N$ on its own that determines whether the TWPA is long enough to reach a certain gain, but rather the physical length combined with the pumping strength, which is what ξ captures.

4.4.3 Two harmonics

Applying $M = 2$ in Equation (4.56), the propagation equations for 2 harmonics become

$$a_1' = a_2 \bar{a}_1 \mathrm{e}^{\mathrm{i}\mu\xi}, \tag{4.58a}$$

$$a_2' = -a_1^2 \mathrm{e}^{-\mathrm{i}\mu\xi}. \tag{4.58b}$$

The case of 2 harmonics has been solved analytically [35], but here we present the numerically determined solution, see Figures 4.7 and 4.8. The results can be summarised as:

- $\mu = 0$: All amplitude in the first harmonic up-converts to the second harmonic.

- $\mu \in (0, \sqrt{2})$: The amplitudes oscillate, and the minimum amplitude of the first harmonic is smaller than the maximum amplitude of the second harmonic.

- $\mu = \sqrt{2}$: Both amplitudes oscillate, and the minimum of the first harmonic is exactly equal to the maximum of the second harmonic.

- $\mu > \sqrt{2}$: The amplitudes oscillate but the amplitude of the first harmonic is always larger than the amplitude of the second harmonic.

- $\mu \gg \sqrt{2}$: There is practically no up-conversion.

In short, the first harmonic oscillates between full transmission and some lower bound. The larger the μ, the smaller the oscillation amplitude and period.

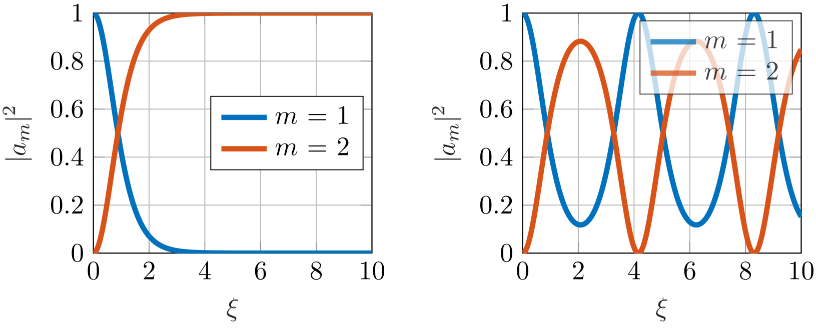

(a) $\mu = 0$ **(b)** $\mu = 0.25$

Figure 4.7: Numerical solution to Equations (4.58a) and (4.58b) for $\mu = \{0, 0.25\}$.

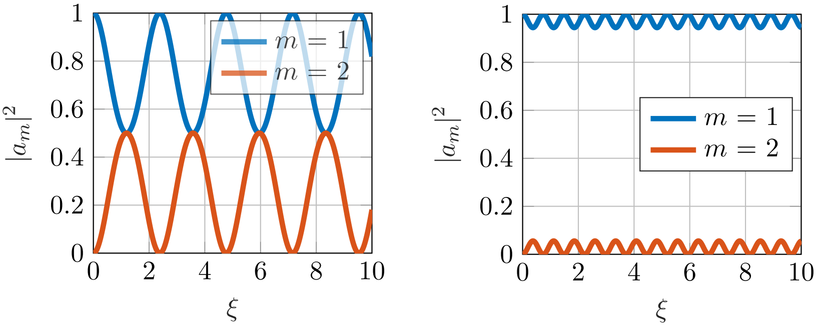

(a) $\mu = \sqrt{2}$ **(b)** $\mu = 8$

Figure 4.8: Numerical solution to Equations (4.58a) and (4.58b) for $\mu = \{\sqrt{2}, 8\}$.

4.4.4 Three harmonics

Applying $M = 3$ in Equation (4.56), the propagation equations for 3 harmonics become

$$a_1' = a_2\bar{a}_1 \mathrm{e}^{\mathrm{i}\mu\xi} + a_3\bar{a}_2 \mathrm{e}^{3\mathrm{i}\mu\xi}, \tag{4.59a}$$

$$a_2' = 2a_3\bar{a}_1 \mathrm{e}^{3\mathrm{i}\mu\xi} - a_1^2 \mathrm{e}^{-\mathrm{i}\mu\xi}, \tag{4.59b}$$

$$a_3' = -3a_2a_1 \mathrm{e}^{-3\mathrm{i}\mu\xi}. \tag{4.59c}$$

We solve these equations numerically for multiple values of μ, see Figures 4.9 and 4.10.

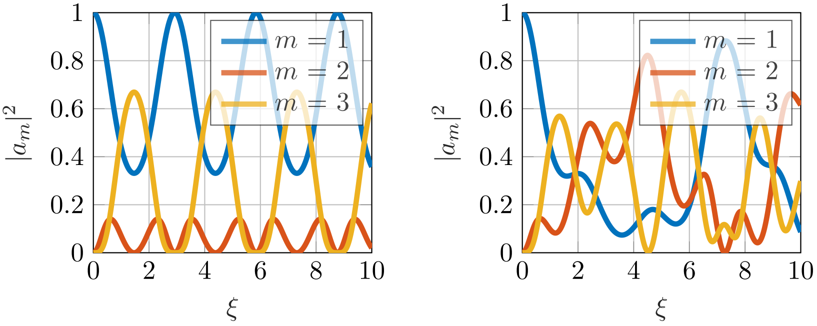

(a) $\mu = 0$ **(b)** $\mu = 0.25$

Figure 4.9: Numerical solution to Equations (4.59a) to (4.59c) for $\mu = \{0, 0.1\}$.

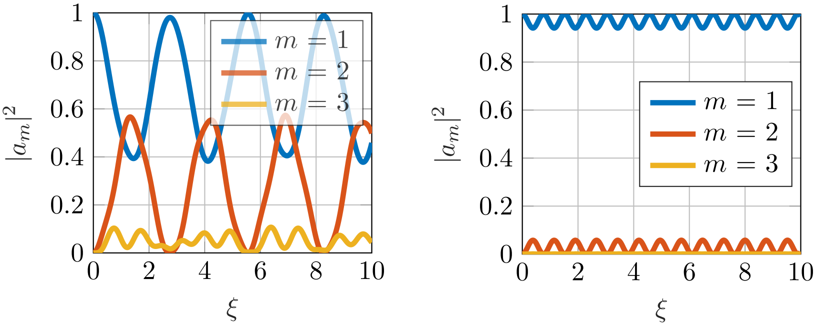

(a) $\mu = \sqrt{2}$ **(b)** $\mu = 8$

Figure 4.10: Numerical solution to Equations (4.59a) to (4.59c) for $\mu = \{\sqrt{2}, 8\}$.

The results can be summarised as:

- $\mu = 0$: The first harmonic does not completely deplete, but oscillates heavily. The second harmonic remains small and instead the third harmonic oscillates heavily.
- $\mu \approx 0.25$: Chaotic behaviour.

- $\mu \approx \sqrt{2}$: Similar behaviour to $M = 2$, but the third harmonic slightly perturbs the transmission of the first and second harmonics.

- $\mu \gg \sqrt{2}$: The third harmonic is negligibly small and we retrieve the results from $M = 2$.

4.4.5 Multiple harmonics

We could of course continue to study specific values of M, such as 4, 5, 6 and so on, but a more interesting question is how many harmonics are *necessary* to include? This is what we tried to answer in Section 4.3.4 but we could not, due to reasons we shall soon discover. In this section we will generalise the results for an arbitrary number of harmonics and, through a numerical study, find the number of harmonics M_c needed to be included so that adding more harmonics practically makes no difference. In other words, if $M < M_\mathrm{c}$, adding harmonics will change the results, while for $M \geq M_\mathrm{c}$ there will be negligible change within some error bound.

If we look back at, and compare, Sections 4.4.3 and 4.4.4, we see that for small values of μ, adding the third harmonic makes a large difference, while for large values of μ, it makes a small difference (if any). It seems as the value of μ is strongly correlated with the necessary number of harmonics M_c.

To find M_c we hence pick a value of μ and solve the general propagation equations, recall Equation (4.56), for $M = \{1, 2, ...\}$ and study how the transmission of the first harmonic (the main tone) evolves with M. We keep increasing M until the propagation of the main tone changes less than a desired error bound. The convergence parameter for a specific M is the absolute value of the difference of the M and $M + 1$ solutions for the main tone. If the largest difference between these two solutions is smaller than the desired error tolerance, say 0.01, we say that it has converged and hence that $M = M_\mathrm{c}$, otherwise it has not converged. We repeat this process for multiple values of μ. Different solutions to Equation (4.56) for $\mu = \{\sqrt{2}, 8\}$ and values of M up to $M_\mathrm{c} + 1$ are shown in Figures 4.11 and 4.12.

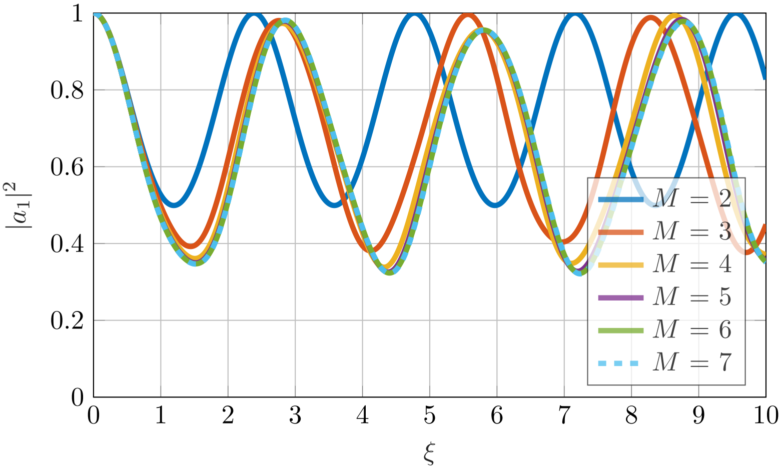

Figure 4.11: Numerical solution to Equation (4.56) for $\mu = \sqrt{2}$ and different values of M up to $M_c + 1 = 7$ on the length $\xi \in [0, 10]$ and error tolerance 0.01.

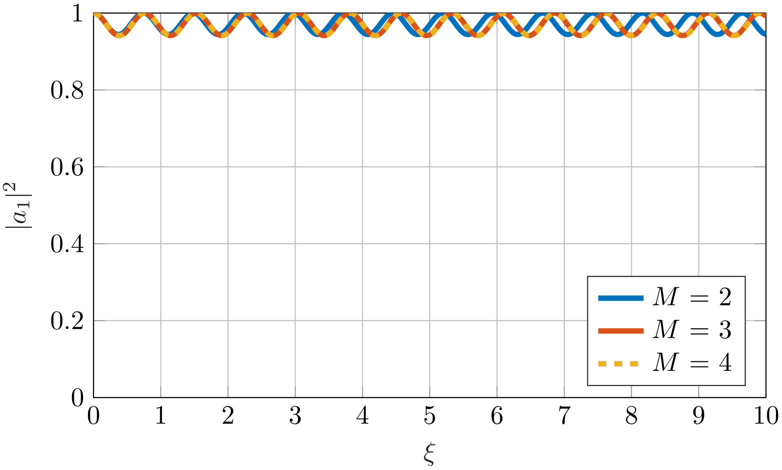

Figure 4.12: Numerical solution to Equation (4.56) for $\mu = 8$ and different values of M up to $M_c + 1 = 4$ on the length $\xi \in [0, 10]$ and error tolerance 0.01.

As we can clearly see, between the two lowest values of M in both figures, there is a clear difference between the solutions. However, for M_c and $M_c + 1$, there is no noticeable difference. We can also note that M_c is clearly larger for $\mu = \sqrt{2}$ than for $\mu = 8$. We find the value of M_c for multiple values of $\mu \in [0.25, 30]$, see Figure 4.13.

Looking at Figure 4.13, it seems as M_c diverges as $\mu \to 0$. We have not confirmed this analytically nor numerically, but we have checked that for $\mu = 0$ there is indeed no convergence for at least up to 196 harmonics. This explains why we never got converging eigenvalues in Section 4.3. We had assumed that we were in the purely linear regime where $\mu = 0$, but we now know that one would need an infinite number of harmonics, which is not realistic as the frequencies of the harmonics will surely reach the cutoff frequency at some point.

Solutions of Equation (4.56) for different values of μ using $M = M_c$ are shown in Figure 4.14. For $\mu = 0.25$ we have $M_c = 12$, for $\mu = \sqrt{2}$ we have $M_c = 6$ and for $\mu = 8$ we have $M_c = 3$.

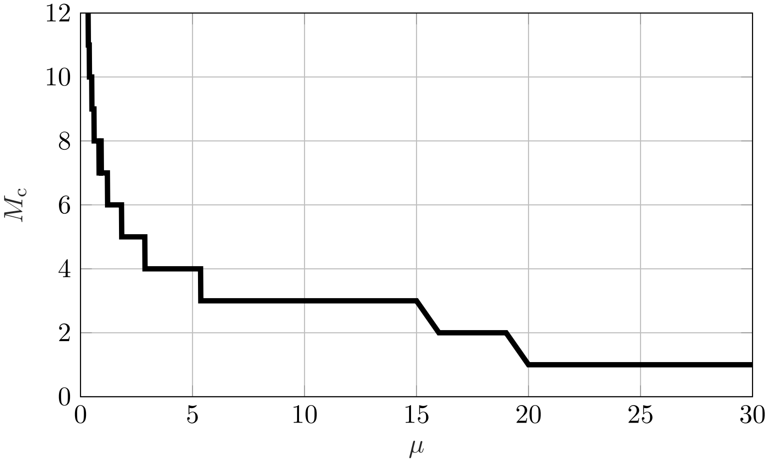

Figure 4.13: The critical number of harmonics M_c to satisfy the convergence criterion of the main tone up to length $\xi = 10$ with error tolerance of 0.01.

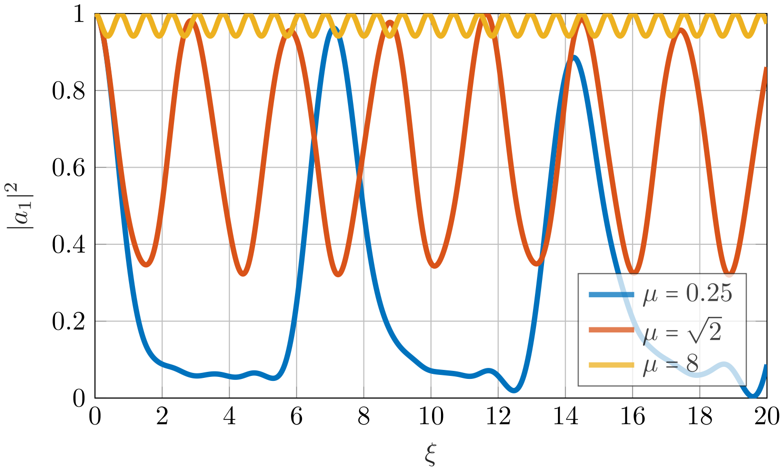

Figure 4.14: The solutions of Equation (4.56) for different values of μ using $M = M_\mathrm{c}$ with error tolerance 0.01.

4.4.6 Conclusions

In this section we investigated what happens with a single tone inserted into the TWPA. We found the propagation equations and then generalised and rescaled them to a form such that every single combination of system parameters can be described by a single scaling parameter, the effective phase mismatch μ. Then we showed that in order to correctly describe the propagation of the main tone, also known as the first harmonic, one needs to use at least the number of harmonics $M = M_\mathrm{c}$. In turn, M_c is highly dependent on μ and seems to diverge as $\mu \to 0$, while it is 1 for $\mu \geq 20$. It is also worth pointing out that M_c is also dependent on the desired error tolerance as well as the largest value of ξ.

The transmission of the main tone can be described as follows: For large enough μ, $\mu \gtrsim 20$, the tone propagates with negligible up-conversion. For fairly large μ, $\mu \approx 8$, the tone propagates with small and fast oscillations. As μ gets smaller, the oscillation amplitude and period become larger. For very small values, $\mu < 1$, the behaviour is less predictable but seems in general to mostly deplete the inserted tone except for small bursts at certain lengths where it regains most of its initial amplitude.

An important question is, what happens if for a value of μ some of the harmonics fall above the cutoff frequency, and what can we say about the main tone's propagation in this scenario? Unfortunately not much. The model we have developed here relies on the assumption that *all* harmonics are well below cutoff. That is in fact a requirement for being able to use the differential equations at all, recall Section 3.2. In other words, if one calculates the value of μ and the corresponding effective length ξ, and sees that $M_\mathrm{c}\omega_1 \ll \omega_\mathrm{c}$, the simulated results *should* be accurate, otherwise we do not know what will happen. We will discuss the accuracy of this model in Section 4.6, once we have extended it in Section 4.5 to include two inputs; the pump and the signal.

4.5 Generalised 3WM model

In this section we will develop a generalised model to capture all up- and down-conversion processes when inserting both a pump and a signal into a TWPA. The generalisation steps will very closely follow the steps taken in Section 4.4, so it is recommended to read that section first.

The ansatz of tones we will develop this model with is the pump-mediated tones ansatz [39], where the waves have frequencies

$$\begin{aligned} \tilde{\omega}_{m\mathrm{p}} &= m\tilde{\omega}_\mathrm{p}, \quad m \in [1, M] \cap \mathbb{N} \\ \tilde{\omega}_{\mathrm{s}+m\mathrm{p}} &= \tilde{\omega}_\mathrm{s} + m\tilde{\omega}_\mathrm{p}, \quad m \in [0, M-1] \cap \mathbb{N}, \\ \tilde{\omega}_{\mathrm{i}+m\mathrm{p}} &= \tilde{\omega}_\mathrm{i} + m\tilde{\omega}_\mathrm{p}, \quad m \in [0, M-1] \cap \mathbb{N}, \end{aligned} \tag{4.60}$$

where M is the number of modes for both pump, signal and idler. In Section 4.5.4 we will show that this is indeed a good ansatz.

4.5.1 Possible mixing processes

First we must identify what mixing processes can take place, as this is the foundation when deriving the propagation equations. We know from the definition of the idler that $\tilde{\omega}_\mathrm{s} + \tilde{\omega}_\mathrm{i} = \tilde{\omega}_\mathrm{p}$. However, we can also go to higher modes of both signal and idler, and their sum will still be a pump harmonic. All the possible mixing processes of these transitions can be summarised as

$$\{m, n \in [0, M-1] \cap \mathbb{N} : m + n < M\} : \tilde{\omega}_{\mathrm{s}+m\mathrm{p}} + \tilde{\omega}_{\mathrm{i}+n\mathrm{p}} = \tilde{\omega}_{(m+n+1)\mathrm{p}}. \tag{4.61}$$

We also know that the signal and its up-converted modes can be up-converted by the pump, $\tilde{\omega}_{\mathrm{s}+m\mathrm{p}} + \tilde{\omega}_{\mathrm{p}} = \tilde{\omega}_{\mathrm{s}+(m+1)\mathrm{p}}$, as discussed in Section 4.3. However, now that we include harmonics of the pump, every pump harmonic can induce similar processes. All these possible mixing processes can be summarised as

$$\begin{aligned} \{m \in [0, M-1] \cap \mathbb{N}, n \in [1, M] \cap \mathbb{N} : m + n < M\} :& \\ \tilde{\omega}_{\mathrm{s}+m\mathrm{p}} + \tilde{\omega}_{n\mathrm{p}} = \tilde{\omega}_{\mathrm{s}+(m+n)\mathrm{p}}&. \end{aligned} \tag{4.62}$$

The same is valid for the idler, simply replace s→i in the equation above.

4.5.2 The propagation equations

Now that we have identified the possible mixing processes, let us determine what the propagation equations are. Using the simplified propagation equations, recall Equation (4.13), the equation for the pump is

$$\begin{aligned} A'_{m\mathrm{p}} &= \sum_{n=m+1}^{M} \frac{c_3}{4} \tilde{\omega}_{n\mathrm{p}} \tilde{\omega}_{(n-m)\mathrm{p}} A_{n\mathrm{p}} \bar{A}_{(n-m)\mathrm{p}} \mathrm{e}^{\mathrm{i}\left(\tilde{k}_{n\mathrm{p}} - \tilde{k}_{m\mathrm{p}} - \tilde{k}_{(n-m)\mathrm{p}}\right)\tilde{x}} \\ &- \frac{1}{2} \sum_{n=1}^{m-1} \frac{c_3}{4} \tilde{\omega}_{n\mathrm{p}} \tilde{\omega}_{(m-n)\mathrm{p}} A_{n\mathrm{p}} A_{(m-n)\mathrm{p}} \mathrm{e}^{-\mathrm{i}\left(\tilde{k}_{m\mathrm{p}} - \tilde{k}_{n\mathrm{p}} - \tilde{k}_{(m-n)\mathrm{p}}\right)\tilde{x}} \\ &+ \sum_{n=m}^{M-1} \frac{c_3}{4} \tilde{\omega}_{\mathrm{s}+n\mathrm{p}} \tilde{\omega}_{\mathrm{s}+(n-m)\mathrm{p}} A_{\mathrm{s}+n\mathrm{p}} \bar{A}_{\mathrm{s}+(n-m)\mathrm{p}} \mathrm{e}^{\mathrm{i}\left(\tilde{k}_{\mathrm{s}+n\mathrm{p}} - \tilde{k}_{n\mathrm{p}} - \tilde{k}_{\mathrm{s}+(n-m)\mathrm{p}}\right)\tilde{x}} \\ &+ \sum_{n=m}^{M-1} \frac{c_3}{4} \tilde{\omega}_{\mathrm{i}+n\mathrm{p}} \tilde{\omega}_{\mathrm{i}+(n-m)\mathrm{p}} A_{\mathrm{i}+n\mathrm{p}} \bar{A}_{\mathrm{i}+(n-m)\mathrm{p}} \mathrm{e}^{\mathrm{i}\left(\tilde{k}_{\mathrm{i}+n\mathrm{p}} - \tilde{k}_{n\mathrm{p}} - \tilde{k}_{\mathrm{i}+(n-m)\mathrm{p}}\right)\tilde{x}} \\ &- \sum_{n=0}^{m-1} \frac{c_3}{4} \tilde{\omega}_{\mathrm{s}+n\mathrm{p}} \tilde{\omega}_{\mathrm{i}+(m-n-1)\mathrm{p}} A_{\mathrm{s}+n\mathrm{p}} A_{\mathrm{i}+(m-n-1)\mathrm{p}} \mathrm{e}^{-\mathrm{i}\left(\tilde{k}_{m\mathrm{p}} - \tilde{k}_{\mathrm{s}+n\mathrm{p}} - \tilde{k}_{\mathrm{i}+(m-n-1)\mathrm{p}}\right)\tilde{x}}. \end{aligned} \tag{4.63a}$$

However, if we assume that the amplitudes of the signal and idler modes are much smaller than the pump amplitude, we can neglect the three latter sums where we have products of amplitudes of signal and idler modes. We call this the *back-action* as it describes the action the signal and idler modes exert back on the pump harmonics when being amplified. Neglecting back-action when there are no pump harmonics other than the first is usually called *the stiff pump approximation.* Then we get the same equations for the pump harmonics as in the single input study, Section 4.4, and we can use the results from that section to describe the propagation of the pump harmonics.

The effects of back-action, *i.e.* how the energy of the pump and its harmonics is depleted when the signal and idler modes are amplified, is analysed and discussed in Section 4.5.6.

For the signal modes we get the equation

$$
\begin{aligned}
A'_{\mathrm{s}+m\mathrm{p}} = & \sum_{n=m+1}^{M} \frac{c_3}{4} \tilde{\omega}_{n\mathrm{p}} \tilde{\omega}_{\mathrm{s}+(n-m-1)\mathrm{p}} A_{n\mathrm{p}} \bar{A}_{\mathrm{i}+(n-m-1)\mathrm{p}} \mathrm{e}^{\mathrm{i}\left(\tilde{k}_{n\mathrm{p}}-\tilde{k}_{\mathrm{s}+m\mathrm{p}}-\tilde{k}_{\mathrm{i}+(n-m-1)\mathrm{p}}\right)\tilde{x}} \\
& + \sum_{n=m+1}^{M-1} \frac{c_3}{4} \tilde{\omega}_{\mathrm{s}+n\mathrm{p}} \tilde{\omega}_{(n-m)\mathrm{p}} A_{\mathrm{s}+n\mathrm{p}} \bar{A}_{(n-m)\mathrm{p}} \mathrm{e}^{\mathrm{i}\left(\tilde{k}_{\mathrm{s}+n\mathrm{p}}-\tilde{k}_{\mathrm{s}+m\mathrm{p}}-\tilde{k}_{(n-m)\mathrm{p}}\right)\tilde{x}} \\
& - \sum_{n=1}^{m} \frac{c_3}{4} \tilde{\omega}_{n\mathrm{p}} \tilde{\omega}_{\mathrm{s}+(m-n)\mathrm{p}} A_{n\mathrm{p}} A_{\mathrm{s}+(m-n)\mathrm{p}} \mathrm{e}^{-\mathrm{i}\left(\tilde{k}_{\mathrm{s}+m\mathrm{p}}-\tilde{k}_{n\mathrm{p}}-\tilde{k}_{\mathrm{s}+(m-n)\mathrm{p}}\right)\tilde{x}}.
\end{aligned} \tag{4.63b}
$$

The equations for the idler modes are the same as in Equation (4.63b) with replacement s↔i.

4.5.3 Rescaling the propagation equations

Now we will rescale the propagation equations above in the same way as we did in Section 4.4.2, to get the generalised propagation equations. We express the frequencies as

$$
\begin{aligned}
\tilde{\omega}_{m\mathrm{p}} &= m\tilde{\omega}_{\mathrm{p}}, \\
\tilde{\omega}_{\mathrm{s}+m\mathrm{p}} &= \tilde{\omega}_{\mathrm{s}} + m\tilde{\omega}_{\mathrm{p}} = \left(m + \frac{1+\delta}{2}\right)\tilde{\omega}_{\mathrm{p}}, \\
\tilde{\omega}_{\mathrm{i}+m\mathrm{p}} &= \tilde{\omega}_{\mathrm{i}} + m\tilde{\omega}_{\mathrm{p}} = \left(m + \frac{1-\delta}{2}\right)\tilde{\omega}_{\mathrm{p}}
\end{aligned} \tag{4.64}
$$

where δ is the detuning (recall Equation (4.27)) and hence the rescaled amplitudes as

$$
\begin{aligned}
a_{m\mathrm{p}} &= m\frac{A_{\mathrm{p}}}{A_{\mathrm{p}0}}, \\
a_{\mathrm{s}+m\mathrm{p}} &= \left(m + \frac{1+\delta}{2}\right)\frac{A_{\mathrm{s}+m\mathrm{p}}}{A_{\mathrm{p}0}}, \\
a_{\mathrm{i}+m\mathrm{p}} &= \left(m + \frac{1-\delta}{2}\right)\frac{A_{\mathrm{i}+m\mathrm{p}}}{A_{\mathrm{p}0}}
\end{aligned} \tag{4.65}
$$

where $A_{\mathrm{p}0}$ is the initial pump amplitude. We rescale length in the same way as in Section 4.4. With the replacements $\tilde{\omega}_1 \to \tilde{\omega}_{\mathrm{p}}, \tilde{k}_1 \to \tilde{k}_{\mathrm{p}}$ and $A_1 \to A_{\mathrm{p}}$, recall Equations (4.53) and (4.55), we get that ξ and μ become

$$
\xi = \frac{c_3\tilde{\omega}_{\mathrm{p}}^2}{4}A_{\mathrm{p}0} \cdot \tilde{x} \approx \frac{1}{4}c_3\tilde{\omega}_{\mathrm{p}}\Delta_{\mathrm{p}0}\tilde{x} \tag{4.66}
$$

and

$$\mu = \frac{\tilde{k}_{2\mathrm{p}} - 2\tilde{k}_{\mathrm{p}}}{c_3\tilde{\omega}_{\mathrm{p}}^2 A_{\mathrm{p}0}/4} \approx \frac{\tilde{\omega}_{\mathrm{p}}^2}{c_3\Delta_{\mathrm{p}0}}. \tag{4.67}$$

All that remains is finding a way to approximate the phase mismatches with numerical factors. We once again expand the dispersion relation to its cubic order and divide each phase mismatch by $\tilde{k}_{2\mathrm{p}} - 2\tilde{k}_{\mathrm{p}}$. Then we get the numerical factors

$$d_{\mathrm{p}:n,m} = \frac{1}{6}\left(n^3 - \left(m + \frac{1+\delta}{2}\right)^3 - \left(n - m - 1 + \frac{1-\delta}{2}\right)^3\right), \tag{4.68a}$$

$$d_{\mathrm{s}:n,m} = \frac{1}{6}\left(\left(n + \frac{1+\delta}{2}\right)^3 - \left(m + \frac{1+\delta}{2}\right)^3 - (n-m)^3\right), \tag{4.68b}$$

$$d_{\mathrm{i}:n,m} = \frac{1}{6}\left(\left(n + \frac{1-\delta}{2}\right)^3 - \left(m + \frac{1-\delta}{2}\right)^3 - (n-m)^3\right), \tag{4.68c}$$

as well as $d_{n,m}$ defined in Equation (4.49). The propagation equations, recall Equation (4.63), neglecting back-action of signal and idler modes on the pump harmonics (as discussed in Section 4.5.2), can then be written as

$$a'_{m\mathrm{p}} = m\left(\sum_{n=m+1}^{M} a_{n\mathrm{p}}\bar{a}_{(n-m)\mathrm{p}}\mathrm{e}^{\mathrm{i}\mu\xi d_{n,m}} - \frac{1}{2}\sum_{n=1}^{m-1} a_{n\mathrm{p}}a_{(m-n)\mathrm{p}}\mathrm{e}^{-\mathrm{i}\mu\xi d_{m,n}}\right), \tag{4.69a}$$

$$\begin{aligned} a'_{\mathrm{s}+m\mathrm{p}} = \left(m + \frac{1+\delta}{2}\right) \times \Bigg(&\sum_{n=m+1}^{M} a_{n\mathrm{p}}\bar{a}_{\mathrm{i}+(n-m-1)\mathrm{p}}\mathrm{e}^{\mathrm{i}\mu\xi d_{\mathrm{p}:n,m}} \\ + &\sum_{n=m+1}^{M-1} a_{\mathrm{s}+n\mathrm{p}}\bar{a}_{(n-m)\mathrm{p}}\mathrm{e}^{\mathrm{i}\mu\xi d_{\mathrm{s}:n,m}} - \sum_{n=1}^{m} a_{n\mathrm{p}}a_{\mathrm{s}+(m-n)\mathrm{p}}\mathrm{e}^{-\mathrm{i}\mu\xi d_{\mathrm{s}:m,m-n}}\Bigg), \end{aligned} \tag{4.69b}$$

$$\begin{aligned} a'_{\mathrm{i}+m\mathrm{p}} = \left(m + \frac{1-\delta}{2}\right) \times \Bigg(&\sum_{n=m+1}^{M} a_{n\mathrm{p}}\bar{a}_{\mathrm{s}+(n-m-1)\mathrm{p}}\mathrm{e}^{\mathrm{i}\mu\xi d_{\mathrm{p}:n,n-m-1}} \\ + &\sum_{n=m+1}^{M-1} a_{\mathrm{i}+n\mathrm{p}}\bar{a}_{(n-m)\mathrm{p}}\mathrm{e}^{\mathrm{i}\mu\xi d_{\mathrm{i}:n,m}} - \sum_{n=1}^{m} a_{n\mathrm{p}}a_{\mathrm{i}+(m-n)\mathrm{p}}\mathrm{e}^{-\mathrm{i}\mu\xi d_{\mathrm{i}:m,m-n}}\Bigg). \end{aligned} \tag{4.69c}$$

Due to the rescaling, the initial condition is $a_{\mathrm{p}0} = 1$, $a_{\mathrm{s}0} = A_{\mathrm{s}0}/A_{\mathrm{p}0} \ll 1$ and 0 for all other amplitudes. However, if back-action is neglected, as done in the equations above, the value of $a_{\mathrm{s}0}$ makes no difference and can be set to 1 for convenience, which simplifies the gain to $|a_{\mathrm{s}}/a_{\mathrm{s}0}|^2 = |a_{\mathrm{s}}|^2$. Another way to phrase this: the value of the initial signal amplitude only makes a difference for the back-action terms, so once the back-action terms are neglected, we can freely set the value of the initial signal amplitude to whatever value we wish, without it having any impact on the transmission of the signal, where 1 is a convenient starting value.

To investigate the transmission of a signal with a frequency larger than the pump, we instead set the initial amplitude of the appropriate up-converted mode of the signal to 1. For example, if $\tilde{\omega}_{\mathrm{s}} = 2.5\tilde{\omega}_{\mathrm{p}}$, we set $a_{\mathrm{s}0} = 0$ and $a_{\mathrm{s+2p}}(0) = 1$. At this frequency the gain is given by $|a_{\mathrm{s+2p}}|^2$.

4.5.4 The single idler model

Now that we have developed the generalised multimode propagation equations, let us begin with a case we explored before, the single idler model, whose equations we get by using $M = 1$ in Equation (4.69). Without pump harmonics and back-action, the pump amplitude is constant and can be neglected from the equations. We then get

$$a_{\mathrm{s}}' = \frac{1+\delta}{2}\bar{a}_{\mathrm{i}}\mathrm{e}^{\mathrm{i}\mu\xi\cdot\frac{1}{8}(1-\delta^2)}, \tag{4.70a}$$

$$a_{\mathrm{i}}' = \frac{1-\delta}{2}\bar{a}_{\mathrm{s}}\mathrm{e}^{\mathrm{i}\mu\xi\cdot\frac{1}{8}(1-\delta^2)}. \tag{4.70b}$$

We can solve these with the same method as used in Section 4.2. We then get that the gain coefficient is given by

$$g = \frac{1}{2}\sqrt{(1-\delta^2)\left(1 - \frac{\mu^2}{8^2}(1-\delta^2)\right)}. \tag{4.71}$$

This is illustrated in Figure 4.15 for multiple values of μ. The first factor in the square root may make the gain coefficient equal to zero, when $|\delta| \to 1$, but never imaginary. The second factor, however, will make it imaginary if μ is too large. This happens when

$$1 < \frac{\mu^2}{8^2}\left(1-\delta^2\right) \quad \Longrightarrow \quad \mu > \frac{8}{\sqrt{1-\delta^2}}. \tag{4.72}$$

In other words, when $\mu < 8$, the single idler model predicts exponential gain in the full band, but for values of $\mu > 8$, exponential gain will be suppressed in the centre of the band. The width of this central band without exponential gain depends on how large μ is.

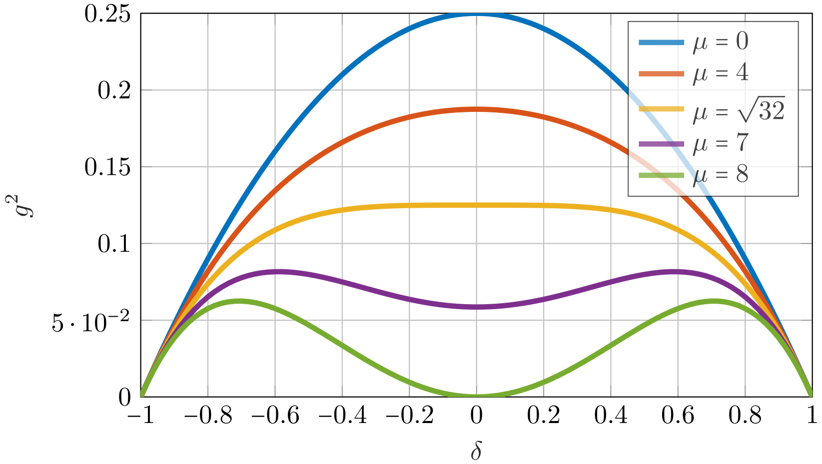

Figure 4.15: The gain coefficient squared as a function of δ for multiple values of μ. The largest values of g are achieved for $\mu = 0$, while for $\mu = 8$, g becomes 0 at 0 detuning.

With this knowledge, we can now say why ignoring signal and idler self-mixing (the pump-mediated model) in our TWPA is a good assumption, or in other words, why we do not need to worry about waves with frequencies such as $2\tilde{\omega}_\mathrm{s}, 3\tilde{\omega}_\mathrm{i}$ and so on. From the conclusion above, we know that the pump amplitude must be such that $\mu < 8$ if we want exponential gain in the full band (which we do). Furthermore, we can assume that the signal is much smaller than the pump, since if it were of the similar size as the strong pump we would not require quantum-limited amplification, which implies that the initial signal amplitude is also much smaller than the initial pump amplitude. Let us assume that the initial signal amplitude is a thousandth of the initial pump amplitude, and that the pump amplitude is such that $\mu \approx 4$. Then the corresponding μ-value for the signal, let us call it μ_s, is approximately $\mu_\mathrm{s} \approx 4000$. Furthermore, we know from Section 4.4 that μ-values much larger than $\sqrt{2}$ prevent up-conversion. Looking at Figure 4.14, we find very limited up-conversion for $\mu \sim 10$, and since $\mu_\mathrm{s} \gg 10$, we conclude that it is large enough to ignore signal and idler self-mixing.

4.5.5 Multiple modes

In Section 4.5.4 we investigated the solution to Equation (4.69) for $M = 1$. It is of course possible to try other values of M, but just as in Section 4.4, a more important question is how many modes *are needed*?

From the conclusions of Section 4.4, we guess that the critical number of modes is also dependent on the value of μ, but to verify this we solve Equation (4.69) for different values of μ, M, and δ, and investigate how many pump harmonics and up-converted signal and idler modes are required so that the transmission of the signal converges.

In Figure 4.16 we see the simulation results for $\mu = 7$ for different values of M at zero detuning. As predicted, for $M = 1$, we get exponential gain. However, when we add more pump harmonics and up-converted signal and idler modes, the transmission converges towards oscillatory transmission. As we guessed, only a few modes were required for convergence for this μ-value.

In Figure 4.17 we instead see the simulation results for $\mu = 1$. For $M = 1$ the signal now grows faster, due to smaller effective phase mismatch. However now also, as we guessed, more modes are required for convergence. Whether transmission is oscillatory or not for the converged solution is unclear.

To summarise, we solved the generalised propagation equations for multiple different values of $\mu \in [0.25, 30]$ and found that the smaller the value of μ is, the larger number of modes are required to get convergence. The number of required modes is also dependent on the detuning; the larger the detuning, the more required modes. It is also dependent on the length of the TWPA. In short, the needed number of modes is $M_\mathrm{c} = M_\mathrm{c}(\mu, \delta, \xi)$.

Furthermore, we see that the converged transmission for small values $\mu \sim 1$ shows much less gain than what was predicted by the single idler model. It grows slower and also deamplifies at certain lengths.

Thus an important conclusion of our analysis is that the gain is much smaller than predicted by the 3 mode model due to a large amount of up-conversion whenever the effective phase mismatch is small.

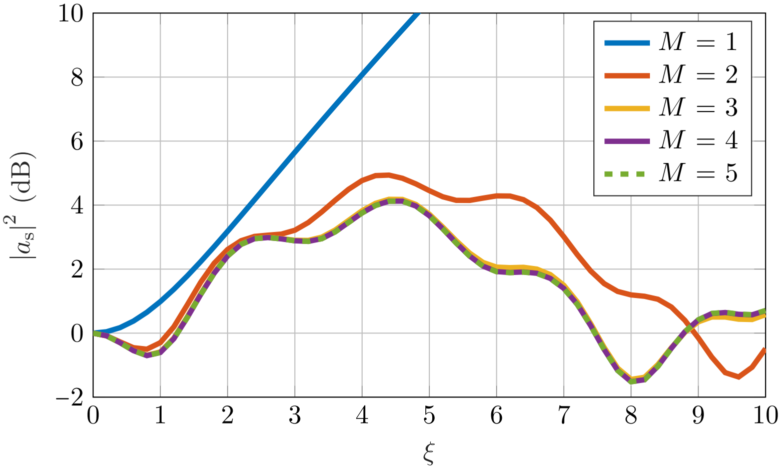

Figure 4.16: Transmission of signal for $\mu = 7$ at zero detuning for several values of M up to $M_c + 1$.

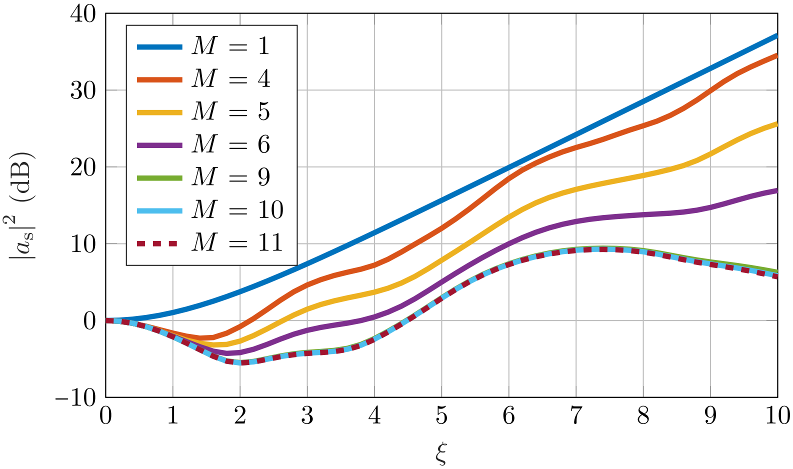

Figure 4.17: Transmission of signal for $\mu = 1$ at zero detuning for several values of M up to $M_c + 1$.

4.5.6 Effects of back-action

In this section we have a closer look at the pump depletion, *i.e.* how the energy of the pump and its harmonics is depleted when we take the back-action of the signal and idler modes into consideration. We included the back-action terms in Equation (4.63a) (the third, fourth and fifth sums), but neglected them in Equation (4.69a) under the assumption that the amplitudes of the signal and idler modes were much smaller than the pump amplitude. Initially this is a valid assumption, since at the input of the TWPA the amplitudes of all signal and idler modes are zero except the signal amplitude which is supposedly much smaller than the initial pump amplitude. However, what we did not really bring up previously was the fact that after propagating through the TWPA, the pump amplitude will be reduced due to up-conversion while the signal *ideally* will grow exponentially. Then the assumption that signal and idler harmonics are much smaller than the pump might not hold any longer.

To investigate whether back-action makes a difference or not, we simply include the neglected terms in the transformation to the generalised propagation equations. Equations (4.69b) and (4.69c) are unaffected, while Equation (4.69a) becomes

$$\begin{aligned} a'_{m\mathrm{p}} = m\Bigg(& \sum_{n=m+1}^{M} a_{n\mathrm{p}}\bar{a}_{(n-m)\mathrm{p}}\mathrm{e}^{\mathrm{i}\mu\xi d_{n,m}} - \frac{1}{2}\sum_{n=1}^{m-1} a_{n\mathrm{p}}a_{(m-n)\mathrm{p}}\mathrm{e}^{-\mathrm{i}\mu\xi d_{m,n}} \\ & + \sum_{n=m}^{M-1} a_{\mathrm{s}+n\mathrm{p}}\bar{a}_{\mathrm{s}+(n-m)\mathrm{p}}\mathrm{e}^{\mathrm{i}\mu\xi d_{\mathrm{s}:n,n-m}} \\ & + \sum_{n=m}^{M-1} a_{\mathrm{i}+n\mathrm{p}}\bar{a}_{\mathrm{i}+(n-m)\mathrm{p}}\mathrm{e}^{\mathrm{i}\mu\xi d_{\mathrm{i}:n,n-m}} \\ & - \sum_{n=0}^{m-1} a_{\mathrm{s}+n\mathrm{p}}a_{\mathrm{i}+(m-n-1)\mathrm{p}}\mathrm{e}^{-\mathrm{i}\mu\xi d_{\mathrm{p}:m,n}} \Bigg). \end{aligned} \tag{4.73}$$

When including these terms, the initial amplitude of the signal makes a difference to the solution. It is important that it is initially much smaller than the pump amplitude, *i.e.* that $a_{\mathrm{s}0} \ll 1$. We solve the propagation equations, but using Equation (4.73) to describe the propagation of pump harmonics, and compare them with the solution when the back-action is neglected, see Figure 4.18.

Surprisingly, back-action does not seem to make much of a difference. For large values of μ, when the signal transmission is oscillatory, there is no noticeable difference at all. When μ has fairly small values, *e.g.* 1 as in Figure 4.18, there is barely any noticeable difference until $\xi \approx 100$ for $a_{s0} = 1/50$, while for $a_{s0} = 1/25$ the difference starts being noticeable at around $\xi \approx 50$.

In short, we do not see the impact of the back-action unless the amplitude of the signal becomes comparable to that of the pump. However, if we assume the initial value of the signal is much smaller than that of the pump, even at large gains, the signal amplitude will never become strong enough to deplete the pump since the up-conversion processes will limit the gain beforehand.

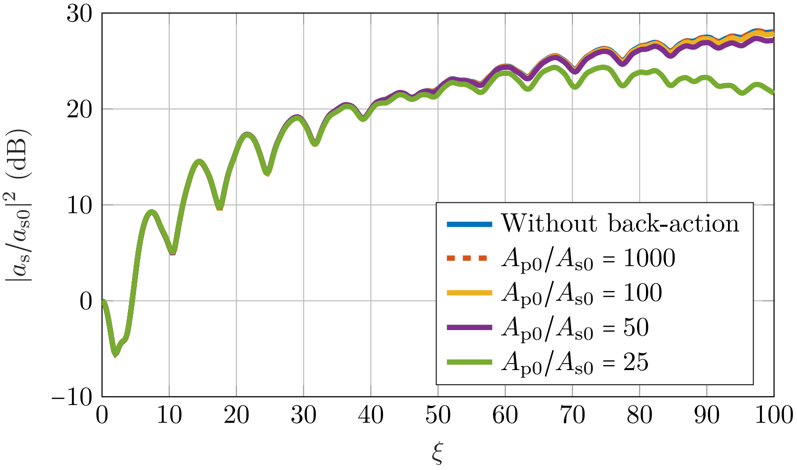

Figure 4.18: The gain for $\mu = 1$ at zero detuning for several initial signal amplitudes.

4.5.7 Conclusions

To conclude, we have developed and investigated a model for an arbitrary number of pump harmonics and up-converted signal and idler modes in the continuous limit. We have shown that it is not the phase mismatch on its own, nor the pumping strength on its own, that determines the wave propagation behaviour throughout the TWPA, but rather the relation between them. We have reduced this relation into a single scaling parameter μ which we call the “effective phase mismatch”. For large values of μ, there is no exponential gain due to the overwhelming phase mismatch. We have also shown that for small values μ, the gain is severely reduced due to a large amount of up-converted modes. A large gain can be achieved for small values of μ, but the propagation is initially lossy due to up-conversion; therefore one must use a very long TWPA to overcome the loss.

We have also shown that, under the assumption that the initial signal is much smaller than the initial pump, the pump depletion will not have any noticeable effect. The up-conversion processes seem to limit the gain before the signal amplitude becomes large enough to perturb the pump.

What our model does *not* capture is what happens when the pumping strength is large enough to make the highest harmonics close to cutoff. This is because of three reasons:

1. We have used the simplified propagation equations, Equation (4.13), where we have assumed linear dispersion for the coupling coefficients, instead of the full expression, Equation (4.12).
2. We have used a cubic approximation of the dispersion relation, Equation (2.16), which is an approximation that only holds for small frequencies, $\omega \ll \omega_\mathrm{c}$.
3. We have used the continuous wave equation instead of the discrete wave equation, that gives us differential equations instead of difference equations.

All of these points are based on the assumption that the wavelengths are much longer than the unit cell length, which is equivalent with the frequencies being well below cutoff. However, as we have seen this is not necessarily true. The larger pumping strength, the more up-converted modes are generated. At some point the largest frequencies will be on the order of cutoff, and then the model will no longer be able to predict the response of the TWPA.

4.6 Comparisons with experiments

We have developed a quite complex model to capture all 3WM processes in the TWPA, in order to determine what actually happens when we insert a pump and a signal. We have fairly conclusive results on the theory model, recall Section 4.5, but in the end the most important question is: does the theory predict the reality well?

In order to experimentally verify the model we use a SNAIL-TWPA. We choose a SNAIL-TWPA, since it is able to suppress 4WM, which is not accounted for in our model yet. Recall the SNAIL, Figure 3.6. The SNAIL-TWPA we used has $N = 440$ unit cells, $\mathcal{N} = 3$ identical junctions on arm one with critical current $I_\mathrm{c} = 3\,\mu\mathrm{A}$, and the lone junction has a critical current of $\alpha I_\mathrm{c} = 0.8\,\mu\mathrm{A}$. The zero-bias inductance of one of the junctions in arm 1 is hence $L_{\mathrm{J}0} \approx 109.7\,\mathrm{pH}$. The capacitance of the SNAIL is expected to be around $C_{\circledcirc} \approx 17.9\,\mathrm{fF}$ and the ground capacitance $C_0 = 154\,\mathrm{fF}$. The flux bias is applied via a coil in the proximity of the TWPA, which we feed a current through. In order to calibrate the current through the coil that corresponds to a flux quantum, we keep increasing the current until we can see several periods of the transmission profile. Then we know the amount of the current that corresponds to a magnetic flux quantum, as well as if there is an offset between zero flux and zero current. The setup is sketched in Figure 4.19.

We bias the SNAIL-TWPA at $\Phi_\mathrm{b} = 0.4\Phi_0$ which makes the mixing coefficients $c_3 \approx 0.82$ and $c_4 \approx 0$, recall Figure 3.8. We set the pump frequency to $f_\mathrm{p} = 8.5\,\mathrm{GHz}$ and increase the pump power until we see that the signal is amplified. We keep increasing the pump power until the gain drops. The gain is measured with a vector network analyser (VNA) by sweeping the frequency of a signal with a power much smaller than the pump power, and comparing it with the transmission we get when the pump is off. This we call the *parametric* gain, as it compares the transmission when there are parametric effects in the TWPA, with when the parametric effects are absent. If one wants to measure the *effective* gain, the transmission of the TWPA is to be compared with the transmission through a bypass SMA cable, as that is what would be used if there were no TWPA. The effective gain is expected to be slightly smaller than the parametric gain, as it includes the losses of the unpumped TWPA.

Once we have the measured gain of the TWPA, the goal is to simulate it and compare the measured data with the simulated data. The parameters for the simulation are the detuning δ, the effective phase mismatch μ and the effective length ξ of the TWPA. The detuning is simple to compute, recall Equation (4.27). The values for μ and ξ do not, in theory, have any degrees of freedom. However, they depend on the pumping strength and the dispersion relation, and we do not know the exact values of these. On the pump line, there are attenuators of 74 dB, and we estimate that the line itself and its connectors have an attenuation of approximately 10 dB, but we do not know the exact value of this attenuation, and hence not the exact pumping strength. Nor do we know the exact inductances and capacitances of the TWPA, and hence not the exact dispersion relation. This gives us two parameters of uncertainty, either μ and ξ, or $\tilde{k}_{\mathrm{p}}$ and $A_{\mathrm{p}0}$.

As the starting point, we use the expected values of the inductance and the capacitances. For the given values $\mathcal{N} = 3$ and $\alpha = 0.8/3$ of the TWPA, and the bias $\Phi_{\mathrm{b}} = 0.4\Phi_0$, we get the inductance $L_0 \approx 3.48 \cdot 109.7\,\mathrm{pH} \approx 381.6\,\mathrm{pH}$. This combined with the ground capacitance of $C_0 = 154\,\mathrm{fF}$ results in $f_0 \approx 20.76\,\mathrm{GHz}$ and hence that $\tilde{\omega}_{\mathrm{p}} \approx 8.5/20.76 \approx 0.41$. Inserting this into the expected dispersion relation of the TWPA we get $\tilde{k}_{\mathrm{p}} \approx 0.42$. Now we only have one parameter of freedom, *i.e.* the pumping strength, so we sweep the pumping strength until we get a transmission comparable to the measured transmission at a pump power $P_{\mathrm{p}}^{\mathrm{source}} = -10\,\mathrm{dBm}$. Next we compare the data obtained from the simulation to the measurement and notice that the measured data has more phase mismatch than the simulated data, see Figure 4.20. This can be either because of too large inductance or too large capacitance, or both. Since the inductance is tunable and increases very fast when approaching $0.5\Phi_0$, recall Figure 3.7, we suspect that it was the inductance that is larger than expected, caused by a nonuniform magnetic flux bias. Other measurements done on other samples also indicate a nonuniform magnetic flux bias. Therefore we try simulating the TWPA with larger inductances and see that the fits capture the shape of the measured data much better for larger values, especially for $L_0 \approx 1.46 L_0^{\mathrm{exp}}$, also shown in Figure 4.20.

Once we found the inductance giving the appropriate amount of phase mismatch, as shown in Figure 4.20 for $L_0 = 1.46 L_0^{\mathrm{exp}}$, we know the pumping strength corresponding to the used pump source power, $P_{\mathrm{p}}^{\mathrm{source}} = -10\,\mathrm{dBm}$. To further verify that the model gives accurate predictions, we now change the pump source power and adjust the determined pumping strength correspondingly. The data for $P_{\mathrm{p}}^{\mathrm{source}} = -15\,\mathrm{dBm}$ and $P_{\mathrm{p}}^{\mathrm{source}} = -5\,\mathrm{dBm}$ with the fits for adjusted pumping strength are shown in Figure 4.21. As we can see, the fits also now capture the shape of the transmission very well, except that it overestimates the gain slightly for all frequencies below the pump frequency.

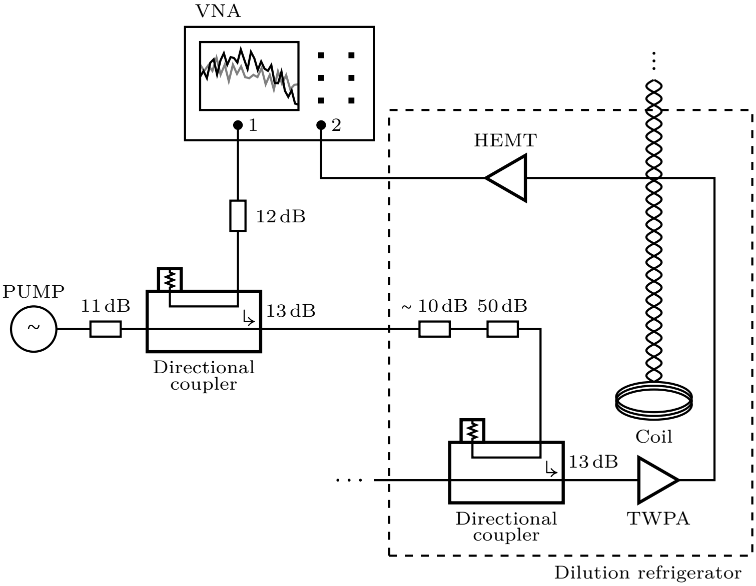

Figure 4.19: A simplified schematic of the experimental setup. The TWPA is placed inside a dilution refrigerator next to a coil. The transmission $|S_{21}|$ is measured with a vector network analyser (VNA). The signal and the pump are coupled together at room temperature using a directional coupler. The magnetic flux bias is applied via a DC voltage source at room temperature. The line into the dilution refrigerator has attenuators with 50 dB attenuation, but the line is estimated to have about ~ 10 dB additional attenuation. The signal line is connected to the coupled port of another directional coupler inside the dilution refrigerator giving an additional 13 dB of attenuation. The total attenuation for the pump, including the estimated line attenuation, is hence 84 dB. There are several details omitted in this schematic, such as circulators, connectors and switches.

For large pump powers, $P_\mathrm{p}^\mathrm{source} \gtrsim -5\,\mathrm{dBm}$, the corresponding fit starts to overestimate the gain more the larger the pump power is. This begins to be visible for $P_\mathrm{p}^\mathrm{source} = -5\,\mathrm{dBm}$ in Figure 4.21, but is more clearly shown for $P_\mathrm{p}^\mathrm{source} = 0\,\mathrm{dBm}$ in Figure 4.22. While this might seem discouraging, it is not surprising that the model does not work for these powers. One assumption we used when deriving this model is that all modes are well below cutoff, and another is that the pump-induced phase drop Δ_p is small. For the small pump powers, $P_\mathrm{p}^\mathrm{source} \lesssim -10\,\mathrm{dBm}$, Δ_p is small, see Table 4.1. Furthermore, $M_\mathrm{c} = 2$ so the highest pump harmonic is at least smaller than cutoff. However, for the larger pump powers, $P_\mathrm{p}^\mathrm{source} \gtrsim 0\,\mathrm{dBm}$, Δ_p is fairly large, and $M_\mathrm{c} \geq 3$, so there are harmonics needed at or above cutoff. In other words, the model does not work for the larger pump powers as the assumptions the model relies on are invalid.

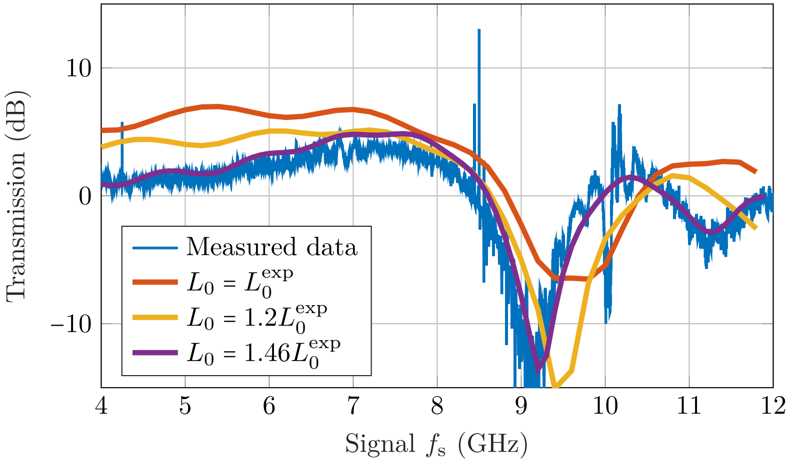

Figure 4.20: The measured data using $P_\mathrm{p}^\mathrm{source} = -10\,\mathrm{dBm}$ for the SNAIL-TWPA transmission (blue) with fits for expected inductance $L_0 = L_0^\mathrm{exp}$ (orange) and larger inductances (yellow and purple).

Features that are not captured in our model are the ripples, as well as the lossy feature seen around 10 GHz in Figure 4.20. The ripples are believed to be a consequence of the discreteness of the chain. We are fairly close to the cutoff frequency where, recall Figure 2.4, the discreteness of the chain results in multiple ripples. After amplification, these ripples may become larger. The lossy feature around 10 GHz is believed to be a resonance due to grounding problems. We have had similar features in other samples, which have disappeared after improving ground bonding.

It is worth pointing out that the theory is based on the assumption that all SNAILs have the same inductance, but both the experiment described above and other independently made experiments imply that the flux, and hence the inductance, is different at different points of the TWPA. While using the larger inductance $L_0 = 1.46L_0^{\mathrm{exp}}$ does seem to fairly well compensate for the nonuniformity of the flux, it is hard to know or predict what other effects it might lead to.

Table 4.1: Parameters extracted from the fitting the data in Figures 4.20 and 4.21. The $P_\mathrm{p}^\mathrm{source}$ is the pump power at the pump signal generator, $P_\mathrm{p}^\mathrm{exp}$ is the expected pump power at the TWPA, given the estimate of the line attenuation, while P_p is the pump power at the TWPA determined from the fits.

$P_\mathrm{p}^\mathrm{source}$ (dBm)	−15	−10	−5	0
$P_\mathrm{p}^\mathrm{exp}$ (dBm)	−99	−94	−89	−84
P_p (dBm)	−101.6	−96.6	−91.6	−86.6
χ	0.0126	0.0224	0.0398	0.0708
μ	15.18	8.54	4.80	2.70
ξ_max	2.77	4.93	8.76	15.58
Δ_p	0.06	0.11	0.19	0.35
I_p (nA)	52	93	165	294

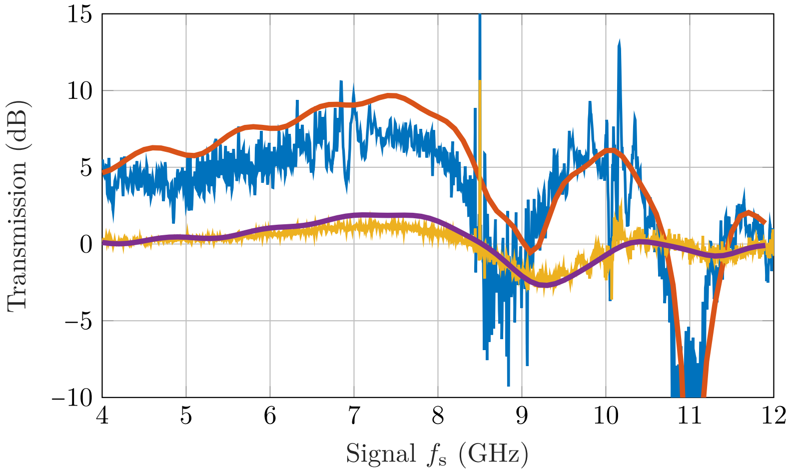

Figure 4.21: The measured data for $P_\mathrm{p}^\mathrm{source} = -5$ dBm (blue) and $P_\mathrm{p}^\mathrm{source} = -15$ dBm (yellow) with their respective fits (orange and purple).

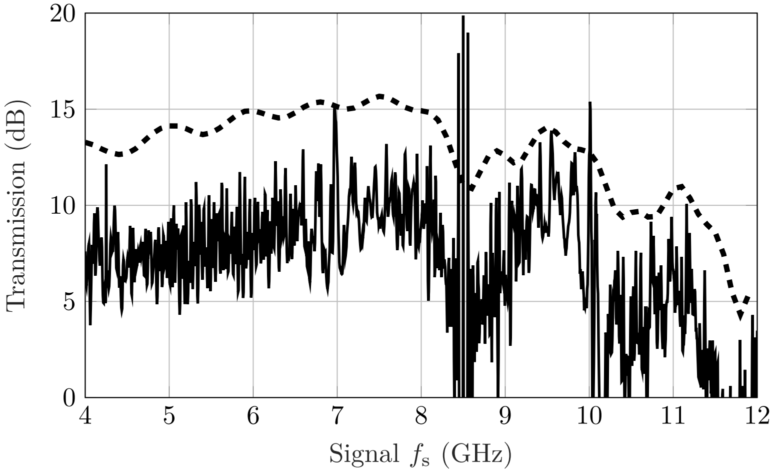

Figure 4.22: The measured data for $P_{\mathrm{p}}^{\mathrm{source}} = 0\,\mathrm{dBm}$ (solid) with its fit (dashed).

CHAPTER 5

Three-wave mixing for arbitrary frequencies

Until now we have used and developed our theory around the continuous wave equation to study wave propagation. However, this theory is only valid as long as all wavelengths are much longer than the length of the unit cell, or equivalently, as long as all frequencies are well below the cutoff frequency. This weak spot of the theory has two major problems. Firstly, for large pumping strengths in the quasi-linear regime, we saw that there was a lot of up-conversion, and at some point the highest pump harmonics reached the cutoff where the theory breaks down. Secondly, we cannot study the propagation of a signal when the signal frequency is close to the cutoff frequency to begin with.

In this chapter we will develop a theory that is built on the discrete propagation equations, which describe the propagation of waves with any frequency within the spectrum. It is complicated to solve the discrete propagation equations for multiple modes, as an equivalent to the general small frequency theory developed in Section 4.5. Therefore, we limit our study to the simplest case of three modes, as a discrete equivalent to the continuous three-mode model [10]. This allows us to investigate whether the pump and the signal can be placed close to the cutoff frequency in order to completely eliminate up-conversion. In the last section of the chapter we will also investigate different kinds of dispersion engineering, in order to reduce phase mismatch at large frequencies.

5.1 Eliminating up-conversion

In Section 4.5 we concluded that it is very challenging to achieve high gain for a TWPA in the small frequency limit, *i.e.* when the pump and the signal are well below the cutoff frequency ω_c, due to the large amount of up-conversion processes. Before doing more complicated measures to hinder up-conversion, such as dispersive engineering [18], we want to investigate if we can use the natural cutoff frequency of the TWPA itself to stop up-conversion, at least for some signal frequencies, and get exponential gain. To find the required pump and signal frequencies to stop up-conversion, we simply assume that the sum of signal and pump frequencies equal the cutoff and find $\omega_\mathrm{p}/\omega_\mathrm{c}$ with respect to $\omega_\mathrm{s}/\omega_\mathrm{p}$, and likewise for the idler. We get

$$\omega_\mathrm{p} + \omega_\mathrm{s} = \omega_\mathrm{c} \quad\Longrightarrow\quad \frac{\omega_\mathrm{p}}{\omega_\mathrm{c}} = \frac{1}{1 + \frac{\omega_\mathrm{s}}{\omega_\mathrm{p}}}, \tag{5.1a}$$

$$\omega_\mathrm{p} + \omega_\mathrm{i} = \omega_\mathrm{c} \quad\Longrightarrow\quad \frac{\omega_\mathrm{p}}{\omega_\mathrm{c}} = \frac{1}{2 - \frac{\omega_\mathrm{s}}{\omega_\mathrm{p}}}, \tag{5.1b}$$

which is illustrated in Figure 5.1. Here we see that if the pump frequency is smaller than half of the cutoff frequency, the pump, the signal and the idler can all up-convert at least once. If the pump is larger than half of the cutoff, the pump itself cannot up-convert, but the signal, the idler or both may still up-convert. However, once the pump frequency becomes larger than 2/3 of the cutoff, there opens up a band around half of the pump frequency where no up-conversion at all is possible. To find the width of this band, we solve Equations (5.1a) and (5.1b) for $\omega_\mathrm{s}/\omega_\mathrm{p}$ with respect to $\omega_\mathrm{p}/\omega_\mathrm{c}$, and find that the band is given by

$$\frac{\omega_\mathrm{c}}{\omega_\mathrm{p}} - 1 < \frac{\omega_\mathrm{s}}{\omega_\mathrm{p}} < 2 - \frac{\omega_\mathrm{c}}{\omega_\mathrm{p}}. \tag{5.2}$$

Expressed in terms of the detuning δ, recall Equation (4.27), we can write this as

$$|\delta| < 3 - 2\frac{\omega_\mathrm{c}}{\omega_\mathrm{p}} \quad \text{or} \quad \frac{\omega_\mathrm{p}}{\omega_\mathrm{c}} > \frac{2}{3 - |\delta|}. \tag{5.3}$$

To find the pump frequency to retrieve 1/3 or 2/3 of the full band, we set $|\delta|$ equal to 1/3 or 2/3 and solve Equation (5.3) for ω_p. These bands are also shown in Figure 5.1.

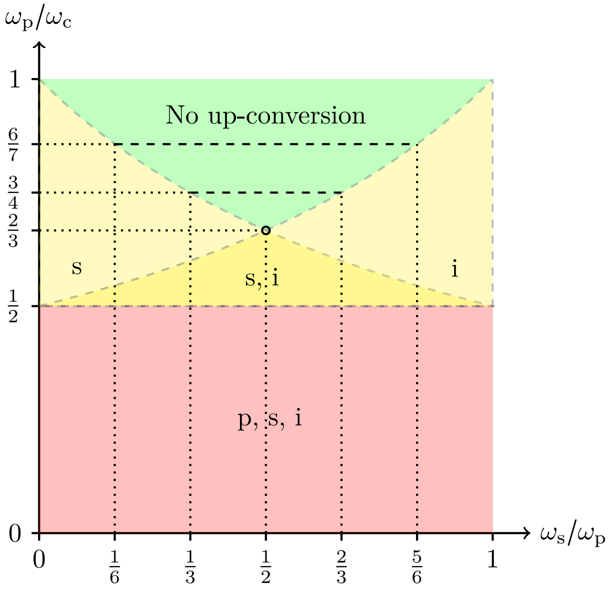

Figure 5.1: The regions of the presence/absence of up-conversion of pump, signal and idler. In the pink region all three modes can be up-converted, in the yellow region both signal and idler are up-converted but pump is not, in the light yellow regions only up-conversion of either signal or idler is possible, and in the green region no up-conversion takes place.

In short, the pump frequency must be larger than 2/3 of the cutoff frequency in order to get a band without up-conversion, and specifically larger than 3/4 of the cutoff in order to get at least 1/3 of the full band without up-conversion. If we try to use the continuous single idler model, described in Section 4.2, to analyse what the gain would be for a pump at any of these large frequencies, we run into 2 problems.

The first problem is that there is more and more phase mismatch the closer to the cutoff we get. From Chapter 4 we know that phase mismatch suppresses, and might prevent, exponential gain. The second problem is that in order to be able to work with the continuous wave equation, instead of the discrete wave equation, we assumed that all wavelengths are much larger than the unit cell length, or equivalently all frequencies are well below the cutoff frequency, recall Figure 2.2. Hence, we cannot use the continuous wave equation to analyse the propagation and transmission in the up-conversion-free regime; instead we must use the discrete wave equation.

5.2 General mixing equations

In this section we will derive general expressions for the mixing equations in the discrete regime. We begin with the discrete wave equation, recall Equation (3.7), but we ignore the four-wave mixing term and implement the unitless definitions used in Chapter 4. The discrete wave equation then reads

$$\begin{aligned}\frac{\mathrm{d}^2}{\mathrm{d}\tilde{t}^2}\phi_n - \left[\tilde{C}\frac{\mathrm{d}^2}{\mathrm{d}\tilde{t}^2} + 1\right](\phi_{n+1} - 2\phi_n + \phi_{n-1}) \\ = -\frac{c_3}{2}\left((\phi_{n+1} - \phi_n)^2 - (\phi_n - \phi_{n-1})^2\right).\end{aligned} \tag{5.4}$$

Now we use the *ansatz* that the node phases ϕ_n are given by

$$\phi_n\left(\tilde{t}\right) = \sum_m \phi_{m,n}\left(\tilde{t}\right) = \frac{1}{2}\sum_m A_{m,n}\mathrm{e}^{\mathrm{i}\left(\tilde{k}_m n - \tilde{\omega}_m\tilde{t}\right)} + \bar{A}_{m,n}\mathrm{e}^{-\mathrm{i}\left(\tilde{k}_m n - \tilde{\omega}_m\tilde{t}\right)} \tag{5.5}$$

where $\phi_{m,n}$ is the node phase of mode m at node n.

5.2.1 Simplifying the free wave terms

As we know from the derivation of the dispersion relation, recall Section 2.2, Equation (5.4) describes the propagation of the free waves if the right-hand side of the equation is equal to zero. However, since the right-hand side is not equal to zero we can no longer assume constant amplitudes, just as in Section 4.1. Hence further analysis is needed.

When applying the second time derivative to the node phases we get

$$\frac{\mathrm{d}^2\phi_n}{\mathrm{d}\tilde{t}^2} = \sum_m -\tilde{\omega}_m^2\phi_{m,n}, \tag{5.6}$$

and the left-hand side can hence be written as

$$\mathrm{LHS} = \sum_m -\tilde{\omega}_m^2 \phi_{m,n} - \left(1 - \tilde{C}\tilde{\omega}_m^2\right)\left(\phi_{m,n+1} - 2\phi_{m,n} + \phi_{m,n-1}\right) \tag{5.7}$$

where the last parenthesis can be written as

$$A_{m,n}\mathrm{e}^{\mathrm{i}\left(\tilde{k}_m n - \tilde{\omega}_m \tilde{t}\right)}\left(\frac{A_{m,n+1}}{A_{m,n}}\mathrm{e}^{\mathrm{i}\tilde{k}_m} - 2 + \frac{A_{m,n-1}}{A_{m,n}}\mathrm{e}^{-\mathrm{i}\tilde{k}_m}\right) + \text{c.c.}, \tag{5.8}$$

where the amplitude fractions would be unity in a linear medium, but will differ when there is mixing.

5.2.2 Simplifying the mixing terms

Just as for the continuous analogue in Section 4.1, the full expression of the right-hand side will contain multiple terms and will be hard to fit on this page, as well as fully analyse. However, we can apply the same technique as before, and only study the mixing terms resonant with each wave, and neglect the rest.

Assume we have the three waves m, q, r, and that the frequencies have the relationship $\tilde{\omega}_m = \tilde{\omega}_q - \tilde{\omega}_r$. There will be two terms from $(\phi_{n+1} - \phi_n)^2$ and another two terms from $(\phi_n - \phi_{n-1})^2$ that will resonate with m. The contribution for this mixing process for $(\phi_{n+1} - \phi_n)^2$ is hence

$$\begin{aligned}
&\frac{1}{2}\left(A_{q,n+1}\mathrm{e}^{\mathrm{i}\left(\tilde{k}_q(n+1) - \tilde{\omega}_q \tilde{t}\right)} - A_{q,n}\mathrm{e}^{\mathrm{i}\left(\tilde{k}_q n - \tilde{\omega}_q \tilde{t}\right)}\right)\\
&\cdot\frac{1}{2}\left(\bar{A}_{r,n+1}\mathrm{e}^{-\mathrm{i}\left(\tilde{k}_r(n+1) - \tilde{\omega}_r \tilde{t}\right)} - \bar{A}_{r,n}\mathrm{e}^{-\mathrm{i}\left(\tilde{k}_r n - \tilde{\omega}_r \tilde{t}\right)}\right)\\
&+\frac{1}{2}\left(\bar{A}_{r,n+1}\mathrm{e}^{-\mathrm{i}\left(\tilde{k}_r(n+1) - \tilde{\omega}_r \tilde{t}\right)} - \bar{A}_{r,n}\mathrm{e}^{-\mathrm{i}\left(\tilde{k}_r n - \tilde{\omega}_r \tilde{t}\right)}\right)\\
&\cdot\frac{1}{2}\left(A_{q,n+1}\mathrm{e}^{\mathrm{i}\left(\tilde{k}_q(n+1) - \tilde{\omega}_q \tilde{t}\right)} - A_{q,n}\mathrm{e}^{\mathrm{i}\left(\tilde{k}_q n - \tilde{\omega}_q \tilde{t}\right)}\right)\\
&=\frac{1}{2}\mathrm{e}^{\mathrm{i}\left(\left(\tilde{k}_q - \tilde{k}_r\right)n - \tilde{\omega}_m \tilde{t}\right)}\left(A_{q,n+1}\mathrm{e}^{\mathrm{i}\tilde{k}_q} - A_{q,n}\right)\left(\bar{A}_{r,n+1}\mathrm{e}^{-\mathrm{i}\tilde{k}_r} - \bar{A}_{r,n}\right)
\end{aligned} \tag{5.9}$$

and analog for $(\phi_n - \phi_{n-1})^2$. For the transition $\tilde{\omega}_m = \tilde{\omega}_q + \tilde{\omega}_r$ we instead get

$$\begin{aligned}
&\frac{1}{2}\left(A_{q,n+1}\mathrm{e}^{\mathrm{i}\left(\tilde{k}_q(n+1)-\tilde{\omega}_q\tilde{t}\right)} - A_{q,n}\mathrm{e}^{\mathrm{i}\left(\tilde{k}_q n-\tilde{\omega}_q\tilde{t}\right)}\right)\\
\cdot&\frac{1}{2}\left(A_{r,n+1}\mathrm{e}^{\mathrm{i}\left(\tilde{k}_r(n+1)-\tilde{\omega}_r\tilde{t}\right)} - A_{r,n}\mathrm{e}^{\mathrm{i}\left(\tilde{k}_r n-\tilde{\omega}_r\tilde{t}\right)}\right)\\
+&\frac{1}{2}\left(A_{r,n+1}\mathrm{e}^{\mathrm{i}\left(\tilde{k}_r(n+1)-\tilde{\omega}_r\tilde{t}\right)} - A_{r,n}\mathrm{e}^{\mathrm{i}\left(\tilde{k}_r n-\tilde{\omega}_r\tilde{t}\right)}\right)\\
\cdot&\frac{1}{2}\left(A_{q,n+1}\mathrm{e}^{\mathrm{i}\left(\tilde{k}_q(n+1)-\tilde{\omega}_q\tilde{t}\right)} - A_{q,n}\mathrm{e}^{\mathrm{i}\left(\tilde{k}_q n-\tilde{\omega}_q\tilde{t}\right)}\right)\\
=&\frac{1}{2}\mathrm{e}^{\mathrm{i}\left((\tilde{k}_q+\tilde{k}_r)n-\tilde{\omega}_m\tilde{t}\right)}\left(A_{q,n+1}\mathrm{e}^{\mathrm{i}\tilde{k}_q} - A_{q,n}\right)\left(A_{r,n+1}\mathrm{e}^{\mathrm{i}\tilde{k}_r} - A_{r,n}\right)
\end{aligned}\tag{5.10}$$

but if it is degenerate, $\tilde{\omega}_m = 2\tilde{\omega}_q$, we only get

$$\begin{aligned}
&\frac{1}{2}\left(A_{q,n+1}\mathrm{e}^{\mathrm{i}\left(\tilde{k}_q(n+1)-\tilde{\omega}_q\tilde{t}\right)} - A_{q,n}\mathrm{e}^{\mathrm{i}\left(\tilde{k}_q n-\tilde{\omega}_q\tilde{t}\right)}\right)\\
\cdot&\frac{1}{2}\left(A_{q,n+1}\mathrm{e}^{\mathrm{i}\left(\tilde{k}_q(n+1)-\tilde{\omega}_q\tilde{t}\right)} - A_{q,n}\mathrm{e}^{\mathrm{i}\left(\tilde{k}_q n-\tilde{\omega}_q\tilde{t}\right)}\right)\\
=&\frac{1}{4}\mathrm{e}^{\mathrm{i}\left(2\tilde{k}_q n-\tilde{\omega}_m\tilde{t}\right)}\left(A_{q,n+1}\mathrm{e}^{\mathrm{i}\tilde{k}_q} - A_{q,n}\right)^2 .
\end{aligned}\tag{5.11}$$

5.2.3 Constructing the discrete propagation equations

Now that we have simplified both sides of Equation (5.4), we can retrieve the discrete analogue of the continuous propagation equations, Equation (4.12) in Section 4.1. In the continuous limit we got differential equations, but now taking the discreteness of the TWPA into consideration we instead get difference equations.

For each wave, we begin by only retrieving the resonant terms and then divide the left-hand side with its exponential factor. The propagation equation for the amplitude of each wave m becomes

$$\begin{aligned}
&A_{m,n}\left(\tilde{\omega}_m^2+\left(1-\tilde{C}\tilde{\omega}_m^2\right)\left(\frac{A_{m,n+1}}{A_{m,n}}\mathrm{e}^{\mathrm{i}\tilde{k}_m}-2+\frac{A_{m,n-1}}{A_{m,n}}\mathrm{e}^{-\mathrm{i}\tilde{k}_m}\right)\right)\\
&=\sum_{q,r:\ \tilde{\omega}_m=\tilde{\omega}_q-\tilde{\omega}_r}\frac{c_3}{2}\mathrm{e}^{\mathrm{i}\left(\tilde{k}_q-\tilde{k}_r-\tilde{k}_m\right)n}A_{q,n}\bar{A}_{r,n}\\
&\cdot\left[\left(\frac{A_{q,n+1}}{A_{q,n}}\mathrm{e}^{\mathrm{i}\tilde{k}_q}-1\right)\left(\frac{\bar{A}_{r,n+1}}{\bar{A}_{r,n}}\mathrm{e}^{-\mathrm{i}\tilde{k}_r}-1\right)\right.\\
&\left.-\left(1-\frac{A_{q,n-1}}{A_{q,n}}\mathrm{e}^{-\mathrm{i}\tilde{k}_q}\right)\left(1-\frac{\bar{A}_{r,n-1}}{\bar{A}_{r,n}}\mathrm{e}^{\mathrm{i}\tilde{k}_r}\right)\right]\\
&+\frac{1}{2}\sum_{q,r:\ \tilde{\omega}_m=\tilde{\omega}_q+\tilde{\omega}_r}\frac{c_3}{2}\mathrm{e}^{-\mathrm{i}\left(\tilde{k}_m-\tilde{k}_q-\tilde{k}_r\right)n}A_{q,n}A_{r,n}\\
&\cdot\left[\left(\frac{A_{q,n+1}}{A_{q,n}}\mathrm{e}^{\mathrm{i}\tilde{k}_q}-1\right)\left(\frac{A_{r,n+1}}{A_{r,n}}\mathrm{e}^{\mathrm{i}\tilde{k}_r}-1\right)\right.\\
&\left.-\left(1-\frac{A_{q,n-1}}{A_{q,n}}\mathrm{e}^{-\mathrm{i}\tilde{k}_q}\right)\left(1-\frac{A_{r,n-1}}{A_{r,n}}\mathrm{e}^{-\mathrm{i}\tilde{k}_r}\right)\right].
\end{aligned}\tag{5.12}$$

5.3 The discrete single idler model

In this section we will study the single idler model, just as in Section 4.2, but now using the discrete propagation equations. In other words, we will assume that there are only three waves present: the pump ‘p’, the signal ‘s’ fulfilling $\tilde{\omega}_\mathrm{s} < \tilde{\omega}_\mathrm{p}$ and the idler ‘i’ given by $\tilde{\omega}_\mathrm{i} = \tilde{\omega}_\mathrm{p} - \tilde{\omega}_\mathrm{s}$. We know from Section 4.5 that the assumption that these waves are the only waves present is a bad assumption *if the waves can up-convert.* But since we now will use the discrete propagation equations, as described in Equation (5.12), we are no longer limited to small frequencies and may place the pump close to the cutoff frequency, which will open up a band free of up-conversion as described in Section 5.1.

5.3.1 The propagation equations

We begin by reusing the assumption of small signal amplitude, $A_{\mathrm{s}0} \ll A_{\mathrm{p}0}$, which combined with a large pump frequency, $\omega_\mathrm{p} > \frac{1}{2}\omega_\mathrm{c}$, lets us assume a constant pump amplitude throughout the TWPA. Let us also reuse the definition for the phase mismatch, $\Delta\tilde{k} = \tilde{k}_\mathrm{p} - \tilde{k}_\mathrm{s} - \tilde{k}_\mathrm{i}$, then the propagation equations for the signal and the idler become

$$\begin{aligned} &A_{\mathrm{s},n}\left(\tilde{\omega}_\mathrm{s}^2 + \left(1 - \tilde{C}\tilde{\omega}_\mathrm{s}^2\right)\left(\frac{A_{\mathrm{s},n+1}}{A_{\mathrm{s},n}}\mathrm{e}^{\mathrm{i}\tilde{k}_\mathrm{s}} - 2 + \frac{A_{\mathrm{s},n-1}}{A_{\mathrm{s},n}}\mathrm{e}^{-\mathrm{i}\tilde{k}_\mathrm{s}}\right)\right) \\ &= \frac{c_3}{2}\mathrm{e}^{\mathrm{i}\Delta\tilde{k}n} A_{\mathrm{p},n}\bar{A}_{\mathrm{i},n} \\ &\cdot\left[\left(\mathrm{e}^{\mathrm{i}\tilde{k}_\mathrm{p}} - 1\right)\left(\frac{\bar{A}_{\mathrm{i},n+1}}{\bar{A}_{\mathrm{i},n}}\mathrm{e}^{-\mathrm{i}\tilde{k}_\mathrm{i}} - 1\right) - \left(1 - \mathrm{e}^{-\mathrm{i}\tilde{k}_\mathrm{p}}\right)\left(1 - \frac{\bar{A}_{\mathrm{i},n-1}}{\bar{A}_{\mathrm{i},n}}\mathrm{e}^{\mathrm{i}\tilde{k}_\mathrm{i}}\right)\right], \end{aligned} \tag{5.13a}$$

$$\begin{aligned} &A_{\mathrm{i},n}\left(\tilde{\omega}_\mathrm{i}^2 + \left(1 - \tilde{C}\tilde{\omega}_\mathrm{i}^2\right)\left(\frac{A_{\mathrm{i},n+1}}{A_{\mathrm{i},n}}\mathrm{e}^{\mathrm{i}\tilde{k}_\mathrm{i}} - 2 + \frac{A_{\mathrm{i},n-1}}{A_{\mathrm{i},n}}\mathrm{e}^{-\mathrm{i}\tilde{k}_\mathrm{i}}\right)\right) \\ &= \frac{c_3}{2}\mathrm{e}^{\mathrm{i}\Delta\tilde{k}n} A_{\mathrm{p},n}\bar{A}_{\mathrm{s},n} \\ &\cdot\left[\left(\mathrm{e}^{\mathrm{i}\tilde{k}_\mathrm{p}} - 1\right)\left(\frac{\bar{A}_{\mathrm{s},n+1}}{\bar{A}_{\mathrm{s},n}}\mathrm{e}^{-\mathrm{i}\tilde{k}_\mathrm{s}} - 1\right) - \left(1 - \mathrm{e}^{-\mathrm{i}\tilde{k}_\mathrm{p}}\right)\left(1 - \frac{\bar{A}_{\mathrm{s},n-1}}{\bar{A}_{\mathrm{s},n}}\mathrm{e}^{\mathrm{i}\tilde{k}_\mathrm{s}}\right)\right]. \end{aligned} \tag{5.13b}$$

5.3.2 Solving the propagation equations

To solve Equations (5.13a) and (5.13b), we take inspiration from Section 4.2 and use similar transformations,

$$A_{\mathrm{s},n} = B_\mathrm{s} \cdot \mathrm{e}^{\mathrm{i}\Delta\tilde{k}n/2} \cdot \mathrm{e}^{\mathrm{i}\lambda n}, \tag{5.14a}$$

$$A_{\mathrm{i},n} = \bar{B}_\mathrm{i} \cdot \mathrm{e}^{\mathrm{i}\Delta\tilde{k}n/2} \cdot \mathrm{e}^{\mathrm{i}\lambda n}. \tag{5.14b}$$

Here λ is very similar to the gain coefficient, with the relation $\lambda = -\mathrm{i}g$, *i.e.* a negative imaginary component of λ gives rise to exponential gain. This way of defining λ simplifies the calculations at a later point. With these transformations, the amplitude fractions become

$$\frac{A_{\mathrm{s},n+1}}{A_{\mathrm{s},n}} = \frac{B_\mathrm{s} \cdot \mathrm{e}^{\mathrm{i}\Delta\tilde{k}(n+1)/2} \cdot \mathrm{e}^{\mathrm{i}\lambda(n+1)}}{B_\mathrm{s} \cdot \mathrm{e}^{\mathrm{i}\Delta\tilde{k}n/2} \cdot \mathrm{e}^{\mathrm{i}\lambda n}} = \mathrm{e}^{\mathrm{i}\left(\lambda+\Delta\tilde{k}/2\right)}, \tag{5.15a}$$

$$\frac{A_{\mathrm{s},n-1}}{A_{\mathrm{s},n}} = \frac{B_\mathrm{s} \cdot \mathrm{e}^{\mathrm{i}\Delta\tilde{k}(n-1)/2} \cdot \mathrm{e}^{\mathrm{i}\lambda(n-1)}}{B_\mathrm{s} \cdot \mathrm{e}^{\mathrm{i}\Delta\tilde{k}n/2} \cdot \mathrm{e}^{\mathrm{i}\lambda n}} = \mathrm{e}^{-\mathrm{i}\left(\lambda+\Delta\tilde{k}/2\right)}, \tag{5.15b}$$

$$\frac{A_{\mathrm{i},n+1}}{A_{\mathrm{i},n}} = \frac{\bar{B}_\mathrm{i} \cdot \mathrm{e}^{\mathrm{i}\Delta\tilde{k}(n+1)/2} \cdot \mathrm{e}^{-\mathrm{i}\bar{\lambda}(n+1)}}{\bar{B}_\mathrm{i} \cdot \mathrm{e}^{\mathrm{i}\Delta\tilde{k}n/2} \cdot \mathrm{e}^{-\mathrm{i}\bar{\lambda} n}} = \mathrm{e}^{\mathrm{i}\left(\Delta\tilde{k}/2-\bar{\lambda}\right)}, \tag{5.15c}$$

$$\frac{A_{\mathrm{i},n-1}}{A_{\mathrm{i},n}} = \frac{\bar{B}_\mathrm{i} \cdot \mathrm{e}^{\mathrm{i}\Delta\tilde{k}(n-1)/2} \cdot \mathrm{e}^{-\mathrm{i}\bar{\lambda}(n-1)}}{\bar{B}_\mathrm{i} \cdot \mathrm{e}^{\mathrm{i}\Delta\tilde{k}n/2} \cdot \mathrm{e}^{-\mathrm{i}\bar{\lambda} n}} = \mathrm{e}^{-\mathrm{i}\left(\Delta\tilde{k}/2-\bar{\lambda}\right)}. \tag{5.15d}$$

Inserting these values of the fractions into Equations (5.13a) and (5.13b), they are simplified to

$$\begin{aligned} &B_\mathrm{s}\left(\tilde{\omega}_\mathrm{s}^2 - 4\left(1-\tilde{C}\tilde{\omega}_\mathrm{s}^2\right)\sin^2\!\left(\frac{\lambda+\Delta\tilde{k}/2+\tilde{k}_\mathrm{s}}{2}\right)\right) = \frac{c_3}{2}A_\mathrm{p}B_\mathrm{i} \\ &\times\left[\left(\mathrm{e}^{\mathrm{i}\tilde{k}_\mathrm{p}}-1\right)\left(\mathrm{e}^{\mathrm{i}\left(\lambda-\Delta\tilde{k}/2-\tilde{k}_\mathrm{i}\right)}-1\right)-\left(1-\mathrm{e}^{-\mathrm{i}\tilde{k}_\mathrm{p}}\right)\left(1-\mathrm{e}^{\mathrm{i}\left(\Delta\tilde{k}/2+\tilde{k}_\mathrm{i}-\lambda\right)}\right)\right] \end{aligned} \tag{5.16a}$$

and

$$\begin{aligned} &B_\mathrm{i}\left(\tilde{\omega}_\mathrm{i}^2 - 4\left(1-\tilde{C}\tilde{\omega}_\mathrm{i}^2\right)\sin^2\!\left(\frac{\lambda-\Delta\tilde{k}/2-\tilde{k}_\mathrm{i}}{2}\right)\right) = \frac{c_3}{2}A_\mathrm{p}B_\mathrm{s} \\ &\times\left[\left(\mathrm{e}^{-\mathrm{i}\tilde{k}_\mathrm{p}}-1\right)\left(\mathrm{e}^{\mathrm{i}\left(\lambda+\Delta\tilde{k}/2+\tilde{k}_\mathrm{s}\right)}-1\right)-\left(1-\mathrm{e}^{\mathrm{i}\tilde{k}_\mathrm{p}}\right)\left(1-\mathrm{e}^{-\mathrm{i}\left(\lambda+\Delta\tilde{k}/2+\tilde{k}_\mathrm{s}\right)}\right)\right]. \end{aligned} \tag{5.16b}$$

Let us note that

$$\begin{aligned} \Delta\tilde{k}/2+\tilde{k}_\mathrm{s} &= \frac{1}{2}\left(\tilde{k}_\mathrm{p}-\tilde{k}_\mathrm{s}-\tilde{k}_\mathrm{i}\right)+\tilde{k}_\mathrm{s} = \frac{1}{2}\left(\tilde{k}_\mathrm{p}+\tilde{k}_\mathrm{s}-\tilde{k}_\mathrm{i}\right), \\ \Delta\tilde{k}/2+\tilde{k}_\mathrm{i} &= \frac{1}{2}\left(\tilde{k}_\mathrm{p}-\tilde{k}_\mathrm{s}-\tilde{k}_\mathrm{i}\right)+\tilde{k}_\mathrm{i} = \frac{1}{2}\left(\tilde{k}_\mathrm{p}-\left(\tilde{k}_\mathrm{s}-\tilde{k}_\mathrm{i}\right)\right), \end{aligned} \tag{5.17}$$

so by defining

$$\tilde{\kappa} = \tilde{k}_\mathrm{s}-\tilde{k}_\mathrm{i}-2\lambda, \tag{5.18}$$

we can write Equations (5.16a) and (5.16b) as

$$\begin{aligned} &B_\mathrm{s}\left(\tilde{\omega}_\mathrm{s}^2 - 4\left(1 - \tilde{C}\tilde{\omega}_\mathrm{s}^2\right)\sin^2\left(\frac{\tilde{k}_\mathrm{p} + \tilde{\kappa}}{4}\right)\right) = \frac{c_3}{2}A_\mathrm{p}B_\mathrm{i} \\ &\times\left[\left(\mathrm{e}^{\mathrm{i}\tilde{k}_\mathrm{p}} - 1\right)\left(\mathrm{e}^{\mathrm{i}\left(\tilde{k}_\mathrm{p}-\tilde{\kappa}\right)/2} - 1\right) - \left(1 - \mathrm{e}^{-\mathrm{i}\tilde{k}_\mathrm{p}}\right)\left(1 - \mathrm{e}^{\mathrm{i}\left(\tilde{k}_\mathrm{p}-\tilde{\kappa}\right)/2}\right)\right] \end{aligned} \tag{5.19a}$$

and

$$\begin{aligned} &B_\mathrm{i}\left(\tilde{\omega}_\mathrm{i}^2 - 4\left(1 - \tilde{C}\tilde{\omega}_\mathrm{i}^2\right)\sin^2\left(\frac{\tilde{k}_\mathrm{p} - \tilde{\kappa}}{4}\right)\right) = \frac{c_3}{2}A_\mathrm{p}B_\mathrm{s} \\ &\times\left[\left(\mathrm{e}^{-\mathrm{i}\tilde{k}_\mathrm{p}} - 1\right)\left(\mathrm{e}^{\mathrm{i}\left(\tilde{k}_\mathrm{p}+\tilde{\kappa}\right)/2} - 1\right) - \left(1 - \mathrm{e}^{\mathrm{i}\tilde{k}_\mathrm{p}}\right)\left(1 - \mathrm{e}^{-\mathrm{i}\left(\tilde{k}_\mathrm{p}+\tilde{\kappa}\right)/2}\right)\right]. \end{aligned} \tag{5.19b}$$

We can rewrite Equations (5.19a) and (5.19b) using the matrix form,

$$\underbrace{\begin{bmatrix} \mathcal{M}_{1,1} & \mathcal{M}_{1,2} \\ \mathcal{M}_{2,1} & \mathcal{M}_{2,2} \end{bmatrix}}_{\mathcal{M}}\begin{bmatrix} B_\mathrm{s} \\ B_\mathrm{i} \end{bmatrix} = \begin{bmatrix} 0 \\ 0 \end{bmatrix} \tag{5.20}$$

where

$$\mathcal{M}_{1,1} = \tilde{\omega}_\mathrm{s}^2 - 4\left(1 - \tilde{C}\tilde{\omega}_\mathrm{s}^2\right)\sin^2\left(\frac{\tilde{k}_\mathrm{p} + \tilde{\kappa}}{4}\right), \tag{5.21a}$$

$$\mathcal{M}_{1,2} = -\frac{c_3}{2}A_\mathrm{p}\left[\left(\mathrm{e}^{\mathrm{i}\tilde{k}_\mathrm{p}} - 1\right)\left(\mathrm{e}^{-\mathrm{i}\left(\tilde{k}_\mathrm{p}-\tilde{\kappa}\right)/2} - 1\right) - \left(1 - \mathrm{e}^{-\mathrm{i}\tilde{k}_\mathrm{p}}\right)\left(1 - \mathrm{e}^{\mathrm{i}\left(\tilde{k}_\mathrm{p}-\tilde{\kappa}\right)/2}\right)\right], \tag{5.21b}$$

$$\mathcal{M}_{2,1} = -\frac{c_3}{2}A_\mathrm{p}\left[\left(\mathrm{e}^{-\mathrm{i}\tilde{k}_\mathrm{p}} - 1\right)\left(\mathrm{e}^{\mathrm{i}\left(\tilde{k}_\mathrm{p}+\tilde{\kappa}\right)/2} - 1\right) - \left(1 - \mathrm{e}^{\mathrm{i}\tilde{k}_\mathrm{p}}\right)\left(1 - \mathrm{e}^{-\mathrm{i}\left(\tilde{k}_\mathrm{p}+\tilde{\kappa}\right)/2}\right)\right], \tag{5.21c}$$

$$\mathcal{M}_{2,2} = \tilde{\omega}_\mathrm{i}^2 - 4\left(1 - \tilde{C}\tilde{\omega}_\mathrm{i}^2\right)\sin^2\left(\frac{\tilde{k}_\mathrm{p} - \tilde{\kappa}}{4}\right). \tag{5.21d}$$

Now, if $\det(\mathcal{M}) \neq 0$, the only solution to Equation (5.20) is $B_\mathrm{s} = B_\mathrm{i} = 0$, which does not agree with Equation (5.14a) if the initial signal amplitude is nonzero. Therefore we know that $\det(\mathcal{M}) = 0$, which gives us the equation

$$\mathcal{M}_{1,1}\mathcal{M}_{2,2} - \mathcal{M}_{1,2}\mathcal{M}_{2,1} = 0, \tag{5.22}$$

which we numerically solve for λ.

5.3.3 Comparison with the continuous model

In Figure 5.2 we compare the numerical solution of Equation (5.22) derived using the discrete theory for $g = -\mathrm{Im}(\lambda)$ with the solutions from the continuous equations, both for the full expression using nonlinear coupling coefficients (Equation (4.12)) as well as the simplified expression using linear coupling coefficients (Equation (4.13)). We note 3 key features in this figure:

1. In the low frequency limit, all solutions match. This is expected since the continuous equations are the approximation of the discrete equations in the low frequency limit, and the difference between linear coupling and nonlinear coupling goes to zero when the frequencies become small.

2. More importantly, we can see that neither of the continuous equations can predict the correct gain coefficient in the large frequency limit. More specifically, the nonlinear coupling equations (solution to Equation (4.12)) overestimate the gain coefficient, while the linear coupling equations (solution to Equation (4.13)) underestimate the gain coefficient.

3. Most importantly, it is theoretically possible to get exponential gain for a pump at large frequencies, *e.g.* $\omega_{\mathrm{p}} = 3\omega_{\mathrm{c}}/4 = 1.5\omega_0$ where we get $1/3$ of the full band free of up-conversion (recall Figure 5.1), as long as the pumping strength is large enough, $\chi \approx 0.1$. We solve Equation (5.22) for multiple pumping strengths and multiple pump frequencies. For each pumping strength we determine the threshold pump frequency $\tilde{\omega}_{\mathrm{th}}$ where exponential gain is completely hindered, *i.e.* where the real part of the gain coefficient becomes zero, see Figure 5.3.

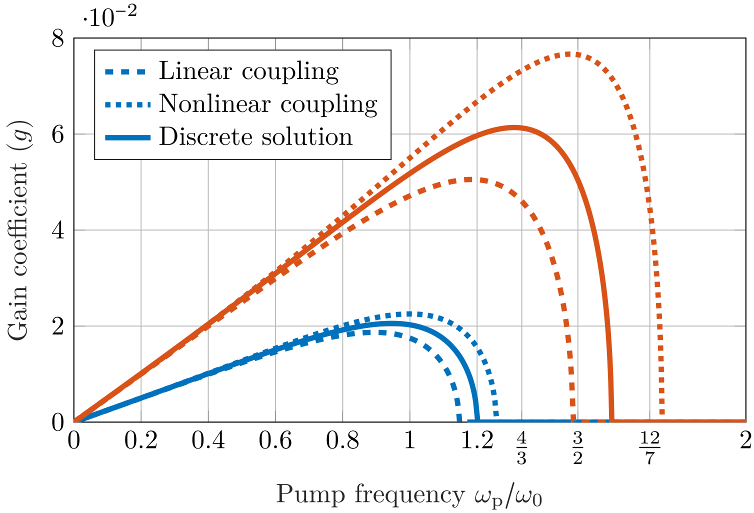

Figure 5.2: The gain coefficient from numerically solving Equation (5.22) (solid) compared with the solution to Equation (4.12) (dotted) and the solution to Equation (4.13) for different pumping strengths, $\chi = 0.05$ (blue) and $\chi = 0.1$ (orange). The solutions are found for $\tilde{C} = 0$ and $\delta = 0$.

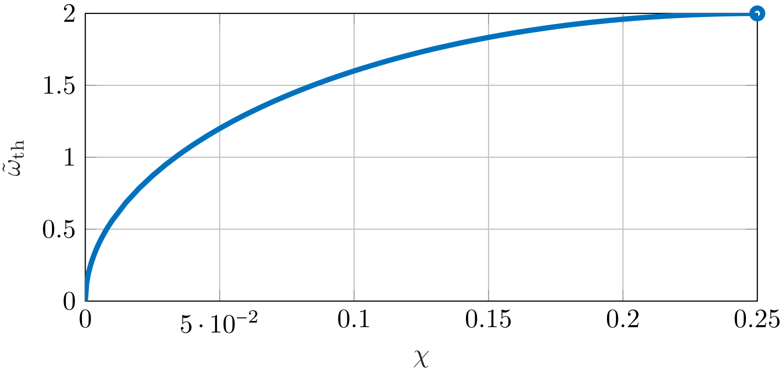

Figure 5.3: The pump frequency $\tilde{\omega}_{\text{th}}$ for a given pumping strength χ where the phase mismatch becomes so large that it hinders exponential gain. When $\chi \geq 0.25$, there is exponential gain even for the largest possible pump frequency, $\tilde{\omega}_p = 2$.

5.3.4 Realistic pumping strengths

Now, an important question is: how large of pumping strength can we achieve? From Equation (5.3) we know the pump frequency that is required to achieve a desired bandwidth. Furthermore, from Figure 5.3, we know the pumping strength to overcome the phase mismatch at a given pump frequency. The pump frequency where the up-conversion free band starts existing is at $\omega_\text{p} = 2\omega_\text{c}/3$, while to get one third of the full bandwidth, we need $\omega_\text{p} = 3\omega_\text{c}/4$. The required pumping strengths when using these pump frequencies, for $\tilde{C} = 0$, are $\chi \gtrsim 0.064$ and $\chi \gtrsim 0.085$ respectively. Let us investigate if we can realistically achieve these pumping strengths.

The pump amplitude

The pumping strength χ is partly dependent on the mixing coefficient c_3, and partly dependent on the pump-induced phase drop Δ_p0, *i.e.* $\chi = \frac{1}{4}c_3\Delta_\text{p0}$. The phase drop Δ_p0 is related to the pump amplitude as

$$\Delta_\text{p} = \tilde{\omega}_\text{p} A_\text{p}. \tag{5.23}$$

We calculate the pump amplitude as

$$A_\text{p} = \frac{I_\text{p} Z_\text{char}}{\varphi_0 \omega_\text{p}} = \frac{i_\text{p}}{\tilde{\omega}_\text{p}} \frac{L_0}{L_\text{J0}} \frac{1}{\sqrt{1 - \tilde{C}\tilde{\omega}_\text{p}^2}} \tag{5.24}$$

which gives us that

$$\Delta_\text{p} = i_\text{p} \frac{L_0}{L_\text{J0}} \frac{1}{\sqrt{1 - \tilde{C}\tilde{\omega}_\text{p}^2}}. \tag{5.25}$$

It is important to note here that when we transformed Equation (3.5) into Equation (3.7), we made an assumption that Δ_p0 is small, or otherwise the resulting conclusion is invalid.

Single junction TWPA

For a single junction TWPA with $\tilde{C} = 0$, the pump-induced phase drop is

$$\Delta_\text{p} = \frac{i_\text{p}}{\sqrt{1 - i_\text{b}^2}} \tag{5.26}$$

and hence the pumping strength

$$\chi = \frac{1}{4} c_3 \Delta_{\mathrm{p}} = \frac{1}{4} \frac{i_{\mathrm{b}} i_{\mathrm{p}}}{1 - i_{\mathrm{b}}^2}. \tag{5.27}$$

With the constraint that the total current must not exceed the critical current, $i_{\mathrm{b}} + i_{\mathrm{p}} < 1$, we can find the maximum value of the pumping strength by assuming that we have a total current $i_{\mathrm{tot}} = i_{\mathrm{b}} + i_{\mathrm{p}}$. Then express the pumping strength in terms of i_{b} and $i_{\mathrm{p}} = i_{\mathrm{tot}} - i_{\mathrm{b}}$, which makes it a function of only one variable, i_{b}, and then we differentiate it and find where the derivative is zero. We then get that the optimal bias current $i_{\mathrm{b}}^{\mathrm{opt}}$ and optimal pump current $i_{\mathrm{p}}^{\mathrm{opt}}$ given the total current i_{tot} is given by

$$i_{\mathrm{b}}^{\mathrm{opt}} = \frac{1 - \sqrt{1 - i_{\mathrm{tot}}^2}}{i_{\mathrm{tot}}}, \quad i_{\mathrm{p}}^{\mathrm{opt}} = i_{\mathrm{tot}} - i_{\mathrm{b}}^{\mathrm{opt}} \tag{5.28}$$

which results in a pumping strength of

$$\chi = \frac{1 - \sqrt{1 - i_{\mathrm{tot}}^2}}{8}. \tag{5.29}$$

From Equation (5.29) we can see that χ approaches its maximum of 1/8 when $i_{\mathrm{tot}} \to 1$. However, this limit is achievable only when the total current consists solely of the bias current, which then violates the assumption that the pump current is much larger than the signal current. Another problem is that for a single junction, when the bias current is too close to the critical current, there are no energy levels left in the potential well. To avoid this let us assume a total current $i_{\mathrm{tot}} = 0.9$, which gives us $i_{\mathrm{b}}^{\mathrm{opt}} \approx 0.63$, $i_{\mathrm{p}}^{\mathrm{opt}} \approx 0.27$ and $\chi \approx 0.07 < 0.085$. For this value of $\chi \approx 0.07$, and a pump frequency at $\tilde{\omega}_{\mathrm{p}} = 1.38$, the bandwidth is about 10 % of the full band and the increment is around 0.01. Therefore, we do not seem to be able to get 1/3 of the full band free from up-conversion. Another problem is that for a biased single junction TWPA, there is still 4WM, *i.e.* $c_4 \neq 0$, which our model does not consider.

RF-SQUID TWPA

An rf-SQUID can be biased such that there is no 4WM. Since our model only captures the effects of pure 3WM, let us assume that it is biased at this point. Then the SQUID has the inductance of the linear inductor, $L_0 = L$, recall

Equation (3.21). The pump-induced phase drop is hence

$$\Delta_{\mathrm{p}} = i_{\mathrm{p}} \frac{L}{L_{\mathrm{J0}}} \tag{5.30}$$

and the mixing coefficient $c_3 = \frac{L}{L_{\mathrm{J0}}}$, recall Equation (3.23). The pumping strength is hence

$$\chi = \frac{1}{4} c_3 \Delta_{\mathrm{p}} = \frac{1}{4} i_{\mathrm{p}} \left(\frac{L}{L_{\mathrm{J0}}} \right)^2 . \tag{5.31}$$

Here too, let us make our assumptions in a way to ensure Δ_{p0} is not too large. For a very large inductance $L = L_{\mathrm{J0}}$ and a fairly large current $i_{\mathrm{p}} = 0.3$, we get $\chi = 0.075$, *i.e.* very similar to the biased single junction TWPA. Once again, it seems we cannot get as much as 1/3 of the full band free from up-conversion, but possibly a small band around half of the pump frequency.

SNAIL TWPA

For a SNAIL TWPA it is not as easy to give an explicit number of c_3 as it is dependent on both α and $\mathcal{N}$. However, from the previously shown values we note that c_3 is typically around unity. That combined with the fact that Δ_{p} must be small, gives us similar results as the ones for an rf-SQUID TWPA.

Conclusions

In short, we conclude that the pumping strength for all designs we have investigated, even for very optimistic values, seems to be just too small to get at least 1/3 of the full band free from up-conversion.

It is worth to point out that our predictions are based on the assumption that Δ_{p0} is small, which limits the pumping strength. We can not overrule the possibility of achieving a large enough pumping strength if the pump amplitude is increased; however, we can not theoretically investigate this regime with our model.

It is also worth to point out that we have not made any assumption on the value of c_3. A possible solution to get a large enough pumping strength could hence be to find a nonlinear inductance element with a large enough c_3.

5.4 Dispersion engineering

To this point, we have studied a nondispersively engineered TWPA, *i.e.* a TWPA with the standard dispersion relation derived in Section 2.2, especially with the relation given by $\tilde{C} = 0$. We saw in Chapter 4 that it is hard to achieve a large gain in the small frequency limit due to either too large phase mismatch, or due to a lot of up-conversion. And in this chapter, so far, we have seen that it is also hard to achieve a large gain in the high frequency limit due to large phase mismatch.

Now we will look at ways to still place the pump at a high frequency, *i.e.* close to the cutoff frequency, and to overcome the phase mismatch problem we add dispersive features to the design. We have two suggestions to do this: either adding LC-oscillators known as resonant phase matching (RPM) features, similar to what has been done for TWPAs implementing 4WM [18], or by periodically modulating the chain parameters [29].

5.4.1 Resonant phase matching (RPM)

To implement resonant phase matching, we add weakly coupled LC-oscillators to the ground in each unit cell, see Figure 5.4. Here the sum of the two capacitances is equal to the single capacitance in the standard unit cell, *i.e.* $C_0 = C_1 + C_\mathrm{c}$, to ensure approximate impedance matching, $Z_\mathrm{char} \approx Z_0$.

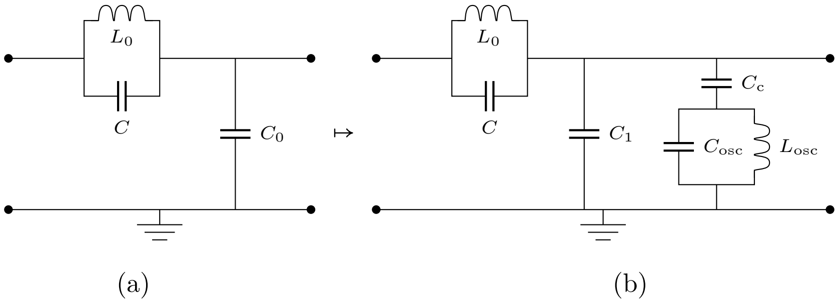

Figure 5.4: The standard unit cell (a) and the unit cell with the RPM features added (b).

The dispersion relation

Using $\cos(\tilde{k}) = \frac{A+D}{2}$ [42], where A and D are element (1,1) and (2,2) of the transmission ($ABCD$) matrix (recall Section 2.3) and where $\tilde{k} = ka$ now is the wave number normalised to the RPM unit cell, the dispersion relation for a TWPA with the unit cell shown in Figure 5.4b is given by

$$\begin{aligned}\cos(\tilde{k}) &= 1 - \frac{1}{2} \cdot \frac{\mathrm{i}\omega L_0}{1-\omega^2 L_0 C} \cdot \left(\mathrm{i}\omega C_1 + \frac{\mathrm{i}\omega C_\mathrm{c}\left(1-\omega^2 L_\mathrm{osc} C_\mathrm{osc}\right)}{1-\omega^2 L_\mathrm{osc}\left(C_\mathrm{c}+C_\mathrm{osc}\right)} \right) \\ &= 1 - \frac{1}{2} \cdot \frac{\omega^2/\omega_0^2}{1-\omega^2/\omega_\mathrm{pl}^2} \cdot \frac{1-\nu\omega^2/\omega_\mathrm{r}^2}{1-\omega^2/\omega_\mathrm{r}^2}\end{aligned} \tag{5.32}$$

where

$$\omega_0^2 = \frac{1}{L_0 C_0}, \quad \omega_\mathrm{pl}^2 = \frac{1}{L_0 C}, \quad \omega_\mathrm{r}^2 = \frac{1}{L_\mathrm{osc}\left(C_\mathrm{c}+C_\mathrm{osc}\right)}, \tag{5.33}$$

where ω_r is the resonance frequency of the RPM feature, and

$$\nu = 1 - \frac{C_\mathrm{c}^2}{\left(C_1+C_\mathrm{c}\right)\left(C_\mathrm{c}+C_\mathrm{osc}\right)} = 1 - \frac{C_\mathrm{c}}{C_0}\frac{C_\mathrm{c}}{C_\mathrm{c}+C_\mathrm{osc}}. \tag{5.34}$$

Further simplification yields

$$4\sin^2\left(\frac{\tilde{k}}{2}\right) = \frac{\omega^2/\omega_0^2}{1-\omega^2/\omega_\mathrm{pl}^2} \cdot \frac{1-\nu\omega^2/\omega_\mathrm{r}^2}{1-\omega^2/\omega_\mathrm{r}^2}. \tag{5.35}$$

Solving this equation for ω^2 yields a second degree polynomial with respect to ω^2,

$$\omega^4 \cdot \left(\frac{4\sin^2\left(\frac{\tilde{k}}{2}\right)}{\omega_\mathrm{pl}^2\omega_\mathrm{r}^2} + \frac{\nu}{\omega_0^2\omega_\mathrm{r}^2} \right) - \omega^2 \cdot \left(4\sin^2\left(\frac{\tilde{k}}{2}\right)\frac{\omega_\mathrm{r}^2+\omega_\mathrm{pl}^2}{\omega_\mathrm{r}^2\omega_\mathrm{pl}^2} + \frac{1}{\omega_0^2} \right) + 4\sin^2\left(\frac{\tilde{k}}{2}\right) = 0. \tag{5.36}$$

One can solve Equation (5.36), but we will simplify it first. The effect of the plasma frequency ω_pl is, similar to before (recall Figure 2.2), that it only pushes the bands to lower frequencies. We ignore this effect by letting $\omega_\mathrm{pl} \to \infty$, which is equivalent with setting $\tilde{C} = 0$. We also express Equation (5.36) in terms of normalised frequencies $\tilde{\omega} = \omega/\omega_0$ and multiply the equation with

$\tilde{\omega}_\mathrm{r}^2$. Then it simplifies to

$$\nu\tilde{\omega}^4 - \tilde{\omega}^2 \cdot \left(\tilde{\omega}_\mathrm{r}^2 + 4\sin^2\left(\frac{\tilde{k}}{2}\right)\right) + 4\tilde{\omega}_\mathrm{r}^2 \sin^2\left(\frac{\tilde{k}}{2}\right) = 0 \tag{5.37}$$

which has two solutions,

$$\tilde{\omega}_\pm^2 = \frac{1}{2\nu}\left[\tilde{\omega}_\mathrm{r}^2 + 4\sin^2\left(\frac{\tilde{k}}{2}\right) \pm \sqrt{\left(\tilde{\omega}_\mathrm{r}^2 + 4\sin^2\left(\frac{\tilde{k}}{2}\right)\right)^2 - 16\nu\tilde{\omega}_\mathrm{r}^2 \sin^2\left(\frac{\tilde{k}}{2}\right)}\right]. \tag{5.38}$$

Now we analyse the solutions for different values of ν. For $\nu = 1$, corresponding to no coupling to the resonators, we retrieve the standard dispersion relation derived in Section 2.2. However, for $\nu < 1$ each resonator is coupled to each unit cell, then a stop-band opens up around the resonance frequency $\tilde{\omega}_\mathrm{r}$, see Figure 5.5. The $\tilde{\omega}_-$ solutions correspond to the lower band and the $\tilde{\omega}_+$ solutions correspond to the upper band. To get the frequency bands, we solve Equation (5.38) for $\tilde{k} \in [0, \pi]$. While $\tilde{\omega}_\pm(\pi)$ gets a fairly long expression which we will not write down here, and $\tilde{\omega}_-(0)$ is trivially equal to 0, it is worth pointing out that $\tilde{\omega}_+(0) = \tilde{\omega}_\mathrm{r}/\sqrt{\nu}$.

Perfect phase matching

The phase mismatch is zero, *i.e.* perfect phase matching, when the pump, signal and idler all lie on a straight line. For the RPM dispersion relation, presented in Figure 5.5, it is not in general possible to find frequencies where this happens at a detuned signal frequency ($\delta \neq 0$). However, at zero detuning ($\delta = 0$), the signal and the idler have the same frequencies and then there exists points of perfect phase matching when the pump is in the upper band and the signal is in the lower band. To find these points, we numerically solve

$$\tilde{\omega}_+\left(\tilde{k}\right) = 2\tilde{\omega}_-\left(\tilde{k}/2\right) \tag{5.39}$$

for $\tilde{k}$, which yields the value of $\tilde{k}_\mathrm{p}$. For $\nu = 0.95$ and $\tilde{\omega}_\mathrm{r} = 1.5$, we find the value to be $\tilde{k}_\mathrm{p} = 1.86$ which translates into the frequencies $\tilde{\omega}_\mathrm{p} \approx 1.77$ and $\tilde{\omega}_\mathrm{s} \approx 0.88$, see Figure 5.6.

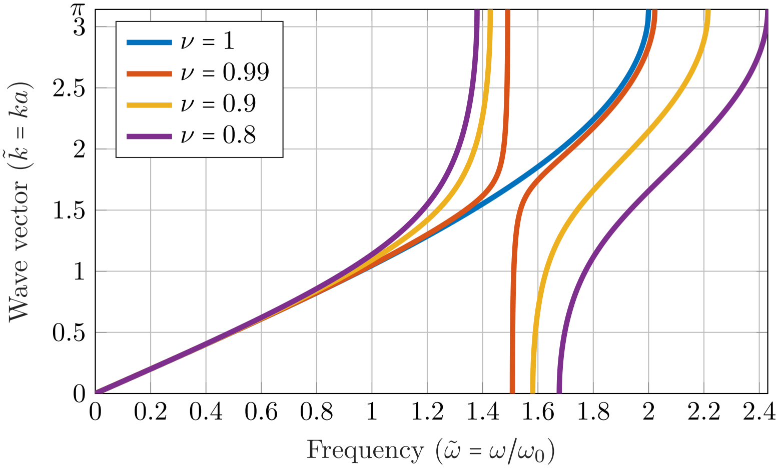

Figure 5.5: The dispersion relation, as given by Equation (5.38), for $\tilde{\omega}_\mathrm{r} = 1.5$, $\omega_\mathrm{pl} = \infty$ and different values of ν.

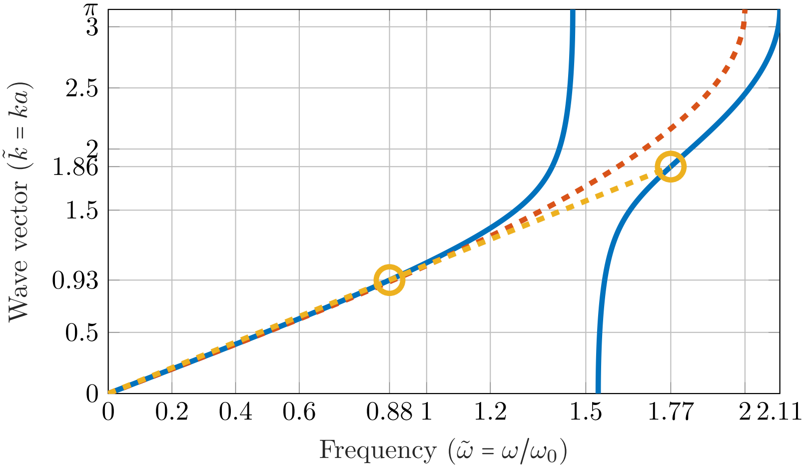

Figure 5.6: The dispersion relation for $\tilde{\omega}_\mathrm{r} = 1.5$, $\tilde{\omega}_\mathrm{J} = \infty$, $\nu = 0.95$ (blue), the standard dispersion relation (orange) as well as the sweet spot for pump and signal (yellow).

The gain coefficient

To find the gain coefficient for this system, we once again numerically solve Equation (5.22). However, we need to take the resonant feature into consideration for $\mathcal{M}_{1,1}$ and $\mathcal{M}_{2,2}$. When initially deriving the discrete wave equation, recall Section 2.1, we only had one capacitance to ground, which gave rise to the first $\tilde{\omega}^2$-terms in Equations (5.21a) and (5.21d), recall Equation (2.4). In order to take the RPM feature into consideration, we hence let

$$\tilde{\omega}^2 \mapsto \tilde{\omega}^2 \cdot \frac{1 - \nu\tilde{\omega}^2/\tilde{\omega}_\mathrm{r}^2}{1 - \tilde{\omega}^2/\tilde{\omega}_\mathrm{r}^2} \tag{5.40}$$

for these terms. The expressions for $\mathcal{M}_{1,1}$ and $\mathcal{M}_{2,2}$ then become

$$\mathcal{M}_{1,1} = \tilde{\omega}_\mathrm{s}^2 \cdot \frac{1 - \nu\tilde{\omega}_\mathrm{s}^2/\tilde{\omega}_\mathrm{r}^2}{1 - \tilde{\omega}_\mathrm{s}^2/\tilde{\omega}_\mathrm{r}^2} - 4\sin^2\left(\frac{\tilde{k}_\mathrm{p} + \tilde{\kappa}}{4}\right), \tag{5.41a}$$

$$\mathcal{M}_{2,2} = \tilde{\omega}_\mathrm{i}^2 \cdot \frac{1 - \nu\tilde{\omega}_\mathrm{i}^2/\tilde{\omega}_\mathrm{r}^2}{1 - \tilde{\omega}_\mathrm{i}^2/\tilde{\omega}_\mathrm{r}^2} - 4\sin^2\left(\frac{\tilde{k}_\mathrm{p} - \tilde{\kappa}}{4}\right). \tag{5.41b}$$

We solve Equation (5.22) with the expressions above for $\mathcal{M}_{1,1}$ and $\mathcal{M}_{2,2}$ for multiple pump frequencies. We note that, even for weak pumping strengths, there is indeed an imaginary part of λ, *i.e.* a real-valued gain coefficient, when the pump is at the sweet spot $\tilde{\omega}_\mathrm{p} \approx 1.77$, see Figure 5.7.

Furthermore, when the pump is at the sweet spot, there is also a band for detuned signals with a real-valued gain coefficient, see Figure 5.8. The width of the band depends on the pumping strength. There are two important points to note in this figure:

1. For the very optimistic pumping strength $\chi = 0.07$, which without dispersion engineering would give about 10 % of the full band and a gain coefficient of ~ 0.01, now gives us a wide band of about 40 % of the full band and a much larger gain coefficient of ~ 0.06.

2. Even for a small, much more realistic, pumping strength $\chi = 0.01$ we still get exponential gain for a fairly large band of about 20 % and a gain coefficient of ~ 0.01.

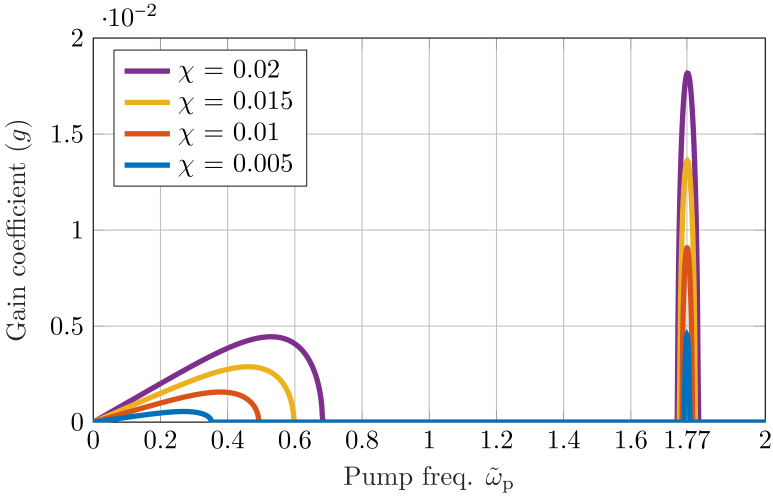

Figure 5.7: The gain coefficient at zero detuning ($\delta = 0$) for an RPM-TWPA with $\nu = 0.95$ and $\tilde{\omega}_{\mathrm{r}} = 1.5$ and different pumping strengths χ.

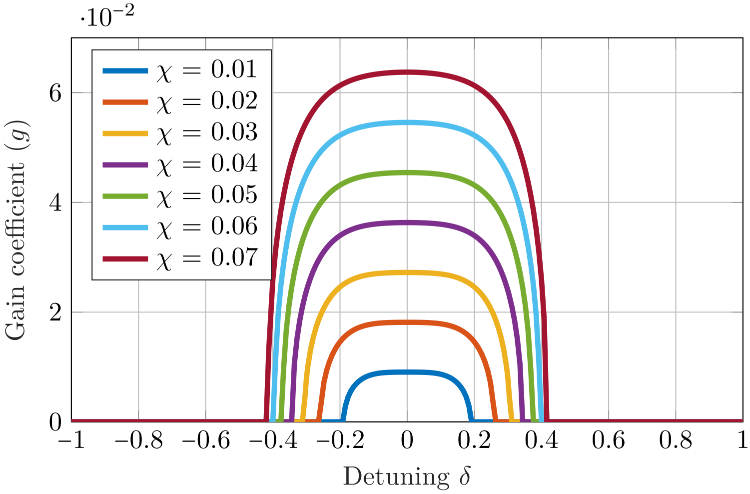

Figure 5.8: The gain coefficient at the sweet spot ($\tilde{\omega}_{\mathrm{p}} \approx 1.77$) for an RPM-TWPA with $\nu = 0.95$ and $\tilde{\omega}_{\mathrm{r}} = 1.5$ at different detunings δ.

In conclusion, by adding the RPM features and putting the pump at the sweet spot, we can achieve low phase mismatch for a fairly wide range of signal frequencies, while also completely disable up-conversion for the pump, the signal and the idler. This leads to a real-valued gain coefficient g, which results in pure exponential gain.

5.4.2 Periodically modulated chain

Another approach of dispersively engineer the TWPA to achieve small phase mismatch at high frequencies is to periodically modulate the chain, see Figure 5.9. With this structure we will once again create two bands where there will exist a sweet spot. Solving for the dispersion relation for this structure with arbitrary parameters $L_1, C_1, C_{0,1}, L_2, C_2, C_{0,2}$ is possible, but the equations become quite tedious. As a simplification, let us disregard the line capacitances, *i.e.* let $C_1 = C_2 = 0$. Let us also assume identical ground capacitances, *i.e.* let $C_{0,1} = C_{0,2} = C_0$. The only difference between the subcells is hence the inductances L_1 and L_2. This is a technique used in several different TWPA designs, although for different reasons, and it is more common to modulate the ground capacitances [28], [29], [33]. Experimental realisation of this approach will be reported separately [45].

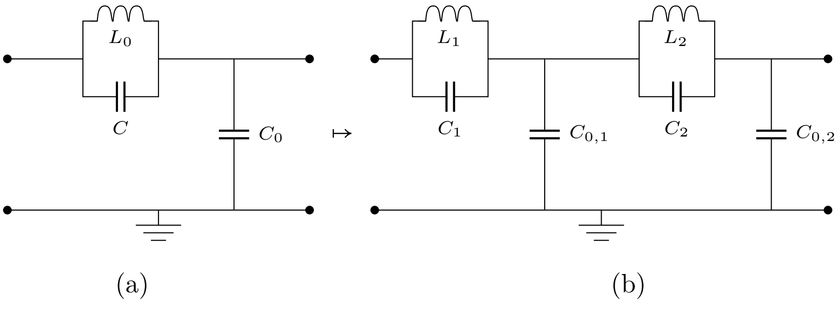

Figure 5.9: The standard unit cell (a) and the unit cell of the modulated chain TWPA (b).

The dispersion relation

To find the dispersion relation, we first find the transmission ($ABCD$) matrix. The transmission matrix of the whole system is given by

$$\begin{aligned}\begin{bmatrix} A & B \\ C & D \end{bmatrix} &= \begin{bmatrix} 1-\omega^2 L_1 C_0 & \mathrm{i}\omega L_1 \\ \mathrm{i}\omega C_0 & 1 \end{bmatrix}\begin{bmatrix} 1-\omega^2 L_2 C_0 & \mathrm{i}\omega L_2 \\ \mathrm{i}\omega C_0 & 1 \end{bmatrix} \\ &= \begin{bmatrix} 1-\omega^2 C_0\left(2L_1+L_2\right)+\omega^4 L_1 L_2 C_0^2 & \mathrm{i}\omega L_1 + \mathrm{i}\omega L_2\left(1-\omega^2 L_1 C_0\right) \\ \mathrm{i}\omega C_0\left(2-\omega^2 L_2 C_0\right) & 1-\omega^2 L_2 C_0 \end{bmatrix}.\end{aligned} \tag{5.42}$$

Using $\cos\left(2\tilde{k}\right) = \frac{A+D}{2}$ [42], where $\tilde{k}$ is the normalised wave number over a subcell and the factor 2 comes from having 2 subcells, we hence get

$$\cos\left(2\tilde{k}\right) = 1-\omega^2 C_0\left(L_1+L_2\right)+\frac{1}{2}\omega^4 L_1 L_2 C_0^2. \tag{5.43}$$

Let us define

$$\omega_1^2 = \frac{1}{L_1 C_0}, \quad \omega_2^2 = \frac{1}{L_2 C_0}. \tag{5.44}$$

Then Equation (5.43) can be written as

$$4\sin^2\left(\tilde{k}\right) = 2\omega^2\left(\frac{1}{\omega_1^2}+\frac{1}{\omega_2^2}\right)-\frac{\omega^4}{\omega_1^2\omega_2^2} \tag{5.45}$$

which we can write as a second degree polynomial with respect to ω^2,

$$\omega^4-\omega^2\cdot 2\left(\omega_1^2+\omega_2^2\right)+4\omega_1^2\omega_2^2\sin^2\left(\tilde{k}\right)=0. \tag{5.46}$$

The solutions are given by

$$\omega_\pm^2 = \omega_1^2+\omega_2^2 \pm \sqrt{\left(\omega_1^2+\omega_2^2\right)^2-4\omega_1^2\omega_2^2\sin^2\left(\tilde{k}\right)}, \tag{5.47}$$

which are shown in Figure 5.10 for multiple values of $\tilde{\omega}_2 = \omega_2/\omega_1$. Note that here we have plotted $\tilde{k}$, which is the wave vector over *one subcell*, as a function of $\tilde{\omega} = \omega/\omega_1$.

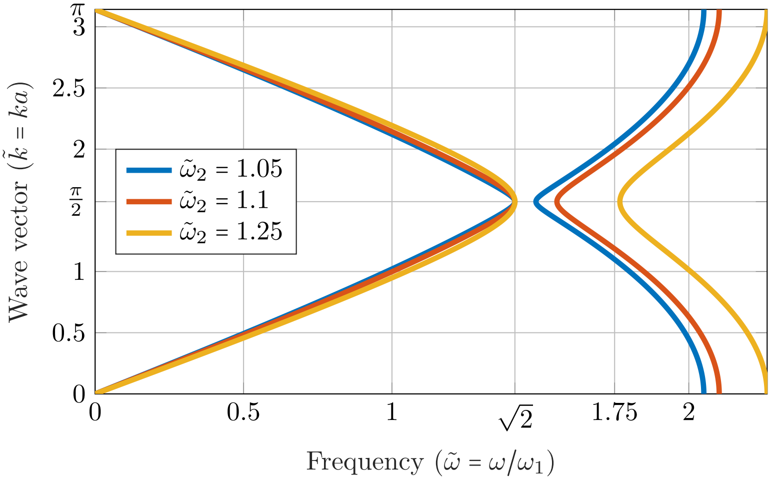

Figure 5.10: The dispersion relation for different values of $\tilde{\omega}_2 = \omega_2/\omega_1$.

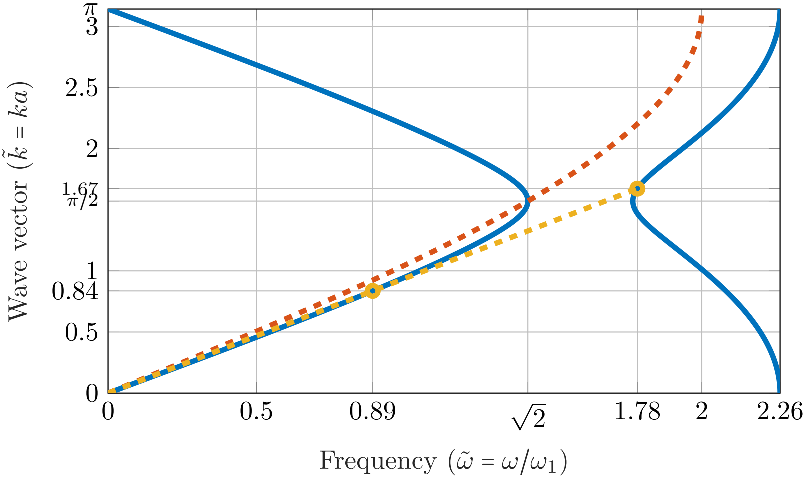

Figure 5.11: The dispersion relation for $\tilde{\omega}_2 = 1.25$ (blue), the standard dispersion relation (orange) as well as the sweet spot for the pump and the signal (yellow).

Solving Equation (5.47) for $\tilde{k} \in \left\{0, \frac{\pi}{2}, \pi\right\}$ gives us that the frequency bands, in terms of $\tilde{\omega} = \omega/\omega_1$, are

$$\begin{aligned} &\tilde{\omega}_- \in \left[0, \sqrt{2}\right], \quad \tilde{\omega}_+ \in \left[\tilde{\omega}_2\sqrt{2}, \sqrt{2 + 2\tilde{\omega}_2^2}\right], \quad (\omega_2 > \omega_1), \\ &\tilde{\omega}_- \in \left[0, \tilde{\omega}_2\sqrt{2}\right], \quad \tilde{\omega}_+ \in \left[\sqrt{2}, \sqrt{2 + 2\tilde{\omega}_2^2}\right], \quad (\omega_1 > \omega_2). \end{aligned} \tag{5.48}$$

Perfect phase matching

We may, by ocular inspection, determine that for certain values of $\tilde{\omega}_2$ there should exist sweet spots similar to the RPM case. To find these sweet spots, we numerically solve Equation (5.39), but now using the solutions presented in Equation (5.47). The solution for $\tilde{\omega}_2 = 1.25$ is presented in Figure 5.11.

The gain coefficient

To actually determine the gain coefficient for a periodically modulated chain of this kind, one needs to develop the equivalent discrete equations to Equations (5.21a) to (5.21d) for the modulated chain. We do not present it here, but it is qualitatively the same as for the RPM case.

CHAPTER 6

Conclusions

In this thesis, we have outlined the theory for several TWPA designs and studied effects of three-wave mixing for both cases of small and large frequency limits. In Chapters 2 and 3 we investigated typical characteristics of the TWPA, such as the dispersion relation, the transmission, the characteristic impedance and the mixing coefficients c_3, c_4. We also derived both the discrete and the continuous wave equations. Then in Chapter 4 we studied three-wave mixing closely in the small frequency limit and developed a general model that describes all mixing processes within the pump-mediated model [39]. We found that there exist two reasons that can limit the gain, phase mismatch and up-conversion. Finally, in Chapter 5, we developed a model to study gain for large frequencies, where up-conversion would no longer be possible but the phase mismatch is large, and we proposed potential ways of reducing phase mismatch at these frequencies.

The general model developed in Chapter 4 works in the small frequency limit for a nondispersively engineered TWPA. It reduces all system parameters, such as wave vectors, frequencies, amplitudes and the mixing coefficient c_3, into *a single scaling parameter* μ, which can be thought of as the "effective phase mismatch". By investigating different values of μ, large and small, we hence cover all possible scenarios. For large values of μ, there is little to no up-conversion, but at the same time the phase mismatch is large and prevents exponential gain. For small values of μ, there is effectively small phase mismatch, but at the same time there is a lot of up-conversion that heavily reduces the gain. In conclusion, within the boundaries of our model, for a TWPA in the small frequency limit without dispersion engineering, it is very hard to achieve a large gain ($> 20\,\mathrm{dB}$) as *either* phase mismatch *or* up-conversion will limit the gain.

To study the mixing effects at large frequencies, one needs to use the discrete wave equation rather than the continuous one, which we presented in Chapter 5. The idea was to investigate whether the intrinsic cutoff frequency of the TWPA could be used to stop up-conversion altogether. After numerically solving the discrete equations we found that in theory it could be possible to put the pump close to the cutoff and still get exponential gain. However, to overcome the large phase mismatch in this region, one needs a very large mixing coefficient c_3. We investigated several TWPA designs and found that none of them had a large enough mixing coefficient to overcome the large phase mismatch. In short, up-conversion can be eliminated by placing the pump close to the cutoff frequency, but to get exponential gain one needs to implement some dispersion engineering to reduce the phase mismatch. Therefore, we focused on dispersion engineering, where we modify the structure of the TWPA to get a dispersion relation such that it satisfies the phase matching condition when the pump is close to the cutoff frequency. We proposed two designs, adding resonant features (RPM) or periodically modulating the parameters of the chain, and we showed that with both of them there exists a sweet spot where there is perfect phase matching between the pump and a signal at half of the pump frequency. Furthermore, we showed that at least for the RPM TWPA, there exists a fairly wide band with exponential gain.

To summarise, it is very hard to get a large gain by using pure three-wave mixing processes without dispersion engineering, as either phase mismatch or up-conversion will limit the gain. Our proposed solution is to place the pump close to the cutoff frequency, while keeping the phase mismatch small by utilising dispersion engineering.

References

[1] C. M. Caves, "Quantum limits on noise in linear amplifiers," *Phys. Rev. D*, vol. 26, pp. 1817–1839, 1982.

[2] T. Yamamoto, K. Inomata, M. Watanabe, *et al.*, "Flux-driven Josephson parametric amplifier," *Applied Physics Letters*, vol. 93, p. 042 510, 2008.

[3] N. Bergeal, F. Schackert, M. Metcalfe, *et al.*, "Phase-preserving amplification near the quantum limit with a Josephson ring modulator," *Nature*, vol. 465, pp. 64–68, 2010.

[4] N. Roch, E. Flurin, F. Nguyen, *et al.*, "Widely tunable, nondegenerate three-wave mixing microwave device operating near the quantum limit," *Phys. Rev. Lett.*, vol. 108, p. 147 701, 2012.

[5] A. Roy and M. Devoret, "Introduction to parametric amplification of quantum signals with Josephson circuits," *Comptes Rendus Physique*, vol. 17, pp. 740–755, 2016, Quantum microwaves / Micro-ondes quantiques.

[6] J. Aumentado, "Superconducting parametric amplifiers: The state of the art in Josephson parametric amplifiers," *IEEE Microwave Magazine*, vol. 21, pp. 45–59, 2020.

[7] R. J. Schoelkopf and S. M. Girvin, "Wiring up quantum systems," *Nature*, vol. 451, pp. 664–669, 2008.

[8] A. A. Clerk, M. H. Devoret, S. M. Girvin, F. Marquardt, and R. J. Schoelkopf, "Introduction to quantum noise, measurement, and amplification," *Rev. Mod. Phys.*, vol. 82, pp. 1155–1208, 2010.

[9] C. S. Macklin, “Quantum feedback and traveling-wave parametric amplification in superconducting circuits,” Ph.D. dissertation, University of California, Berkeley, 2015.

[10] P. K. Tien, “Parametric amplification and frequency mixing in propagating circuits,” *Journal of Applied Physics*, vol. 29, pp. 1347–1357, 1958.

[11] A. L. Cullen, “A travelling-wave parametric amplifier,” *Nature*, vol. 181, pp. 332–332, 1958.

[12] T. Duty, G. Johansson, K. Bladh, D. Gunnarsson, C. Wilson, and P. Delsing, “Observation of quantum capacitance in the Cooper-pair transistor,” *Phys. Rev. Lett.*, vol. 95, p. 206 807, 2005.

[13] P. K. Tien and H. Suhl, “A traveling-wave ferromagnetic amplifier,” *Proceedings of the IRE*, vol. 46, pp. 700–706, 1958.

[14] A. L. Grimsmo and A. Blais, “Squeezing and quantum state engineering with Josephson travelling wave amplifiers,” *npj Quantum Information*, vol. 3, p. 20, 2017.

[15] M. Perelshtein, K. Petrovnin, V. Vesterinen, *et al.*, *Broadband continuous variable entanglement generation using Kerr-free Josephson metamaterial*, 2021.

[16] O. Yaakobi, L. Friedland, C. Macklin, and I. Siddiqi, “Parametric amplification in Josephson junction embedded transmission lines,” *Phys. Rev. B*, vol. 87, p. 144 301, 2013.

[17] K. O’Brien, C. Macklin, I. Siddiqi, and X. Zhang, “Resonant phase matching of Josephson junction traveling wave parametric amplifiers,” *Phys. Rev. Lett.*, vol. 113, p. 157 001, 2014.

[18] C. Macklin, K. O’Brien, D. Hover, *et al.*, “A near quantum-limited Josephson traveling-wave parametric amplifier,” *Science*, vol. 350, pp. 307–310, 2015.

[19] T. C. White, J. Y. Mutus, I.-C. Hoi, *et al.*, “Traveling wave parametric amplifier with Josephson junctions using minimal resonator phase matching,” *Applied Physics Letters*, vol. 106, p. 242 601, 2015.

[20] M. T. Bell and A. Samolov, “Traveling-wave parametric amplifier based on a chain of coupled asymmetric squids,” *Phys. Rev. Applied*, vol. 4, p. 024 014, 2015.

[21] L. Planat, A. Ranadive, R. Dassonneville, *et al.*, "Photonic-crystal Josephson traveling-wave parametric amplifier," *Phys. Rev. X*, vol. 10, p. 021 021, 2020.

[22] A. B. Zorin, "Josephson traveling-wave parametric amplifier with three-wave mixing," *Phys. Rev. Applied*, vol. 6, p. 034 006, 2016.

[23] A. Ranadive, M. Esposito, L. Planat, *et al.*, *A reversed Kerr traveling wave parametric amplifier*, 2021.

[24] A. B. Zorin, "Flux-driven Josephson traveling-wave parametric amplifier," *Phys. Rev. Applied*, vol. 12, p. 044 051, 2019.

[25] V. Sivak, N. Frattini, V. Joshi, A. Lingenfelter, S. Shankar, and M. Devoret, "Kerr-free three-wave mixing in superconducting quantum circuits," *Phys. Rev. Applied*, vol. 11, p. 054 060, 2019.

[26] A. Miano and O. A. Mukhanov, "Symmetric traveling wave parametric amplifier," *IEEE Transactions on Applied Superconductivity*, vol. 29, pp. 1–6, 2019.

[27] B. Ho Eom, P. K. Day, H. G. LeDuc, and J. Zmuidzinas, "A wideband, low-noise superconducting amplifier with high dynamic range," *Nature Physics*, vol. 8, pp. 623–627, 2012.

[28] C. Bockstiegel, J. Gao, M. Vissers, *et al.*, "Development of a broadband NbTiN traveling wave parametric amplifier for mkid readout," *Journal of Low Temperature Physics*, vol. 176, pp. 1–7, 2014.

[29] M. R. Vissers, R. P. Erickson, H.-S. Ku, *et al.*, "Low-noise kinetic inductance traveling-wave amplifier using three-wave mixing," *Applied Physics Letters*, vol. 108, p. 012 601, 2016.

[30] S. Chaudhuri, D. Li, K. D. Irwin, *et al.*, "Broadband parametric amplifiers based on nonlinear kinetic inductance artificial transmission lines," *Applied Physics Letters*, vol. 110, p. 152 601, 2017.

[31] R. P. Erickson and D. P. Pappas, "Theory of multiwave mixing within the superconducting kinetic-inductance traveling-wave amplifier," *Phys. Rev. B*, vol. 95, p. 104 506, 2017.

[32] S. Goldstein, N. Kirsh, E. Svetitsky, *et al.*, "Four wave-mixing in a microstrip kinetic inductance travelling wave parametric amplifier," *Applied Physics Letters*, vol. 116, p. 152 602, 2020.

[33] M. Malnou, M. Vissers, J. Wheeler, *et al.*, "Three-wave mixing kinetic inductance traveling-wave amplifier with near-quantum-limited noise performance," *PRX Quantum*, vol. 2, p. 010 302, 2021.

[34] D. J. Parker, M. Savytskyi, W. Vine, *et al.*, "Degenerate parametric amplification via three-wave mixing using kinetic inductance," *Phys. Rev. Applied*, vol. 17, p. 034 064, 2022.

[35] J. A. Armstrong, N. Bloembergen, J. Ducuing, and P. S. Pershan, "Interactions between light waves in a nonlinear dielectric," *Phys. Rev.*, vol. 127, pp. 1918–1939, 1962.

[36] H. Takahasi, "Information theory of quantum-mechanical channels," in ser. Advances in Communication Systems, A. Balakrishnan, Ed., vol. 1, Elsevier, 1965, pp. 227–310.

[37] M. T. Raiford, "Degenerate parametric amplification with time-dependent pump amplitude and phase," *Phys. Rev. A*, vol. 9, pp. 2060–2069, 1974.

[38] M. Simoen, "Parametric interactions with signals and the vacuum," Ph.D. dissertation, Chalmers University of Technology, 2015.

[39] T. Dixon, J. Dunstan, G. Long, J. Williams, P. Meeson, and C. Shelly, "Capturing complex behavior in Josephson traveling-wave parametric amplifiers," *Phys. Rev. Applied*, vol. 14, p. 034 058, 2020.

[40] M. J. Feldman, P. T. Parrish, and R. Y. Chiao, "Parametric amplification by unbiased Josephson junctions," *Journal of Applied Physics*, vol. 46, pp. 4031–4042, 1975.

[41] A. Barone and G. Paternò, *Physics and applications of the Josephson effect.* New York : Wiley, cop., 1982.

[42] D. M. Pozar, *Microwave Engineering.* Chichester, 2012.

[43] N. E. Frattini, V. V. Sivak, A. Lingenfelter, S. Shankar, and M. H. Devoret, "Optimizing the nonlinearity and dissipation of a SNAIL parametric amplifier for dynamic range," *Phys. Rev. Applied*, vol. 10, p. 054 020, 2018.

[44] A. B. Zorin, "Quasi-phasematching in a poled Josephson traveling-wave parametric amplifier with three-wave mixing," *Applied Physics Letters*, vol. 118, p. 222 601, 2021.

[45] A. Fadavi Roudsari *et al.*, unpublished, 2022.

Part II

Appended paper

PAPER A

A high gain travelling-wave parametric amplifier based on three-wave mixing

Hampus Renberg Nilsson, Anita Fadavi Roudsari, Daryoush Shiri,
Per Delsing, Vitaly Shumeiko

`http://arxiv.org/abs/2205.07758`

The layout has been revised.

A high gain travelling-wave parametric amplifier based on three-wave mixing

Hampus Renberg Nilsson,* Anita Fadavi Roudsari, Daryoush Shiri, Per Delsing, and Vitaly Shumeiko
Department of Microtechnology and Nanoscience - MC2,
Chalmers University of Technology, S-412 96 Göteborg, Sweden.

(Dated: May 17, 2022)

We extend the theory for a Josephson junction travelling wave parametric amplifier (TWPA) operating in the three-wave mixing regime and we propose a scheme for achieving high gain. The continuous three-mode model [P. K. Tien, J. Appl. Phys. **29**, 1347 (1958)] is on one hand extended to describe a discrete chain of Josephson junctions at high frequencies close to the spectral cutoff where there is no up-conversion. On the other hand, we also develop a continuous multimode theory for the low-frequency region where the frequency dispersion is close to linear. We find that in both cases the gain is significantly reduced compared to the prediction by the continuous three-mode model as the result of increasingly strong dispersion at the high frequencies and generation of up-converted modes at the low frequencies. The developed theory is in quantitative agreement with experimental observations. To recover the high gain, we propose to engineer a chain with dispersive features to form a two-band frequency spectrum and to place the pump frequency within the upper band close to the spectral cutoff. We prove that there exists a sweet spot, where the signal and the pump are phase matched, while the up-conversion is inhibited. This results in a high gain which grows exponentially with the length of the TWPA.

I. INTRODUCTION

Quantum limited parametric amplifiers [1] are important tools for measuring and monitoring states of superconducting qubits. Built with nonlinear, superconducting lumped element oscillators or transmission line resonators and demonstrating high gain and small added noise [2–6], the parametric amplifiers became an essential part of the circuit Quantum Electrodynamics (cQED) [7] toolbox.

To build a large-scale multiqubit quantum processor, an optimisation of qubit readout by multiplexing is desirable, which requires amplifiers with a large bandwidth, high gain and low added noise. Such a capability is provided by travelling wave parametric amplifiers (TWPA). During the last few years, the interest has rapidly grown in the development and investigation of the properties of different types of TWPA.

The amplification principle of the TWPA is based on nonlinear interaction of a weak propagating signal with an intense co-propagating wave (pump), which under a phase-matching condition results in an exponential spatial growth in the signal amplitude [8–10]. In the quantum regime, the TWPA is capable to generate signal squeezing and photon entanglement [11, 12].

Within the cQED platform, two types of TWPAs are experimentally tested and theoretically studied: the first type uses the nonlinear kinetic inductance of a superconducting transmission line [13–20], and the second uses the nonlinear inductance of a chain of Josephson junctions [12, 22–32]. The TWPAs are further distinguished depending on the type of nonlinear interaction they employ: three-wave mixing (3WM) or four-wave mixing (4WM).

In this paper, we theoretically investigate the efficiency of the TWPA operating in the 3WM regime, we compare and verify our theoretical model with experimental data and we suggest a way to achieve high gain.

The 3WM amplifiers employ the lowest order, cubic, nonlinearity of the inductive energy, which is similar to the $\chi^{(2)}$ nonlinearity in optical crystals. Such nonlinearity is associated with the broken time-reversal symmetry, which can be introduced by applying a dc current bias, or a magnetic flux bias. The amplification occurs due to a down-conversion process, which is capable to provide an efficient amplification within a large bandwidth in a weakly dispersive medium already at relatively small pump intensity [10]. An important property of this regime is the separation of the amplification band from the pump, and also the possibility of phase preserving as well as phase sensitive amplification.

In practice, however, the amplification performance of 3WM devices with weak frequency dispersion is compromised by the generation of pump harmonics [33] as well as signal and idler up-conversion [15, 34].

The 4WM amplifiers employ the next order, quartic, nonlinearity of the inductive energy, which is similar to the $\chi^{(3)}$ nonlinearity in optical fibers. Amplification in this regime is less efficient since it is a higher order effect with respect to the pumping strength, and it also suffers from dephasing due to Kerr effect that makes exponential amplification impossible without dispersion engineering [23–25]. Furthermore, the pump position in the middle of the gain band is undesirable for certain applications.

Our quest in this paper is to investigate whether it is possible to realise in practice full exponential amplification in a TWPA using 3WM by avoiding the poisoning effect of up-converted modes.

At first glance, the discreteness of the Josephson junction chain allows solving of the problem by placing the pump frequency close to the spectral cutoff, inherent

---

* Hampus.Renberg.Nilsson@chalmers.se

in the discrete chains, and thus eliminating the up-converted modes. Our analysis based on the exact solution for the discrete chain shows that this is in principle possible. However, to overcome the effect of dispersion, which becomes increasingly strong in the vicinity of the spectral cutoff, a rather strong pump signal is required that is unlikely to be realised in practice.

We propose to solve this difficulty by engineering a two-band frequency spectrum of the TWPA and placing the pump within the upper band close to the spectral cutoff. In this case, as we prove, there exists a sweet spot where the pump and the signal belong to the different bands and are exactly phase-matched, while the generation of up-converted modes is inhibited since the pump is close enough to the cutoff. In the vicinity of this sweet spot, a rather broad window opens where a strong exponential amplification occurs. The width of this window is limited by the dispersion and up-conversion effects (c.f. experimental observation in a kinetic inductance TWPA in [19]).

The structure of the paper is the following. In Section II we derive universal dynamic equations for three different kinds of TWPAs, that use either current biased junctions, or magnetic flux biased radio-frequency superconducting quantum interference devices (rf-SQUIDs) [29], or magnetic flux biased superconducting nonlinear asymmetric inductive elements (SNAILs) [31].

In Section III we derive the exact solution to the model containing only three modes involved in the down-conversion, while neglecting up-converted modes, and we evaluate the exponential gain and the frequency region where the exponential gain exists. This part is a generalisation of the solution for a continuous medium in Ref. [10]. Here we also evaluate the pumping strength required for this model to be valid.

In Section IV we investigate the low frequency region with weak frequency dispersion and show that generation of up-converted modes makes it impractically hard to achieve high exponential gain (cf. [34]). We also compare our theoretical results with experimental data obtained on a SNAIL-based TWPA, and find a very good quantitative agreement.

In Section V we pursue the strategy of boosting the gain by engineering a two-band spectrum of the TWPA. We identify the sweet spots, where the high gain is achieved, for the two TWPA designs - adding resonators to unit cells [23–25], and periodically modulating the TWPA parameters [27]. The obtained results are summarised in Section VI.

II. TWPA DYNAMICAL EQUATIONS

The travelling-wave parametric amplifier we study is a chain of identical cells, each consisting of a block of Josephson elements, $\mathcal{L}_\mathrm{J}$, and a capacitor, C, as depicted in Fig. 1.

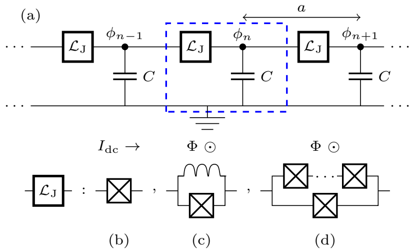

FIG. 1: Circuit diagram of a general discrete TWPA (a), the dashed line indicates a unit cell of length a. Options for the Josephson junction block $\mathcal{L}_\mathrm{J}$: (b) current biased junction, (c) flux-biased rf-SQUID, (d) flux-biased SNAIL.

A convenient starting point for a dynamical description of the TWPA is the Lagrangian [35],

$$\mathcal{L} = \left(\frac{\Phi_0}{2\pi}\right)^2 \sum_{n=1}^{N} \left(\frac{C}{2}\,\dot{\phi}_n^2 + \mathcal{L}_\mathrm{J}[\theta_n]\right), \tag{1}$$

where $\phi_n(t)$ is the dynamical variable - the superconducting phase at node n, $\dot{\phi}_n(t)$ is its time derivative, $\Phi_0 = h/(2e)$ is the magnetic flux quantum, $\mathcal{L}_\mathrm{J}$ is the Lagrangian of the Josephson junction block, and $\theta_n = \phi_n - \phi_{n-1}$ is the superconducting phase difference across the block.

We consider three flavours for the Josephson junction blocks suitable for 3WM. The simplest one is the Josephson junction block consisting of a single Josephson junction, Fig. 1b,

$$\mathcal{L}_\mathrm{J}[\theta_n] = \left(\frac{C_\mathrm{J}}{2}\dot{\theta}_n^2 + \frac{1}{L_\mathrm{J}}\cos\theta_n\right), \tag{2}$$

where C_J and $L_\mathrm{J} = \hbar/(2eI_\mathrm{c})$ are the Josephson junction capacitance and inductance, respectively.

In order to provide the 3WM mechanism, the Josephson junction has to be biased with a dc current, I_dc, which induces a constant shift of the phase difference across each cell, θ_0, defined by equation,

$$\sin\theta_0 = \frac{I_\mathrm{dc}}{I_\mathrm{c}}\,. \tag{3}$$

After including this constant shift to the phase difference, $\theta_n \to \theta_0 + \theta_n(t)$, a dynamical equation for the TWPA is derived by varying the Lagrangian over the dynamical variable $\phi_n(t)$ yielding,

$$\begin{aligned}\ddot{\phi}_n - \frac{C_\mathrm{J}}{C}(\ddot{\theta}_{n+1} - \ddot{\theta}_n) - \bar{\omega}_0^2(\sin\theta_{n+1} - \sin\theta_n)\\ - \bar{\omega}_0^2\tan\theta_0(\cos\theta_{n+1} - \cos\theta_n) = 0\,,\end{aligned} \tag{4}$$

where

$$\bar{\omega}_0^2 = \frac{\cos\theta_0}{L_\mathrm{J}C} \tag{5}$$

is the resonance frequency of the current-biased $L_J C$-oscillator.

The linear terms, with respect to θ_n, in Eq. (4) define the spectral properties of propagating waves in the TWPA, while the nonlinear terms, with respect to θ_n, are responsible for the mixing processes. In the absence of the biasing dc current the 3WM term vanishes.

The TWPA dispersion relation is derived by assuming the solution to a linearised version of Eq. (4) as a discrete analogue to the propagating wave with quasi-wave vector κ, $\phi_n(t) \propto \mathrm{e}^{\mathrm{i}(\kappa n-\omega t)}$, giving the relation,

$$2\bar{\omega}_0 \sin\frac{\kappa}{2} = \frac{\omega}{\sqrt{1-(C_\mathrm{J}/C)(\omega/\bar{\omega}_0)^2}}\,. \tag{6}$$

The dispersion relation has a cutoff at $\kappa_\mathrm{c} = \pi$, where the frequency reaches the maximum value ω_c,

$$\omega_\mathrm{c} = \frac{2\bar{\omega}_0}{\sqrt{1+4C_\mathrm{J}/C}}\,. \tag{7}$$

The dispersion relation cutoff is related to the discrete nature of the TWPA, but it is also affected by the Josephson junction capacitance. In practice, however, the latter is usually small, $C_\mathrm{J} \ll C$, and we will neglect it for most of the theoretical analysis throughout the paper, but keep it when comparing with experiments in Section IV D.

Assuming a small amplitude of the phase oscillation, $|\theta_n| \ll 1$, we expand trigonometric functions in Eq. (4) up to the second order, thus retaining the 3WM term but omitting the higher order 4WM term, to get,

$$\ddot{\phi}_n - \bar{\omega}_0^2(\theta_{n+1}-\theta_n) = -\frac{\bar{\omega}_0^2\tan\theta_0}{2}\left(\theta_{n+1}^2-\theta_n^2\right)\,. \tag{8}$$

An alternative solution for a 3WM TWPA is to use an rf-SQUID instead of a Josephson junction [29], as shown in Fig. 1c. An rf-SQUID includes an inductance L in parallel with the Josephson junction, which allows replacing the dc current bias with a dc magnetic flux bias to achieve 3WM. The Lagrangian $\mathcal{L}_\mathrm{J}$ in this case has the form

$$\mathcal{L}_\mathrm{J}[\theta_n] = \left(\frac{1}{L_\mathrm{J}}\cos(\theta_0+\theta_n) - \frac{(\theta_0+\theta_n+F)^2}{2L}\right)\,, \tag{9}$$

where $F = 2\pi\Phi/\Phi_0$ is the normalised magnetic flux. The dc phase shift θ_0 is now defined, in the absence of net dc current through the rf-SQUID, by the relation

$$\frac{\sin\theta_0}{L_\mathrm{J}} + \frac{\theta_0+F}{L} = 0\,. \tag{10}$$

The dynamic equation now takes a form similar to the one in Eq. (8),

$$\begin{aligned}&\ddot{\phi}_n - \omega_\mathrm{rf}^2(\theta_{n+1}-\theta_n) = -\frac{\bar{\omega}_0^2\tan\theta_0}{2}(\theta_{n+1}^2-\theta_n^2)\,,\\ &\omega_\mathrm{rf}^2 = \left(\bar{\omega}_0^2+\frac{1}{LC}\right)\,.\end{aligned} \tag{11}$$

Another alternative design is to replace the rf-SQUID with a SNAIL circuit [31], as shown in Fig. 1d. This device can be viewed as a modification of a dc-SQUID with several series connected junctions placed in one of the arms. The corresponding Lagrangian reads,

$$\mathcal{L}_\mathrm{J}[\theta_n] = \frac{1}{L_\mathrm{J1}}\cos(\theta_0+\theta_n+F) - \frac{\mathcal{N}}{L_\mathrm{J2}}\cos\frac{\theta_0+\theta_n}{\mathcal{N}}, \tag{12}$$

here $\mathcal{N}$ refers to the number of identical junctions in the top arm in Fig. 1d. The biasing phase difference is defined in the absence of the net dc current through the SNAIL, by

$$\frac{2\pi}{\Phi_0}I_S = \frac{1}{L_\mathrm{J1}}\sin(\theta_0+F) + \frac{1}{L_\mathrm{J2}}\sin\frac{\theta_0}{\mathcal{N}} = 0\,. \tag{13}$$

Proceeding with the derivation in a similar way to the single junction TWPA, we get the following dynamical equation for the SNAIL-TWPA,

$$\ddot{\phi}_n - \omega_S^2(\theta_{n+1}-\theta_n) = -\frac{\omega_S^2\chi_3}{2}\left(\theta_{n+1}^2-\theta_n^2\right)\,, \tag{14}$$

where

$$\begin{aligned}\omega_S^2 &= \frac{1}{L_\mathrm{J1}C}\cos(\theta_0+F) + \frac{1}{L_\mathrm{J2}C\mathcal{N}}\cos\frac{\theta_0}{\mathcal{N}}\,,\\ \chi_3 &= \frac{1}{\omega_S^2}\left(\frac{1}{L_\mathrm{J1}C}\sin(\theta_0+F) + \frac{1}{L_\mathrm{J2}C\mathcal{N}^2}\sin\frac{\theta_0}{\mathcal{N}}\right)\,.\end{aligned} \tag{15}$$

It is worth to note at this point that it is not possible to employ an asymmetric dc-SQUID for 3-wave mixing instead of the SNAIL: in this case $\mathcal{N} = 1$ in Eq. (15), and the nonlinear term in Eq. (14) turns to zero by virtue of Eq. (13).

Comparing Eqs. (4), (11) and (14), we find that they all have similar structures and could be written in a universal form,

$$\begin{aligned}&\frac{1}{\omega_0^2}\ddot{\phi}_n - (\phi_{n+1}-2\phi_n+\phi_{n-1})\\ &= -\frac{\chi_3}{2}\left[(\phi_{n+1}-\phi_n)^2-(\phi_n-\phi_{n-1})^2\right]\,,\end{aligned} \tag{16}$$

where ω_0 is the resonance frequency of the cell, and χ_3 is the 3WM nonlinear coefficient. Particular values of these quantities for different TWPA designs are presented in Table I.

TABLE I: Summary of resonance frequencies and 3WM nonlinear coefficients for different TWPA designs.

TWPA	Bias	ω_0	χ_3
Junction	Current	$\bar{\omega}_0$ Eq. (5)	$\tan\theta_0$
RF-SQUID	Flux	ω_rf Eq. (11)	$\left(\frac{\bar{\omega}_0}{\omega_\mathrm{rf}}\right)^2\tan\theta_0$
SNAIL	Flux	ω_S Eq. (15)	Eq. (15)

III. 3-MODE MODEL

The amplification in a TWPA results from the process of resonant down-conversion, when the frequencies of three interacting waves, *i.e.* pump, signal, and idler, obey the resonance condition, $\omega_\mathrm{p} = \omega_\mathrm{s} + \omega_\mathrm{i}$. Besides this process necessary for amplification, the nonlinear term in Eq. (16) generates a large set of up-converted modes of all the waves involved in the amplification and their combinations. These processes of up-conversion significantly degrade the performance of the amplifier, as we will show in the next section.

To reveal the full amplification potential of the 3WM mechanism, we consider an ideal model where only three waves participating in the down-conversion are taken into account, while all the up-converted modes are neglected. In this model, the field in the TWPA chain consists of a linear combination of three partial harmonic tones,

$$\phi_n(t) = \frac{1}{2} \sum_{\alpha=\mathrm{p,s,i}} \left(A_{\alpha,n} \mathrm{e}^{-\mathrm{i}\omega_\alpha t} + \mathrm{c.c.} \right) \tag{17}$$

whose amplitudes satisfy equation that follows from Eq. (16),

$$\begin{aligned} &\frac{\omega_\alpha^2}{\omega_0^2} A_{\alpha,n} + (A_{\alpha,n+1} - 2A_{\alpha,n} + A_{\alpha,n-1}) = \\ &\frac{\chi_3 \omega_\alpha}{2\pi} \int_0^{\frac{2\pi}{\omega_\alpha}} \left[(\phi_{n+1} - \phi_n)^2 - (\phi_n - \phi_{n-1})^2 \right] \mathrm{e}^{\mathrm{i}\omega_\alpha t}\, \mathrm{d}t \,, \end{aligned} \tag{18}$$

where integration is done over the period of the corresponding mode.

For the pump amplitude, the right-hand side of Eq. (18) only contains the resonant products, $A_{\mathrm{s},n} A_{\mathrm{i},n}$, which are responsible for the pump depletion. For the amplifiers employed for qubit measurements, an input signal is typically $\sim 1\,\mathrm{nA}$, which is by two orders of magnitude smaller than the pump current, which is typically a considerable fraction of the critical current, $I_\mathrm{c} \sim 1\,\mu\mathrm{A}$. Thus, for a power gain up to the order of 40 dB the signal and idler remain weak compared to the pump within the whole TWPA chain, $A_{\mathrm{s},n}$, $A_{\mathrm{i},n} \ll A_{\mathrm{p},n}$, and we will neglect their effect on the pump. As a result, Eq. (18) for the pump becomes linear and has a free propagating wave solution, $A_{\mathrm{p},n} = A_\mathrm{p} \mathrm{e}^{-\mathrm{i}\kappa_\mathrm{p} n}$, with the dispersion relation,

$$\omega_\mathrm{p}^2 = 4\omega_0^2 \sin^2 \frac{\kappa_\mathrm{p}}{2} \,. \tag{19}$$

The dispersion relation has a cutoff at $\omega_\mathrm{c} = 2\omega_0$, $\kappa_\mathrm{c} = \pi$, and is strongly dispersive in the vicinity of the cutoff. In the long-wave limit, $\kappa_\mathrm{p} \ll 1$, the dispersion relation becomes linear, $\omega_\mathrm{p} \approx \omega_0 \kappa_\mathrm{p}$.

Proceeding to the equations for signal and idler we find that the only resonant contributions here come from the products $A_{\mathrm{p},n} A_{\mathrm{i},n}^*$ for the signal, and $A_{\mathrm{p},n} A_{\mathrm{s},n}^*$ for the idler. This implies that the equations form a linear equation set. The solution ansatz has the form,

$$A_{\mathrm{s},n} = A_\mathrm{s} \mathrm{e}^{\mathrm{i}\frac{\kappa_\mathrm{p}+\tilde\kappa}{2} n}, \quad A_{\mathrm{i},n}^* = A_\mathrm{i}^* \mathrm{e}^{-\mathrm{i}\frac{\kappa_\mathrm{p}-\tilde\kappa}{2} n} \,, \tag{20}$$

where $\tilde\kappa$ is an unknown quasi-wave vector. Then the corresponding equations in Eq. (18) reduce to an algebraic equation for spatio-temporally independent amplitude, A_s,

$$\begin{aligned} &\frac{\omega_\mathrm{s}^2}{\omega_0^2} A_\mathrm{s} - 4\sin^2 \frac{\kappa_\mathrm{p} + \tilde\kappa}{4} A_\mathrm{s} = \\ &= -\frac{\chi_3 A_\mathrm{p}}{2} \Big[\left(1 - \mathrm{e}^{-\mathrm{i}\kappa_\mathrm{p}}\right) \left(1 - \mathrm{e}^{\mathrm{i}\frac{\kappa_\mathrm{p}-\tilde\kappa}{2}}\right) \\ &- \left(\mathrm{e}^{\mathrm{i}\kappa_\mathrm{p}} - 1\right) \left(\mathrm{e}^{-\mathrm{i}\frac{\kappa_\mathrm{p}-\tilde\kappa}{2}} - 1\right) \Big] A_\mathrm{i}^* \,, \end{aligned} \tag{21}$$

and a similar equation for A_i with the replacements, $A_\mathrm{s} \leftrightarrow A_\mathrm{i}$, $\omega_\mathrm{s} \to \omega_\mathrm{i}$, and $\kappa_\mathrm{p} \to -\kappa_\mathrm{p}$.

The quasi-wave vector $\tilde\kappa$ is found from the solubility condition for Eq. (21) and equation for A_i, *i.e.* from the condition for the determinant of the system to be equal to zero. After some algebra the corresponding equation can be presented in the form,

$$\begin{aligned} 0 = {} & \sin\frac{\kappa_\mathrm{p} - 2\kappa_\mathrm{s} + \tilde\kappa}{4} \sin\frac{\kappa_\mathrm{p} - 2\kappa_\mathrm{i} - \tilde\kappa}{4} \\ & \times \sin\frac{\kappa_\mathrm{p} + 2\kappa_\mathrm{s} + \tilde\kappa}{4} \sin\frac{\kappa_\mathrm{p} + 2\kappa_\mathrm{i} - \tilde\kappa}{4} \\ & - \chi_3^2 |A_\mathrm{p}|^2 \sin^2\frac{\kappa_\mathrm{p}}{2} \sin^2\frac{\kappa_\mathrm{p} + \tilde\kappa}{4} \sin^2\frac{\kappa_\mathrm{p} - \tilde\kappa}{4} \,. \end{aligned} \tag{22}$$

A solution to this equation generally has the imaginary part that describes the amplification effect. We quantify the amplification with the gain coefficient $g = \mathrm{Im}(\tilde\kappa/2)$, which characterises the amplitude gain per unit cell and is related to the power gain of TWPA as

$$G(\mathrm{dB}) = 20 g N \log_{10}(\mathrm{e}) \,, \tag{23}$$

where N is the number of unit cells.

The exact numerical solution for g at the degeneracy point, $\omega_\mathrm{s} = \omega_\mathrm{i} = \omega_\mathrm{p}/2$, is presented in Fig. 2a for different pumping strengths. The pumping strength here is characterised through the quantity

$$\varepsilon = |\chi_3 \theta_\mathrm{p}| \,, \quad \theta_\mathrm{p} = 2\sin\frac{\kappa_\mathrm{p}}{2} A_\mathrm{p} = \frac{\omega_\mathrm{p}}{\omega_0} A_\mathrm{p} \,. \tag{24}$$

Here θ_p is the the amplitude of oscillation of phase difference across the cell associated with the pump amplitude at the node, A_p. At small frequencies, $\omega_\mathrm{p} \ll \omega_\mathrm{c}$, $\kappa_\mathrm{p} \ll 1$, the gain coefficient is small and grows linearly with frequency. It reaches a maximum and then sharply drops to zero at the gain cutoff frequency, $\omega_\mathrm{p} = \Omega_\mathrm{c}$. The maximum gain and Ω_c depend on the pumping strength as illustrated in Fig. 3. As seen from Fig. 2a, the maximum gain at large frequencies is quite large: for pumping strength $\varepsilon \approx 0.4$, the gain coefficient reaches the value $g \approx 0.06$, which translates to the power gain, $G \approx 26\,\mathrm{dB}$, for a chain with $N = 50$ cells.

A numerical solution of Eq. (22) for the gain coefficient as a function of detuning is presented in Fig. 2b with solid lines. The plots are made for the pump frequency values corresponding to maxima of the gain coefficients in Fig. 2a for the same pump intensities.

To better understand the gain properties, we derive an approximate analytical solution to Eq. (22). To this end we cast $\tilde{\kappa}$ on the form,

$$\tilde{\kappa} = \kappa_{\mathrm{s}} - \kappa_{\mathrm{i}} - 2\mathrm{i}g\,, \tag{25}$$

where quasi-wave vectors, $\kappa_{\mathrm{s,i}}$, are related to the signal and idler respective frequencies via the dispersion relation similar to Eq. (19). We also define the detuning from the degeneracy point,

$$\delta = \frac{\omega_{\mathrm{s}} - \omega_{\mathrm{p}}/2}{\omega_{\mathrm{p}}/2}\,, \tag{26}$$

and the phase mismatch $\Delta(\delta)$,

$$\Delta(\delta) = \kappa_{\mathrm{p}} - \kappa_{\mathrm{s}}(\delta) - \kappa_{\mathrm{i}}(\delta)\,. \tag{27}$$

At weak coupling, $\varepsilon \ll 1$, the gain coefficient is small, as is also seen in Fig. 2a, in comparison with the wave vectors $\kappa_{\mathrm{p}} \sim \kappa_{\mathrm{s}} \sim \kappa_{\mathrm{i}}$, which are of order unity at high frequencies, as given by the dispersion relation in Eq. (6). On the other hand, the phase mismatch, which is sufficient to suppress the gain is also small. Therefore, both g and $\Delta(\delta)$ are small additive corrections to $\kappa_{\mathrm{p,s,i}}$, and can be omitted from the corresponding terms in Eq. (22). This approximation yields the explicit solution for g,

$$\sinh^2\frac{g}{2} = -\sin^2\frac{\Delta(\delta)}{4} + \chi_3^2|A_{\mathrm{p}}|^2\frac{\sin^2\frac{\kappa_{\mathrm{p}}}{2}}{\sin\kappa_{\mathrm{s}}\sin\kappa_{\mathrm{i}}} \times\left(\sin^2\frac{\kappa_{\mathrm{s}}+\kappa_{\mathrm{i}}}{4} - \sin^2\frac{\kappa_{\mathrm{s}}-\kappa_{\mathrm{i}}}{4}\right)^2. \tag{28}$$

The obtained solution is a generalisation to a discrete chain and arbitrary frequency of the result obtained in [10] for a continuous medium. One can see from Eq. (28) that it is the competition between the nonlinear coupling controlled by the intensity of the pump (the second term on the right) and the phase mismatch (the first term on the right) that determines whether g is real or imaginary, *i.e.*, whether exponential amplification occurs or not. The sharp drop of the gain is explained by the increasingly strong dispersion near the cutoff frequency. At zero detuning, Eq. (28) reduces to the form

$$\sinh^2\frac{g}{2} = -\sin^2\frac{\Delta}{4} + \chi_3^2|A_{\mathrm{p}}|^2\sin^4\frac{\kappa_{\mathrm{p}}}{4}\,, \tag{29}$$

where

$$\Delta = \Delta(0) = \kappa_{\mathrm{p}} - 2\kappa_{\mathrm{s}} \tag{30}$$

is the phase mismatch between the frequency points, ω_{p} and $\omega_{\mathrm{p}}/2$. This solution is represented in Fig. 2 with dashed lines.

Equation (22) and its approximate analytical solution, Eq. (28), together with numerical solution presented in Fig. 2 constitute the first main result of this paper.

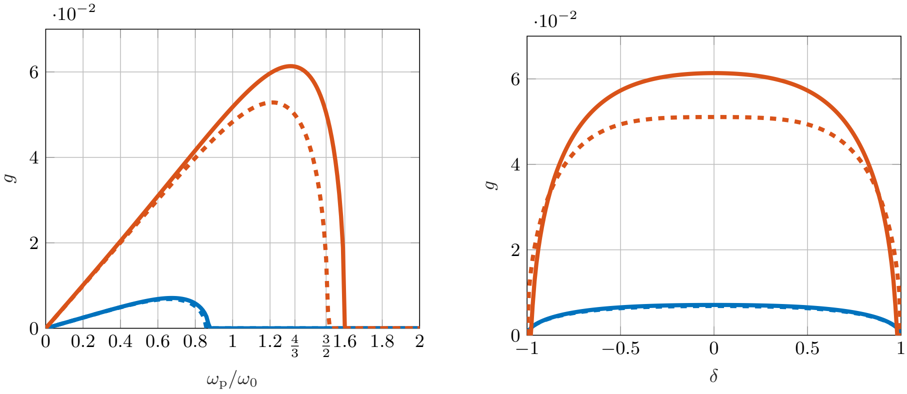

(a)

(b)

FIG. 2: Gain coefficient from numerically solving Eq. (22) (solid), and from Eq. (28) (dashed), for different pumping strengths, $\varepsilon = 0.1$ (blue) and 0.4 (orange). (a) Gain coefficient at zero detuning, $\delta = 0$, as function of pump frequency. (b) Gain coefficient as function of detuning at the pump frequencies, $\omega_{\mathrm{p}}/\omega_0 = 0.67$ and 1.31, corresponding to the maximum gain coefficient at zero detuning.

A. Validity of the model

The validity of the model above relies on the absence of up-converted modes of the pump, signal, and idler. For the pump, the condition, $\omega_{\mathrm{p}} > \omega_0$, guarantees that the

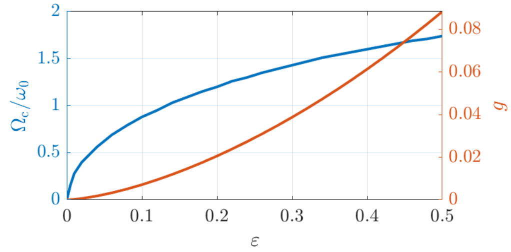

FIG. 3: Maximum value of the gain coefficient (orange) and the gain coefficient cutoff frequency Ω_{c} (blue) as functions of the pumping strength.

second pump harmonic falls above the cutoff, $\omega_{\mathrm{c}} = 2\omega_0$. For the signal/idler the lowest bound is established by condition that the up-converted signal at zero detuning falls above the cutoff, $\omega_{\mathrm{p}}/2 + \omega_{\mathrm{p}} > 2\omega_0$. This yields a more stringent constraint, $\omega_{\mathrm{p}} > \Omega_{\mathrm{th}} = 4\omega_0/3$. At pump frequency larger than this threshold value, the detuned signal and idler are not up-converted within the band defined by equation,

$$|\delta| < 3\left(1 - \frac{\Omega_{\mathrm{th}}}{\omega_{\mathrm{p}}}\right). \tag{31}$$

This situation is illustrated in Fig. 4.

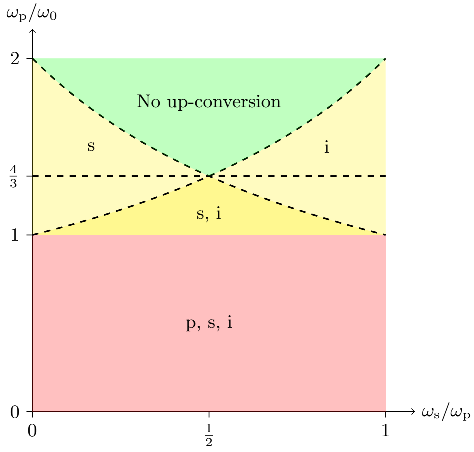

FIG. 4: The regions of the absence/presence of up-conversion of pump, signal and idler. In the green region no up-conversion takes place, horizontal dashed line indicates Ω_{th}; in light yellow regions up-conversion of either signal or idler is possible, while in yellow region both signal and idler are up-converted but pump is not; in pink region all three modes are up-converted.

Therefore we conclude that the three-mode model considered is justified, when the gain cutoff frequency exceeds the threshold for no-up-conversion, $\Omega_{\mathrm{c}}(\varepsilon) > \Omega_{\mathrm{th}}$, and within the bandwidth in Eq. (31). This condition imposes the lowest bound for the required pumping strength. An accurate estimate of the lowest bound is extracted from the numerical solution to Eq. (22),

$$\varepsilon \gtrsim 0.25\,. \tag{32}$$

To obtain an analytical estimate we assume, $g = 0$ in Eq. (29), to get,

$$\chi_3|A_{\mathrm{p}}| > \frac{\sin\frac{\Delta}{4}}{\sin^2\frac{\kappa_{\mathrm{p}}}{4}}\,. \tag{33}$$

At $\omega_{\mathrm{p}} = \Omega_{\mathrm{th}}$, $\kappa_{\mathrm{p}} \approx 0.46\pi$, and for zero detuning, $\delta = 0$, we have $\kappa_{\mathrm{s}} \approx 0.22\pi$, giving $\Delta \approx 0.03\pi$. This results in the bound for the pumping strength, $\chi_3|A_{\mathrm{p}}| > 0.20$, or $\varepsilon \gtrsim 0.27$, which slightly overestimates the exact result from Eq. (32).

The crucial question is now whether the required coupling strength can be experimentally achieved with a feasible pump intensity. Let us first consider the dc current biased TWPA. The pumping strength here is limited by the switching of the Josephson junctions to the resistive branch. In the quantum limit, the maximum dc supercurrent that the junction can sustain corresponds to the disappearance of the last quantized energy level from the well of the tilted Josephson potential. The maximum dc supercurrent can be crudely estimated from the relation, $\hbar\omega_{\mathrm{pl}}/2 \sim \Delta U$, where $\omega_{\mathrm{pl}} = \sqrt{\cos\theta_0/(L_{\mathrm{J}}C_{\Sigma})}$ is the effective plasma frequency for the junction, $C_{\Sigma} = C/2 + C_{\mathrm{J}} \approx C/2$, and $\Delta U \approx (2E_{\mathrm{J}}/3)\cos^3\theta_0$ is the depth of the well of the tilted Josephson potential. Impedance matching of the TWPA with the transmission line, $\sqrt{L_{\mathrm{J}}/(C\cos\theta_0)} = Z_0$, gives for the maximum current, $\cos^2\theta_0 \sim 3\pi\sqrt{2}Z_0/R_q$, where $R_q = h/(2e^2)$ is the quantum resistance; this corresponds to $I_{\mathrm{dc}} \sim 0.97 I_{\mathrm{c}}$. Assuming that the quasi-classical tunnelling rate, $\Gamma \propto \exp(-7.2\Delta U/\hbar\omega_{\mathrm{pl}})$ [36], is valid for the two-three quantized energy levels in the well [37], and also taking into account the experimental observations, *e.g.* in Ref. [38], we may safely assume for the switching current value, $I \approx 0.9 I_{\mathrm{c}}$.

When the pump is on and has a small frequency, $\omega_{\mathrm{p}} \ll \omega_{\mathrm{pl}}$, the instant adiabatic current consists of the dc biasing current, I_{dc}, and the pump ac current, I_{p}, and their sum should not exceed the switching current, $I_{\mathrm{dc}} + I_{\mathrm{p}} < 0.9 I_{\mathrm{c}}$. The maximum pumping strength under this constraint is, $\varepsilon = 0.28$, which is achieved at $I_{\mathrm{dc}} = 0.63 I_{\mathrm{c}}$ and $I_{\mathrm{p}} = 0.27 I_{\mathrm{c}}$. Although this pumping strength is above the bound in Eq. (32), the frequency window where the model is valid is very small, $\Omega_{\mathrm{c}} - \Omega_{\mathrm{th}} \approx 0.06\omega_0$, Fig. 4, making the amplification bandwidth unacceptably narrow. Furthermore, the corresponding pumping current is too large given the theory constraint, $I_{\mathrm{p}} \ll I_{\mathrm{c}}$, more feasible would be the lower current values, $I_{\mathrm{p}} \sim 0.1 I_{\mathrm{c}}$. In addition, a spread of the junction parameters in a real TWPA would also reduce the estimated pumping strength.

More importantly, however, is that the relevant ac regime is non-adiabatic: the pump frequencies above the no-up-conversion threshold, $\omega_\mathrm{p} > \Omega_\mathrm{th} \approx 1.33\bar{\omega}_0$, are close to and even higher than the plasma frequency, $\omega_\mathrm{pl} = \sqrt{2}\bar{\omega}_0 \approx 1.41\bar{\omega}_0$. In this regime, the resonant excitation facilitates tunnelling (especially due to the multi-photon processes at large pump amplitude), therefore the biasing current should be even smaller than in the adiabatic regime, hence the pumping strength would be further reduced.

In the case of an rf-SQUID TWPA, the maximum nonlinear coupling is achieved at $\theta_0 = \pi/2$ [29], when $\chi_3 = L/L_\mathrm{J}$. For a non-hysteretic regime, $L/L_\mathrm{J} < 1$, combination of this constraint with the a small value of the amplitude of phase oscillation, $\theta_\mathrm{p} < 0.1$, results in a pumping strength, $\varepsilon < 0.1$, which is below the threshold, Eq. (32). Similar argument also applies to the SNAIL-TWPA.

To summarise, we conclude that the 3-mode amplification regime, which would provide the high exponential gain at high frequencies, $\omega_\mathrm{p} \sim \omega_0$ cannot be realised in practice with any of the TWPA designs considered here. The desired condition, $\Omega_\mathrm{c}(\varepsilon) > \Omega_\mathrm{th}$, cannot be fulfilled because of small values of nonlinear 3WM coefficients in realistic devices and limited pumping current.

To go beyond the studied 3-mode model, two strategies can be followed. The one is to consider the lower frequencies and include the up-converted modes in the model, while the other is to keep the 3-mode model but consider dispersion engineering at high frequencies. In the next section we will discuss the first option in detail.

IV. QUASILINEAR DISPERSION REGIME

In this section we analyse TWPA performance in the low frequency region, $\omega \ll \omega_0$, $\kappa \ll \pi$, where the dispersion relation is quasi-linear. The limit of the continuous medium is natural for the kinetic inductance TWPA, but it is also considered in most of publications devoted to the Josephson junction TWPAs.

In this limit the discrete chain of the Josephson junctions is described with a continuous variable, $an \to x$, $\phi_n \to \phi(x)$, where a is the physical length of the unit cell. Then the difference equation Eq. (16) turns into a differential equation,

$$\begin{aligned}&\frac{1}{\omega_0^2}\ddot{\phi} + 4\sin^2\frac{a\hat{k}}{2}\phi \\ &= \frac{\chi_3}{2}\left\{\left[\left(1-\mathrm{e}^{-\mathrm{i}a\hat{k}}\right)\phi\right]^2 - \left[\left(\mathrm{e}^{\mathrm{i}a\hat{k}}-1\right)\phi\right]^2\right\}\,,\end{aligned} \tag{34}$$

where $\hat{k} = -\mathrm{i}\partial_x$. Keeping the lowest order terms with respect to a in the expansion of the interaction term, we write Eq. (34) in the form,

$$\frac{1}{\omega_0^2}\ddot{\phi} + 4\sin^2\frac{a\hat{k}}{2}\phi \;=\; \frac{\chi_3 a^3}{2}\, i\hat{k}(\hat{k}\phi)^2\,. \tag{35}$$

This dynamical equation (and a similar one for the 4WM) is a standard object of study in the TWPA literature.

To analyse the resonant wave dynamics described by this equation one has to take into account, in addition to the down-conversion discussed in the previous section, the processes which are efficient for a weakly dispersive medium: (i) generation of pump harmonics with frequencies $n\omega_\mathrm{p}$ [33], (ii) up-conversion of the signal and down-converted idler by the pump tone and its harmonics, $\omega_\mathrm{s,i} + n\omega_\mathrm{p}$ [34]. The processes that can be neglected for a weak signal include pump depletion and generation of signal/idler harmonics and their intermodulation products.

A. Pump harmonics

Let us first consider pump harmonic generation. When a pump tone is injected, the field in the cavity has the form

$$\phi(x,t) = \frac{1}{2}\sum_{m=1}^{M}\left(A_{m\mathrm{p}}(x)\mathrm{e}^{\mathrm{i}(k_{m\mathrm{p}}x - m\omega_\mathrm{p}t)} + \mathrm{c.c.}\right)\,, \tag{36}$$

where k is a wave vector related to ω via the free wave dispersion relation, $ka = 2\arcsin(\omega/(2\omega_0))$, and M is the number of harmonics included in the computation (see below). A slow variation of the amplitudes of the harmonics accounts for the effect of nonlinear interaction.

Substituting Eq. (36) in Eq. (35) we get a set of M coupled nonlinear equations for the pump harmonics,

$$\begin{aligned}&A'_{m\mathrm{p}} = \frac{\chi_3 a}{4}\times \\ &\left(\sum_{n=m+1}^{M} k_{n\mathrm{p}}k_{(n-m)\mathrm{p}}A_{n\mathrm{p}}A^*_{(n-m)\mathrm{p}}\mathrm{e}^{\mathrm{i}\Delta_{n,m}x}\right. \\ &\left.-\frac{1}{2}\sum_{n=1}^{m-1} k_{n\mathrm{p}}k_{(m-n)\mathrm{p}}A_{n\mathrm{p}}A_{(m-n)\mathrm{p}}\mathrm{e}^{-\mathrm{i}\Delta_{m,n}x}\right)\,,\end{aligned} \tag{37}$$

where the prime signifies spatial derivative, $A' = \mathrm{d}A/\mathrm{d}x$, $\Delta_{n,m} = k_{n\mathrm{p}} - k_{m\mathrm{p}} - k_{(n-m)\mathrm{p}}$, and $m \in \{1, ..., M\}$ is the harmonic number. In this equation, the first sum describes coupling to the higher harmonics, while the second sum describes coupling to the lower harmonics, as illustrated in Fig. 5. The factor 1/2 in the second sum accounts for the double counting in the sum, *e.g.* $n = 1$ and $n = m - 1$.

When the number of harmonics is restricted to $M = 2$, an analytical solution is available [33], which shows that for a linear dispersion the injected tone is fully converted to the second harmonic on a length inversely proportional to the amplitude of the injected signal. In the presence of dispersion, both harmonics exhibit oscillatory behaviour (see blue curve in Fig. 7) while preserving the quantity $|A_\mathrm{p}(x)|^2 + 4|A_{2\mathrm{p}}(x)|^2 =$ constant. Analytical solutions are also available for larger number of harmonics, but their behaviour becomes rather complex, so we resort to numerics.

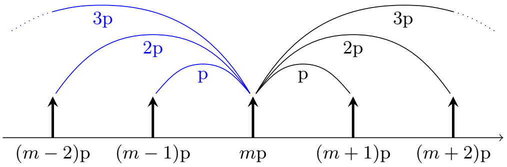

FIG. 5: Interaction of m-th pump harmonic illustrating structure of Eq. (37). Each process is marked with the pump harmonic that is driving the process.

We perform a numerical study under the assumption that all relevant harmonics have frequencies well below the cutoff. For a weak dispersion the pre-exponential factors in Eq. (37) can be approximated with linear functions, $k_{m\mathrm{p}}a = m\omega_\mathrm{p}/\omega_0$, while the exponential dephasing factors are approximated with the lowest order (cubic) corrections. The latter can be expressed through the dephasing $\Delta \approx k_\mathrm{p}^3 a^2/32$ defined in Eq. (26),

$$\begin{aligned}\Delta_{m,n} &= 8\Delta d_{m,n} = \frac{k_\mathrm{p}^3 a^2}{4}\, d_{m,n}\,, \\ d_{m,n} &= \frac{1}{2} mn(m-n)\,.\end{aligned} \tag{38}$$

To compute and analyse the solutions to Eq. (37), it is convenient to introduce dimensionless spatial coordinate and rescaled harmonic amplitudes,

$$\xi = \frac{\varepsilon k_\mathrm{p}}{4} x, \quad a_{m\mathrm{p}}(\xi(x)) = m\frac{A_{m\mathrm{p}}(x)}{A_\mathrm{p}(0)}\,, \tag{39}$$

where ε is the pumping strength defined in Eq. (24), which has the form in the low frequency limit, $\varepsilon = |\chi_3 A_\mathrm{p}(0)|k_\mathrm{p}a$. Then Eq. (37) reduces to a compact form,

$$\begin{aligned}(a_m)'_\xi = m &\sum_{n=m+1}^{M} a_n a_{n-m}^* \mathrm{e}^{\mathrm{i}\mu\xi d_{n,m}} \\ &- \frac{m}{2}\sum_{n=1}^{m-1} a_n a_{m-n} \mathrm{e}^{-\mathrm{i}\mu\xi d_{m,n}}\,,\end{aligned} \tag{40}$$

where the spatial behaviour of all harmonics is described with a *single scaling parameter*,

$$\mu = \frac{32\Delta}{\varepsilon k_\mathrm{p}} \approx \frac{k_\mathrm{p}^2 a^2}{\varepsilon}\,. \tag{41}$$

This parameter is proportional to the ratio of the dephasing and the nonlinear pumping strength, and has clear physical meaning indicating that it is the interplay between the dispersion and the nonlinear coupling (the pumping strength) that defines the behaviour of the harmonics.

The differential equations in Eq. (40) are solved numerically for different values of μ and M using 4th and 5th order Runge-Kutta methods of the MATLAB function `ode45`.

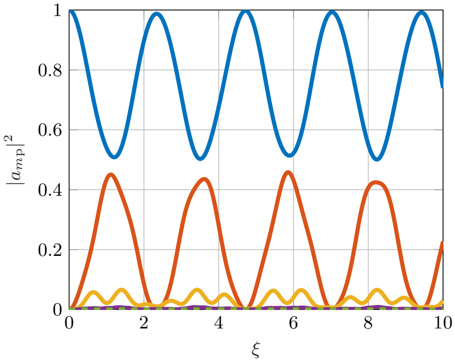

FIG. 6: First five harmonics for $\mu = 2$ and $M = 5$: First (blue), second (orange), third (yellow), fourth (purple) and fifth (dashed green).

The spatial dependence of the solutions truncated at $M = 5$ is shown in Fig. 6 for $\mu = 2$. All the harmonics oscillate but while amplitudes of the first and second harmonics are substantial, the amplitudes of higher harmonics, $m = 3, 4, 5$, are decreasingly small. Correspondingly, the effect of the latter on the main pump tone is small, as illustrated in Fig. 7 for $\mu = 2$ and different values of M. Here the solution for the main pump tone coupled to three harmonics clearly differs from the one coupled to two harmonics, but the more harmonics are included the smaller effect they have on the solution for the main pump tone. The solution for the main pump tone appears to converge at $M \gtrsim 5$.

Our numerical studies show that the number of large-amplitude harmonics depends on the value of μ, the number of large-amplitude harmonics increases when μ decreases, which corresponds to a weaker dispersion or stronger pumping. Furthermore, for a given μ, the amplitudes of harmonics with numbers exceeding a certain critical value, $m > M_\mathrm{c}$, become negligible on a given length, as illustrated in Fig. 8. One can hence truncate Eq. (40) at $M = M_\mathrm{c}(\mu)$ to accurately compute the solution for the main pump tone. The result of such a study is presented in Fig. 9. We solve Eq. (40) for certain val-

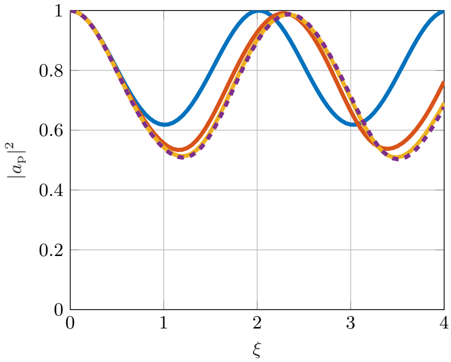

FIG. 7: Solution for $|a_{\rm p}(\xi)|^2$ to Eq. (40), using $\mu = 2$ and different number of harmonics included in computation, $M = 2$ (blue), 3 (orange), 4 (yellow), 5 (dashed magenta).

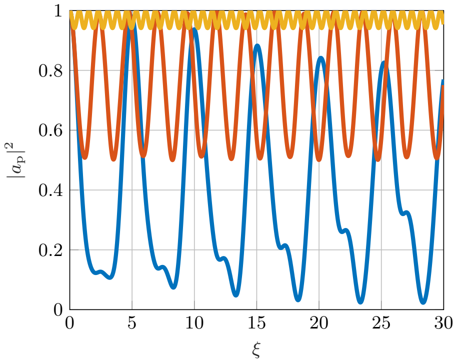

FIG. 9: Solution for $|a_{\rm p}(\xi)|^2$ to Eq. (40), using $\mu = 0.5$ (blue), 2 (orange), and 8 (yellow) and corresponding $M_{\rm c} = 11, 6, 4$.

ues of μ and find the corresponding values for $M_{\rm c}$. For $\mu = 0.5$ we find that $M_{\rm c} = 10$, for $\mu = 2$ we find that $M_{\rm c} = 5$, and for $\mu = 8$, $M_{\rm c} = 3$. Different values of $M_{\rm c}$ as a function of μ is shown in Fig. 8. As seen in Fig. 9, the pump behaviour can in general be summarised as follows: The pump oscillates between full transmission and some lower bound. The larger the μ, the smaller the oscillation amplitude and period.

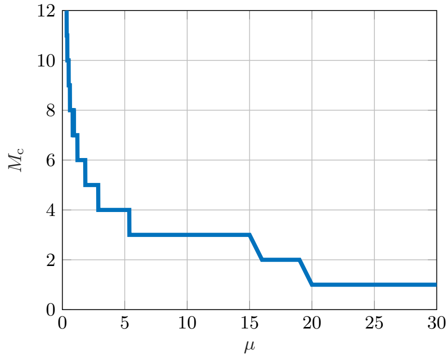

FIG. 8: The critical number of harmonics $M_{\rm c}$ for different values of μ for the length $\xi = 10$ and error tolerance 0.01.

B. Comparison with four-wave mixing

It is instructive to compare the pump harmonic generation studied in the previous section to the pump harmonic generation by the 4WM, where the phase mismatch introduced by the Kerr effect prevents exponential amplification. One should anticipate that a similar mechanism would suppress the generation of pump high harmonics [33]. We test this assumption by computing the third harmonic of the pump using the developed scaling method.

The equations for the pump harmonics are derived in a similar way as for the 3WM. Restricting to the third harmonic, we have,

$$A'_{\rm p} = \mathrm{i}\frac{\chi_4 a^2}{8}\left(k_{\rm p}^3 A_{\rm p}^2 A_{\rm p}^* - k_{3\rm p} k_{\rm p}^2 A_{3\rm p} A_{\rm p}^{*2} \mathrm{e}^{\mathrm{i}(k_{3\rm p}-3k_{\rm p})x}\right) \tag{42a}$$

$$A'_{3\rm p} = \mathrm{i}\frac{\chi_4 a^2}{8}\left(2k_{3\rm p} k_{\rm p}^2 A_{3\rm p} A_{\rm p} A_{\rm p}^* - \frac{1}{3} k_{\rm p}^3 A_{\rm p}^3 \mathrm{e}^{-\mathrm{i}(k_{3\rm p}-3k_{\rm p})x}\right), \tag{42b}$$

where χ_4 is the 4-th order nonlinearity coefficient derived in a similar way to χ_3 in Section II. The value of χ_4 is $\frac{1}{2}$ for a junction TWPA, while it is typically smaller for an rf-SQUID or a SNAIL TWPA at zero bias. With similar rescalings as in Section IV A,

$$\xi = \frac{\chi_4 A_{\rm p}(0)^2 k_{\rm p}^3 a^2}{8} x, \quad a_{m\rm p}(\xi) = m\frac{A_{m\rm p}}{A_{\rm p}(0)}, \tag{43}$$

we write these equations in a dimensionless form,

$$(a_{\rm p})'_\xi = \mathrm{i}\left(a_{\rm p}^2 a_{\rm p}^* - 3a_{3\rm p} a_{\rm p}^{*2} \mathrm{e}^{\mathrm{i}\mu\xi}\right), \tag{44a}$$

$$(a_{3\rm p})'_\xi = 3\mathrm{i}\left(2a_{3\rm p} a_{\rm p} a_{\rm p}^* - \frac{1}{3} a_{\rm p}^3 \mathrm{e}^{-\mathrm{i}\mu\xi}\right). \tag{44b}$$

Here the spatial behaviour of both harmonics is defined by a single scaling parameter,

$$\mu = \frac{256\Delta}{\chi_4 A_{\rm p}(0)^2 k_{\rm p}^3 a^3} \approx \frac{8k_{\rm p}^2 a^2}{\chi_4 \theta_{\rm p}(0)^2}. \tag{45}$$

We solve Eq. (42) numerically for different values of μ, the result is presented in Fig. 10. In contrast to 3WM, where the first harmonic is completely depleted in the absence of frequency dispersion, $\mu = 0$ (blue line), it oscillates for the 4WM (yellow line), similar to 3WM at a considerable dispersion, $\mu = 3$ (orange line).

Thus we conclude that the Kerr effect, caused by the χ_4-term, not only prevents exponential amplification but also suppresses the generation of higher harmonics, which makes up-conversion processes less dangerous for 4WM amplification compared to 3WM.

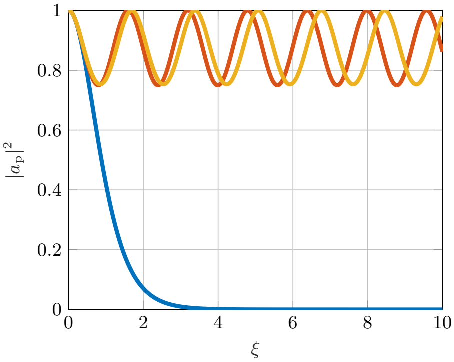

FIG. 10: Spatial dependence of pump signal under 4WM including one up-converted mode for non-dispersive spectrum, $\mu = 0$ (yellow); for comparison the pump signal under 3WM is shown for $\mu = 0$ (blue), and for dispersive spectrum, $\mu = 3$ (orange).

C. Full multimode model

Now we proceed with the discussion of the amplification in the 3WM regime and assume a weak signal tone being injected in addition to the strong pump tone, $A_{\rm s}(0) \ll A_{\rm p}(0)$. We perform our analysis under the same assumption as in Section III of small amplitudes of signal and idler compared to the pump amplitude within the whole TWPA, $A_{\rm s}(x), A_{\rm i}(x) \ll A_{\rm p}(x)$. This assumption allows us to neglect the back-action of signal and idler on the pump (pump depletion), and also neglect the generation of signal and idler harmonics while allowing the up-conversion of signal and idler by the pump harmonics. The latter assumption implies a linearisation of the equations with respect to all signal and idler harmonics.

With the adopted approximations, the field in the TWPA will consist of a linear combination of the pump and pump harmonics, $m\omega_{\rm p}$, signal $\omega_{\rm s}$, down-converted idler, $\omega_{\rm i} = \omega_{\rm p} - \omega_{\rm s}$, and all their up-converted modes by the pump and pump harmonics, $\omega_{{\rm s}+m{\rm p}} = \omega_{\rm s} + m\omega_{\rm p}$, $\omega_{{\rm i}+m{\rm p}} = \omega_{\rm i} + m\omega_{\rm p}$, see Fig. 11. The ansatz is therefore,

$$\begin{aligned}\phi(x,t) &= \frac{1}{2}\sum_{m=1}^{M}\left[A_{m{\rm p}}{\rm e}^{{\rm i}k_{m{\rm p}}x-{\rm i}m\omega_{\rm p}t} + {\rm c.c}\right]\\ &+ \frac{1}{2}\sum_{m=0}^{M-1}\Big[A_{{\rm s}+m{\rm p}}{\rm e}^{{\rm i}k_{{\rm s}+m{\rm p}}x-{\rm i}(\omega_{\rm s}+m\omega_{\rm p})t}\\ &+ A_{{\rm i}+m{\rm p}}{\rm e}^{{\rm i}k_{{\rm i}+m{\rm p}}x-{\rm i}(\omega_{\rm i}+m\omega_{\rm p})t} + {\rm c.c.}\Big]\,.\end{aligned} \tag{46}$$

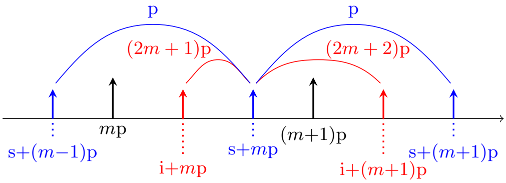

FIG. 11: Frequency diagram illustrating structure of Eq. (47) for the signal m-th harmonic, $a_{{\rm s}+m{\rm p}}$; signal modes (blue), idler modes (red), pump harmonics (black), down-conversion processes (red) and up-conversion processes (blue). Each process is marked with the pump harmonic that is driving the process.

Using the reduced variables introduced in Eqs. (27), (39) and (41) and detuning δ defined in Eq. (26), the equations for the signal modes take the form,

$$\begin{aligned}(a_{{\rm s}+m{\rm p}})'_\xi &= \left(m + \frac{1+\delta}{2}\right)\\ &\times\Bigg(\sum_{n=m+1}^{M} a_{n{\rm p}}a^*_{{\rm i}+(n-m-1){\rm p}}{\rm e}^{{\rm i}\mu\xi d^{\rm p}_{n,m}}\\ &+ \sum_{n=m+1}^{M-1} a_{{\rm s}+n{\rm p}}a^*_{(n-m){\rm p}}{\rm e}^{{\rm i}\mu\xi d^{\rm s}_{n,m}}\\ &- \sum_{n=1}^{m} a_{n{\rm p}}a_{{\rm s}+(m-n){\rm p}}{\rm e}^{-{\rm i}\mu\xi d^{\rm s}_{m,(m-n)}}\Bigg)\,,\end{aligned} \tag{47}$$

where $m \in [0, M-1]$. The numerical factors in the exponents are derived by using the cubic approximation of the dispersion relation and have the form,

$$\begin{aligned}d^{\rm p}_{n,m} &= \frac{k_{n{\rm p}} - k_{{\rm s}+m{\rm p}} - k_{{\rm i}+(n-m-1){\rm p}}}{8\Delta}\\ &= \frac{1}{6}\left(n^3 - \left(m + \frac{1+\delta}{2}\right)^3 - \left(n - m - 1 + \frac{1-\delta}{2}\right)^3\right),\\ d^{\rm s}_{n,m} &= \frac{k_{{\rm s}+n{\rm p}} - k_{{\rm s}+m{\rm p}} - k_{(n-m){\rm p}}}{8\Delta}\\ &= \frac{1}{6}\left(\left(n + \frac{1+\delta}{2}\right)^3 - \left(m + \frac{1+\delta}{2}\right)^3 - (n-m)^3\right),\end{aligned} \tag{48}$$

where Δ is defined in Eq. (27). The equations for the idler modes are similar, but with the replacements s↔i and $\delta \leftrightarrow -\delta$.

For $M = 1$, Eq. (47) reduces to the continuous analog of the 3-mode model in Section III,

$$\begin{aligned}(a_{\mathrm{s}})'_\xi &= \frac{1+\delta}{2} a_{\mathrm{i}}^* \mathrm{e}^{\mathrm{i}\mu\xi\left(1-\delta^2\right)/8} \\ (a_{\mathrm{i}})'_\xi &= \frac{1-\delta}{2} a_{\mathrm{s}}^* \mathrm{e}^{\mathrm{i}\mu\xi\left(1-\delta^2\right)/8}\,.\end{aligned} \tag{49}$$

The solution has an exponential form, $a_{\mathrm{s}},\, a_{\mathrm{i}} \propto \mathrm{e}^{g\xi}$, with the gain coefficient [10],

$$g = \frac{1}{2}\sqrt{\left(1-\delta^2\right)\left[1-\frac{\mu^2}{8^2}\left(1-\delta^2\right)\right]}\,, \tag{50}$$

that coincides with the long-wave length asymptotic in Eq. (28). The exponential gain occurs only for small values of the scaling parameter given by, $\mu < 8/\sqrt{1-\delta^2}$.

We solve Eq. (47) numerically in the same way as we solved them for the pump harmonics, including the spatial dependence of the pump harmonics. The results for the power gain as the function of length, $G(\xi) = |a_{\mathrm{s}}(\xi)/a_{\mathrm{s}0}|^2$, are shown in Figs. 12 and 13 for $\mu = 1$ and $\mu = 10$ at zero detuning ($\delta = 0$). These results demonstrate two distinctly different amplification regimes: For small values of μ, the gain grows on average with the TWPA length, but much slower than expected from 3-mode model, Eq. (50). The gain suppression is the result of the up-conversion with many up-converted modes affecting the signal. In Fig. 12, the gain reaches value $G \sim 20\,\mathrm{dB}$ at scaled length $\xi \approx 30$. In the opposite case of large μ, the gain profile converges quickly, and the number of modes included in the simulation is small. Correspondingly, the gain spatial profile becomes oscillatory and has a relatively small amplitude, Fig. 13. This reduction of the gain is the effect of phase mismatch, in accord with the criterion of a non-exponential amplification of the three-mode model, $\mu > 8$.

While one should not expect the gain larger than few dB for TWPA with any length when μ is large, for small μ the gain grows with the length and interesting question is what gain can be achieved for realistic Josephson junction TWPA. The limitation is imposed by the necessity to accommodate all relevant modes within the spectral range. For the ten pump harmonics involved, as in Fig. 12, the pump frequency should be limited, $\omega_{\mathrm{p}} < 0.1\omega_{\mathrm{c}}$, which corresponds to $ka < 0.2$. From Eqs. (39) and (41), we then deduce the real space length, $x \sim 500a\xi = 15000$ unit cells. Such a long TWPA is unpractical.

Summarising, we formulate the second important result of this paper: in weakly dispersive spectral region of low frequencies the gain above 20 dB is hard to achieve. For small μ, the gain is reduced by a strong up-conversion effect, while for large μ, the gain is small and oscillatory because of a large effective phase mismatch.

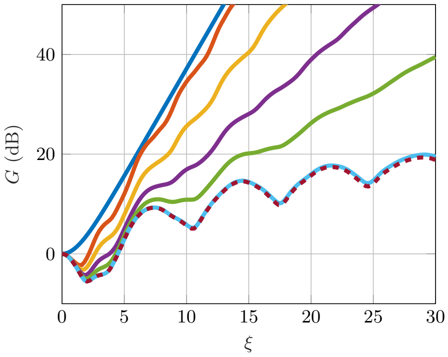

FIG. 12: Gain G for $\mu = 1$ at zero detuning, $\delta = 0$, and $M = 1$, 4, 5, 6, 7, and 10 (from top to bottom), and $M = 11$ (dashed magenta).

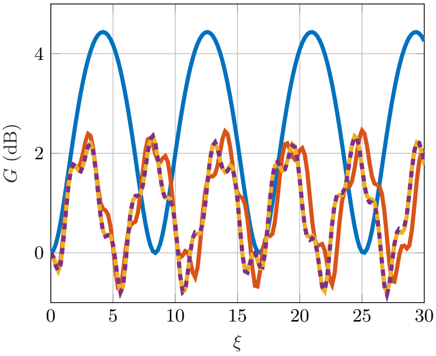

FIG. 13: Gain G for $\mu = 10$ at zero detuning, $\delta = 0$, and $M = 1$ (blue), 2 (red), 3 (yellow), and 4 (dashed purple).

D. Comparison with experiment

In this section we compare our theoretical predictions with experiments performed on a SNAIL-TWPA, Fig. 1d. The device consists of $N = 440$ unit cells, each unit cell contains one junction with $I_{\mathrm{c}1} = 0.8\,\mu\mathrm{A}$, and $\mathcal{N} = 3$ identical junctions with $I_{\mathrm{c}2} = 3\,\mu\mathrm{A}$, Eq. (12). The biasing magnetic flux is applied at $\Phi \approx 0.4\Phi_0$, where $\chi_3(\Phi) \approx 0.82$ (recall Eq. (15)), and the four-wave mixing vanishes. The pump frequency is placed at $f_{\mathrm{p}} = 8.5\,\mathrm{GHz}$, and the transmission ($S_{21}$) is measured using a VNA while sweeping the signal frequency within the band $4-12\,\mathrm{GHz}$. We determine the gain by comparing the transmission of the signal for pump on versus pump off. The data is presented in Figs. 14 and 15 with black lines for the expected pump powers $P_{\mathrm{p}}^{\mathrm{exp}} \approx -99\,\mathrm{dBm}$ and $P_{\mathrm{p}}^{\mathrm{exp}} \approx -94\,\mathrm{dBm}$, respectively. The red lines represent

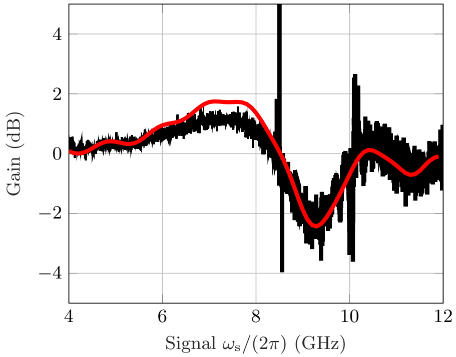

FIG. 14: Measured data for a SNAIL-TWPA for the expected pump power $P_p^{\text{exp}} \approx -99\,\text{dBm}$ (black) and pump frequency $\omega_p/(2\pi) = 8.5\,\text{GHz}$, and a theory fit (red) computed using the generalized quasi-linear model with $\mu = 15.18$ and $\xi = 2.77$, Eqs. (40) and (47).

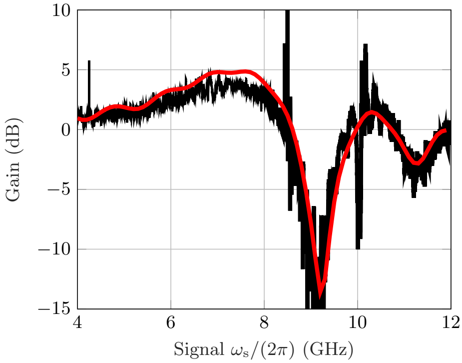

FIG. 15: Measured data for a SNAIL-TWPA for the expected pump power $P_p^{\text{exp}} \approx -94\,\text{dBm}$ (black) and pump frequency $\omega_p/(2\pi) = 8.5\,\text{GHz}$, and a theory fit (red) computed using the generalised quasi-linear model with $\mu = 8.54$ and $\xi = 4.93$, Eqs. (40) and (47).

the theoretical fit.

The fitting is done by using Eqs. (40) and (47). These equations contain two parameters, the scaling parameter μ, and the signal detuning δ. We generate the solution, $a_s(\xi; \delta, \mu)$ for chosen δ and μ and compute the gain at the end of the chain for a range of detunings, $G(\xi_{\max}, \delta, \mu)$. Then we sweep the two parameters, $\xi_{\max}$ and μ, to obtain the best fit to the data. Equivalently, one can use the parameters, $k_p a$ - normalised pump wave vector and ε - strength of coupling, which are related to $\xi_{\max}$ and μ by virtue of Eq. (39) for the given length of the chain and Eq. (41), in which we use the exact dispersion relation, Eq. (6), including the junction capacitances.

The parameter values extracted from the fitting are presented in Table II. The values of ε are found different for both datasets, which agrees quantitatively with the difference in the pump powers. At the same time, the value of $k_p a$ is the same in both cases as expected. The found value of the pump wave vector, $k_p a = 0.51$, however, differs from the theoretical value, $k_p a = 0.42$, computed from the dispersion relation, Eq. (6) using the SNAIL parameters, $\omega_S = 2\pi \cdot 20.6\,\text{GHz}$, and $C = 154\,\text{fF}$ and $C_J = 17.9\,\text{fF}$. We attribute this discrepancy to a non-uniform magnetic flux bias. The on-chip pump current, I_p, is determined by computing the pump-induced phase difference, $|\theta_p(0)| = \varepsilon/|\chi_3|$, Eq. (24), and then connecting it to the current using Eq. (13). The found values of the on-chip pump power are consistent with the expected values, as the estimated loss of the line is $\sim 84\,\text{dB}$.

Summarising, the theory reproduces very well the measured frequency dependence of the gain, $G(\omega_s)$, despite that only two fitting parameters are at hand to describe an intricate interplay of the pump, signal, idler and their up-converted modes. Furthermore, our analysis reveals that the measurements are done in the regime of non-exponential amplification of large μ, Fig. 13, which explains the small measured values of the gain.

TABLE II: Parameters extracted from the fitting the data in Figs. 14 and 15.

P_p^{exp} (dBm)	−99	−94
ε	0.0504	0.0896
$k_p a$	0.51	0.51
μ	15.18	8.54
$\xi_{\max}$	2.77	4.93
I_p (nA)	52	93
P_p (dBm)	−101.6	−96.6
Fig.	14	15

V. A SOLUTION: TWO-BAND FREQUENCY SPECTRUM

In this section we revisit the 3-mode model of Section III and consider the possibility of reducing the dispersion at high frequencies, in the no-up-conversion region, $\omega_p > \Omega_{\text{th}} = 4\omega_0/3$, to maintain the high gain. The idea is to create a sweet spot in the TWPA frequency spectrum where the signal injected at the degeneracy point, $\omega_s = \omega_p/2$, is exactly phase matched with the pump, $\kappa_s = \kappa_p/2$. Such a possibility does not exist for the TWPA studied in Section III. However, as we theoretically prove in this section, such a possibility appears for a TWPA with a two-band frequency spectrum (cf. [19]). At such a sweet spot a strong exponential amplification is predicted to occur and, moreover, it persists within a wide frequency band.

A common way to create a gap in the TWPA spectrum is to periodically modulate the device parameters along the propagation direction. This is routinely done for kinetic inductance TWPAs by modulating the geometry, and thereby the impedance, of the transmission line [13]. For the Josephson junction TWPAs another method is used – adding linear LC-oscillators to the TWPA cells. In this case, a spectral gap opens at the resonance frequency of the oscillators. This method of dispersion engineering is used in four-wave mixing devices to mitigate the Kerr effect [23–25].

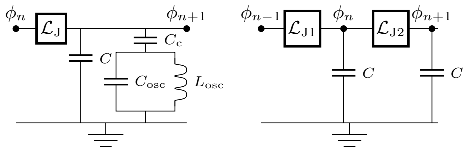

(a) (b)

FIG. 16: Circuit diagrams for TWPAs with two-band frequency spectrum; (a) LC-oscillators added to the unit cells, and (b) periodically modulated parameters of the unit cells.

A. Chain with oscillators

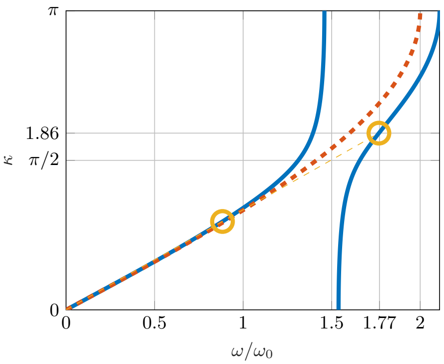

FIG. 17: 2-band frequency dispersion relation for a TWPA with LC-oscillators with $\omega_1 = 1.5\omega_0$ and $\nu = 0.95$ (solid lines). The dispersion relation exhibits a frequency gap at the resonance frequency of the LC-oscillator, the dashed line indicates the dispersion relation in the absence of oscillators, the circles indicate the positions of phase matched points which lie on a straight line within the no-up-conversion region (shown in Fig. 4).

Let us consider the TWPA with LC-oscillators. The corresponding circuit is presented in Fig. 16a. The derivation of the dynamical equation is straightforward: we add the oscillator circuit variables to the Lagrangian, Eq. (1), and eliminate the oscillator variables from the dynamic equations. Specifically we consider the dc current biased TWPA. In this case, Eq. (21) for the chain without oscillators remains valid with the only difference, the factor ω^2/ω_0^2 in the first term is replaced with

$$\frac{\omega^2}{\omega_0^2} \to \frac{\omega^2}{\omega_0^2}\frac{\nu\omega^2 - \omega_1^2}{\omega^2 - \omega_1^2} \tag{51}$$

where

$$\omega_1^2 = \frac{1}{L_\mathrm{osc}(C_\mathrm{osc} + C_\mathrm{c})}, \tag{52}$$

$$\nu = 1 - \frac{C_\mathrm{c}^2}{(C + C_\mathrm{c})(C_\mathrm{osc} + C_\mathrm{c})}. \tag{53}$$

The dispersion equation then takes the form

$$4\omega_0^2 \sin^2\frac{\kappa}{2} = \omega^2 \frac{\nu\omega^2 - \omega_1^2}{\omega^2 - \omega_1^2}. \tag{54}$$

Solving for ω we get

$$\begin{aligned}\omega_\pm^2 = \frac{1}{2\nu}\Bigg[&\left(\omega_1^2 + 4\omega_0^2\sin^2\frac{\kappa}{2}\right) \\ &\pm\sqrt{\left(\omega_1^2 + 4\omega_0^2\sin^2\frac{\kappa}{2}\right)^2 - 16\nu\omega_1^2\omega_0^2\sin^2\frac{\kappa}{2}}\,\Bigg].\end{aligned} \tag{55}$$

The derived spectrum is depicted in Fig. 17; it consists of two bands separated by a gap.

To identify the sweet spot we assume the pump frequency within the upper band, and the signal frequency within the lower band, and solve equation, $\omega_-(\kappa_\mathrm{p}/2) = \omega_+(\kappa_\mathrm{p})/2$. Converted for the pump frequency, this equation has the explicit form

$$\frac{3(1-\nu)}{\omega_\mathrm{p}^2 - \omega_1^2} = \frac{1}{16\omega_0^2\omega_1^2}\frac{(4\omega_1^2 - \nu\omega_\mathrm{p}^2)^2}{4\omega_1^2 - \omega_\mathrm{p}^2}. \tag{56}$$

One can check by direct calculation that the solution indeed possesses the property, $\kappa_\mathrm{s} = \kappa_\mathrm{p}/2$, as illustrated in Fig. 17: the pump and signal points are located on a straight line. Moreover, the pump frequency is located in the no-up-conversion frequency region (recall Fig. 4).

The equations for the gain coefficient, Eqs. (28) and (29), derived in Section III do not change their form in the present case; however, the dependence of the gain coefficient on the frequency is now different due to the different dispersion relation. Dependence of the gain coefficient at the signal degeneracy on the pump frequency is illustrated in Fig. 18. As soon as the pump is placed within the lower frequency band, the gain coefficient behaves similarly to the one in Fig. 2a for a TWPA without oscillators. However, when the pump is placed within the upper band at the sweet spot, the amplification dramatically increases up to $g \approx 0.014$ for a rather weak pumping strength, $\varepsilon = 0.06$, about seven times smaller than the maximum pumping strength in Fig. 2a and definitely

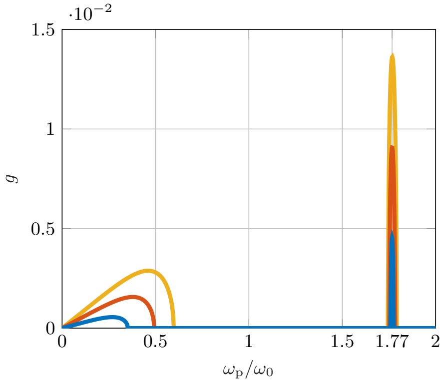

FIG. 18: Gain coefficient for a signal at zero detuning, $\delta = 0$, for a TWPA with a two-band dispersion relation with $\omega_1 = 1.5\omega_0$, $\nu = 0.95$ and $\varepsilon = 0.02$ (blue), 0.04 (orange) and 0.06 (yellow). When the pump is placed within the lower band, the gain coefficient is similar to the case in the absence of oscillators (curves at the lower left corner). The sharp high-amplification peak emerges when the pump is placed within the upper band at the sweet spot, $\omega_\mathrm{p} = 1.77\omega_0$. The peak widths are $0.018\omega_0$, $0.032\omega_0$ and $0.048\omega_0$ respectively.

achievable in experiments. This g-value corresponds to the gain $G \approx 24\,\mathrm{dB}$ for $N = 200$ unit cells. The pump position is rather flexible, the gain remains high within the pump bandwidth $\sim 0.05\omega_0$.

For a detuned signal, large amplification persists within a quite wide frequency band, $\sim 0.5\omega_\mathrm{p}$ that could be of order of few GHz, as shown in Fig. 19. This is due to a relatively weak dispersion in the low frequency region.

B. Sweet spot in periodically modulated chain

Here we examine a periodically modulated TWPA and prove that there also exists a sweet spot. Experimental realisation of such a device will be reported elsewhere [39]. The circuit is presented in Fig. 16b, here each unit cell consists of two subcells with different Josephson junction parameters. Consider the dc current biased TWPA with different Josephson inductances in the subcells. The Lagrangian can be written for odd and even circuit nodes in analogy with Eqs. (1) and (2),

$$\begin{aligned}\mathcal{L}_\mathrm{J}[\theta_n] = &\sum_{2n} \frac{1}{L_{\mathrm{J}1}} \cos(\theta_{01} + \theta_{2n}) \\ &+ \sum_{2n+1} \frac{1}{L_{\mathrm{J}2}} \cos(\theta_{02} + \theta_{2n+1})\,.\end{aligned} \tag{57}$$

The biasing phases here obey the equations, $\sin\theta_{0j} = I_\mathrm{dc}/I_{\mathrm{c}j}$. Dynamical equations for such a chain have the form,

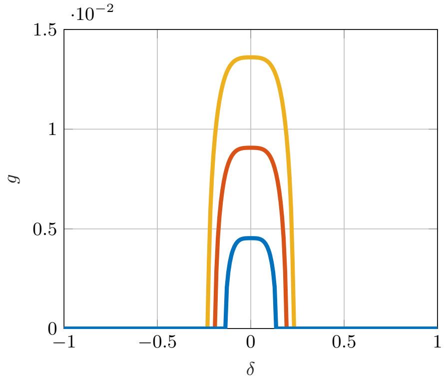

FIG. 19: Gain coefficient as function of detuning for a TWPA with two-band dispersion relation with $\omega_1 = 1.5\omega_0$ and $\nu = 0.95$, for pump at optimal phase matching point $\approx 1.77\omega_0$ and different pumping strengths, $\varepsilon = 0.02$ (blue), 0.04 (orange), and 0.06 (yellow). The corresponding bandwidths are $\omega_\mathrm{s} - \omega_\mathrm{p}/2 = (0.14,\, 0.19,\, 0.23)\,\omega_\mathrm{p}$, respectively.

$$\begin{aligned}&-\ddot{\phi}_{2n} - \left(\omega_1^2\theta_{2n} - \omega_2^2\theta_{2n+1}\right) \\ &+ \frac{1}{2}\left(\omega_1^2 \tan\theta_{01}\theta_{2n}^2 - \omega_2^2 \tan\theta_{02}\theta_{2n+1}^2\right) = 0\,,\end{aligned} \tag{58}$$

$$\begin{aligned}&-\ddot{\phi}_{2n+1} - \left(\omega_2^2\theta_{2n+1} - \omega_1^2\theta_{2n+2}\right) \\ &+ \frac{1}{2}\left(\omega_2^2 \tan\theta_{02}\theta_{2n+1}^2 - \omega_1^2 \tan\theta_{01}\theta_{2n+2}^2\right) = 0\,,\end{aligned} \tag{59}$$

where $\omega_j^2 = \cos\theta_{0j}/L_{\mathrm{J}j}C$ are the subcell resonance frequencies. The linearised equations define the spectral properties of the chain. Assume the solution having the form, $\phi_{2n} = A\mathrm{e}^{\mathrm{i}\kappa(2n) - \mathrm{i}\omega t}$, $\phi_{2n+1} = B\mathrm{e}^{\mathrm{i}\kappa(2n+1) - \mathrm{i}\omega t}$, then equations for amplitudes, A and B, read,

$$\begin{aligned}&\left(\omega^2 - \omega_1^2 - \omega_2^2\right)A + \left(\omega_1^2\mathrm{e}^{-\mathrm{i}\kappa} + \omega_2^2\mathrm{e}^{\mathrm{i}\kappa}\right)B = 0 \\ &\left(\omega^2 - \omega_2^2 - \omega_1^2\right)B + \left(\omega_2^2\mathrm{e}^{-\mathrm{i}\kappa} + \omega_1^2\mathrm{e}^{\mathrm{i}\kappa}\right)A = 0\,,\end{aligned} \tag{60}$$

and the dispersion relation has the form,

$$\omega^2 = \left(\omega_1^2 + \omega_2^2\right) \pm \sqrt{\left(\omega_1^2 + \omega_2^2\right)^2 - 4\omega_1^2\omega_2^2 \sin^2\kappa}\,. \tag{61}$$

The dispersion relation is depicted in Fig. 20; it has two bands separated by a gap. The sweet spot is found from equations, $\omega_\mathrm{s} = \omega_\mathrm{p}/2$, $\kappa_\mathrm{s} = \kappa_\mathrm{p}/2$, whose solution reads,

$$\omega_\mathrm{p}^2 = 8\left[\left(\omega_1^2 + \omega_2^2\right) - \sqrt{3}\omega_1\omega_2\right]\,, \tag{62}$$

$$\sin^2\frac{\kappa_\mathrm{p}}{2} = \frac{\sqrt{3}\left[\left(\omega_1^2 + \omega_2^2\right) - \sqrt{3}\omega_1\omega_2\right]}{\omega_1\omega_2}\,. \tag{63}$$

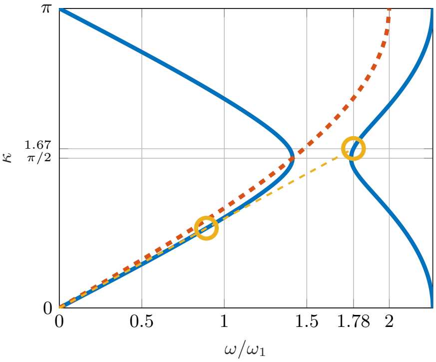

FIG. 20: Dispersion relation of a periodically modulated Josephson junction chain with $\omega_2 = 1.25\omega_1$; it consists of two bands separated by a gap (solid lines), dashed line indicates the dispersion relation in the absence of modulation, the circles indicate positions of phase matched points, they lie on a straight line within the no-up-conversion frequency region.

This solution is illustrated in Fig. 20: the positions of the pump and the signal at the degeneracy are indicated with the circles; they lie on a straight line at different sides of the gap in the region where the up-conversion is not possible. The gain in this setup is qualitatively similar to the TWPA with LC-oscillators.

VI. CONCLUSION

In this paper, we propose a method for achieving a high gain for a lumped-element TWPA operating in the 3WM regime. The simple model of amplification in weakly dispersive medium [9, 10], relevant for kinetic inductance TWPAs and Josephson junction TWPAs at low frequencies predicts the gain up to 40 dB for a chain with 100 unit cells and a reasonable pump intensity. However, in practice, such a gain was never demonstrated. This was explained with a parasitic effect of generation of high harmonics and up-conversion processes [34]. We performed a detailed theoretical analysis of this regime including multiple pump harmonics and signal and idler up-converted modes. We identified a scaling parameter μ that controls the gain and quantifies an interplay between the dispersion and the nonlinear wave interaction and found that the gain is strongly reduced for both small values as well as large values of μ, although for different reasons. When the dispersion is weak in relation to the interaction, *i.e.* for small μ, the generation of up-converted modes is prominent. In the opposite limit of strong dispersion in relation to the interaction, *i.e.* for large μ, the phase mismatch becomes the dominant effect. This finding is supported by the experimental observations on a SNAIL-TWPA, and the data are in quantitative agreement with the theoretical simulations.

Our proposal concerns a different operation regime for which the cutoff frequency of the TWPA plays the central role. We proposed to place the pump close to the cutoff such that generation of up-converted modes is inhibited. Then, by solving the difference equations for discrete Josephson junction chain we found that there is a sweet spot where the pump and the signal are exactly phase matched. The sweet spot was proven to exist when the TWPA frequency spectrum consists of two bands separated by a gap. Studying different ways of engineering the two-band spectrum - by adding LC-oscillators or periodically modulating the chain parameters, we predicted that the gain at the sweet spot may achieve the values of order 25 dB within a few GHz amplification bandwidth for a chain with ~ 200 unit cells and for moderate pump intensities.

VII. ACKNOWLEDGEMENTS

The project was supported by the Knut and Alice Wallenberg foundation via the Wallenberg Centre for Quantum Technology, and the EU Consortium OpenSuperQ. The authors acknowledge the use of the Nanofabrication Laboratory (NFL) at Chalmers University of Technology.

[1] C. M. Caves, Quantum limits on noise in linear amplifiers, Phys. Rev. D **26**, 1817(1982).

[2] T. Yamamoto *et al.,* Flux-driven Josephson parametric amplifier, Appl. Phys. Lett., **93**, 042510 (2008).

[3] N. Bergeal, *et al.*, Phase-preserving amplification near the quantum limit with a Josephson ring modulator, Nature **465**, 64 (2010).

[4] N. Roch, *et al.*, Tunable Nondegenerate Three-Wave Mixing Microwave Device Operating near the Quantum Limit, Phys. Rev. Lett. **108**, 147701 (2012).

[5] A. Roy and M. Devoret, Introduction to parametric amplification of quantum signals with Josephson circuits, Comptes Rendus Phys. **17**, 740 (2016).

[6] J. Aumentado, Superconducting Parametric Amplifiers (Review), IEEE Microwave magazine, August 2020, p.45 (2020).

[7] R. J. Schoelkopf and S. M. Girvin, Wiring up quantum systems, Nature **451**, 664 (2008).

[8] A. L. Cullen, A travelling-Wave Parametric Amplifier, Nature (London) **181**, 332 (1958).

[9] P. K. Tien and H. Suhl, A Traveling-Wave Ferromagnetic Amplifier, Proc. lnst. Radio Engrs. **46**, 700 (1958).

[10] P. K. Tien, Parametric amplification and frequency mixing in propagating circuits, J. Appl. Phys. **29**, 1347

(1958).

[11] A. L. Grimsmo and A. Blais, Squeezing and quantum state engineering with Josephson travelling wave amplifiers, npj Quantum Information 3:20 (2017).

[12] M. R. Perelshtein, *et al.,* Broadband continuous variable entanglement generation using Kerr-free Josephson metamaterial, arXiv:2111.06145 (2021).

[13] Byeong Ho Eom, Peter K. Day, Henry G. LeDuc, and Jonas Zmuidzinas, A wideband, low-noise superconducting amplifier with high dynamic range, Nature Phys. **8**, 623 (2012).

[14] C. Bockstiegel, J. Gao, M. R. Vissers, M. Sandberg, S. Chaudhuri, A. Sanders, L.R. Vale, K.D. Irwin, and D. P. Pappas, Development of a Broadband NbTiN Traveling-WaveParametric Amplifier for MKID Readout, J. Low Temp. Phys. **176**, 476 (2014).

[15] M. R. Vissers, R. P. Erickson, H.-S. Ku, Leila Vale, Xian Wu, G. C. Hilton, and D. P. Pappas, Low-noise kinetic inductance traveling-wave amplifier using three-wave mixing, Appl. Phys. Lett. **108**, 012601 (2016).

[16] S. Chaudhuri, D. Li, K. D. Irwin, C. Bockstiegel, J. Hubmayr, J. N. Ullom, M. R. Vissers, and J. Gao, Broadband parametric amplifiers based on nonlinear kinetic inductance artificial transmission lines, Appl. Phys. Lett. **110**, 152601 (2017).

[17] R. P. Erickson and D. P. Pappas, Theory of multiwave mixing within the superconducting kinetic-inductance traveling-wave amplifier, Phys. Rev. B **95**, 104506 (2017).

[18] S. Goldstein, N. Kirsh, E. Svetitsky, Y. Zamir, O. Hachmo, C.E. Mazzotti de Oliveira, and N. Katz Four wave-mixing in a microstrip kinetic inductance travelling wave parametric amplifier, Appl. Phys. Lett. **116**, 152602 (2020).

[19] M. Malnou, M. R. Vissers, J. D. Wheeler, J. Aumentado , J. Hubmayr, J. N. Ullom, and J. Gao, Three-Wave Mixing Kinetic Inductance Traveling-Wave Amplifier with Near-Quantum-Limited Noise Performance, PRX Quantum **2**, 010302 (2021).

[20] D. J. Parker, M. Savytskyi, W. Vine, A. Laucht, T. Duty, A. Morello, A.L. Grimsmo, and J.J. Pla, A near-ideal degenerate parametric amplifier, arXiv:2108.10471 (2021).

[21] M. J. Feldman, P. T. Parrish, and R. Y. Chiao, Parametric amplification by unbiased Josephson junctions, J. Appl. Phys. **46**, 4031 (1975).

[22] O. Yaakobi, L. Friedland, C. Macklin, and I. Siddiqi, Phys. Rev. B 87, 144301 (2013); Phys. Rev. B 88, 219904(E) (2013).

[23] K. O'Brien, C. Macklin, I. Siddiqi. and Xiang Zhang, Resonant Phase Matching of Josephson Junction Traveling Wave Parametric Amplifiers, Phys. Rev. Lett. **113**, 157001 (2014).

[24] C. Macklin, K. O'Brien, D. Hover, M. E. Schwartz, V. Bolkhovsky, X. Zhang, W. D. Oliver, I. Siddiqi, A near-quantum-limited Josephson traveling wave parametric amplifier, Science **350**, 325 (2015).

[25] T.C. White, *et al.,* Traveling wave parametric amplifier with Josephson junctions using minimal resonator phase matching, Appl. Phys. Lett. **106**, 242601 (2015).

[26] M.T. Bell and A. Samolov, Traveling-Wave Parametric Amplifier Based on a Chain of Coupled Asymmetric SQUIDs, Phys. Rev. Applied **4**, 024014 (2015).

[27] L. Planat, *et al.*, Photonic-Crystal Josephson Traveling-Wave Parametric Amplifier Phys. Rev. X **10**, 021021 (2020).

[28] A. Ranadive, M. Esposito, L. Planat, E. Bonet, C. Naud, O. Buisson, W. Guichard, and N. Roch, A reversed Kerr traveling wave parametric amplifier arXiv:2101.05815 (2021).

[29] A. B. Zorin, Josephson Traveling-Wave Parametric Amplifier with Three-Wave Mixing, Phys. Rev. Appl. **6**, 034006 (2016).

[30] A. B. Zorin, Flux-Driven Josephson Traveling-Wave Parametric Amplifier, Phys. Rev. Appl. **12**, 044051 (2019).

[31] V. V. Sivak, N. E. Frattini, V. R. Joshi, A. Lingenfelter, S. Shankar, and M. H. Devoret, Kerr-Free Three-Wave Mixing in Superconducting Quantum Circuits, Phys. Rev. Appl. **11**, 054060 (2019).

[32] A. Miano and O. A. Mukhanov, Symmetric Traveling Wave Parametric Amplifier, IEEE Trans. Appl. Supercond. **29**, 1501706 (2019).

[33] J. A. Armstrong, N. Bloembergen, J. Ducuning, and P. S. Pershan, Interactions between Light Waves in a Nonlinear Dielectric, Phys. Rev. **127**, 1918 (1962).

[34] T. Dixon, J. W. Dunstan, G. B. Long, J. M. Williams, P. J. Meeson, and C. D. Shelly, Capturing Complex Behavior in Josephson Traveling-Wave Parametric Amplifiers, Phys. Rev. Appl. **14**, 034058 (2020).

[35] M. H. Devoret, in *Quantum Entanglement and Information Processing*, edited by D. Esteve, J. M. Raimond, and J. Dalibard, Proceedings of the Les Houches Summer School of Theoretical Physics, LXIII, 1995 (Elsevier, Amsterdam, 2004).

[36] A. O. Caldeira and A. J. Leggett, Quantum tunnelling in a dissipative system, Ann. Phys. **149**, 374 (1983).

[37] P. Hänggi, Dissipative tunneling, Z. Phys. B **68**,181 (1987).

[38] H. F. Yu, X. B. Zhu, Z. H. Peng, W. H. Cao, D. J. Cui, Ye Tian, G. H. Chen, D. N. Zheng, X. N. Jing, Li Lu, and S. P. Zhao, Quantum and classical resonant escapes of a strongly driven Josephson junction, Phys. Rev. B **81**, 144518 (2010).

[39] A. Fadavi Roudsari *et al.*, unpublished (2022).